Chemical and Biological Oceanographic Conditions in the Estuary and Gulf of St. Lawrence during 2022

Marjolaine Blais, Peter S. Galbraith, Stéphane Plourde and Caroline Lehoux

Fisheries and Oceans Canada,
Québec Region,
Maurice Lamontagne Institute,
P.O. Box 1000,
Mont-Joli, QC,
G5H 3Z4

2023

Canadian Technical Report of
Hydrography and Ocean Sciences 357

Fisheries and Oceans Canada | Pêches et Océans Canada

Canada

Canadian Technical Report of Hydrography and Ocean Sciences

Technical reports contain scientific and technical information of a type that represents a contribution to existing knowledge but which is not normally found in the primary literature. The subject matter is generally related to programs and interests of the Oceans and Science sectors of Fisheries and Oceans Canada.

Technical reports may be cited as full publications. The correct citation appears above the abstract of each report. Each report is abstracted in the data base *Aquatic Sciences and Fisheries Abstracts.*

Technical reports are produced regionally but are numbered nationally. Requests for individual reports will be filled by the issuing establishment listed on the front cover and title page.

Regional and headquarters establishments of Ocean Science and Surveys ceased publication of their various report series as of December 1981. A complete listing of these publications and the last number issued under each title are published in the *Canadian Journal of Fisheries and Aquatic Sciences*, Volume 38: Index to Publications 1981. The current series began with Report Number 1 in January 1982.

Rapport technique canadien sur l'hydrographie et les sciences océaniques

Les rapports techniques contiennent des renseignements scientifiques et techniques qui constituent une contribution aux connaissances actuelles mais que l'on ne trouve pas normalement dans les revues scientifiques. Le sujet est généralement rattaché aux programmes et intérêts des secteurs des Océans et des Sciences de Pêches et Océans Canada.

Les rapports techniques peuvent être cités comme des publications à part entière. Le titre exact figure au-dessus du résumé de chaque rapport. Les rapports techniques sont résumés dans la base de données *Résumés des sciences aquatiques et halieutiques*.

Les rapports techniques sont produits à l'échelon régional, mais numérotés à l'échelon national. Les demandes de rapports seront satisfaites par l'établissement auteur dont le nom figure sur la couverture et la page de titre.

Les établissements de l’ancien secteur des Sciences et Levés océaniques dans les régions et à l'ad- ministration centrale ont cessé de publier leurs diverses séries de rapports en décembre 1981. Vous trouverez dans l'index des publications du volume 38 du *Journal canadien des sciences halieutiques et aquatiques*, la liste de ces publications ainsi que le dernier numéro paru dans chaque catégorie. La nouvelle série a commencé avec la publication du rapport numéro 1 en janvier 1982.

Canadian Technical Report
of Hydrography and Ocean Sciences 357

2023

Chemical and Biological Oceanographic Conditions in the Estuary and Gulf of St. Lawrence during 2022

Marjolaine Blais, Peter S. Galbraith, Stéphane Plourde and Caroline Lehoux

Fisheries and Oceans Canada
Québec Region
Maurice Lamontagne Institute
P.O. Box 1000
Mont-Joli, QC
G5H 3Z4

Cat. No. Fs 97-18/357E-PDF ISBN 978-0-660-49436-4 ISSN 1488-5417

Correct citation for this publication:

Blais, M., Galbraith, P.S., Plourde, S. and Lehoux, C. 2023. Chemical and Biological Oceanographic Conditions in the Estuary and Gulf of St. Lawrence during 2022. Can. Tech. Rep. Hydrogr. Ocean Sci. 357 : v + 70 p.

TABLE OF CONTENTS

ABSTRACT

Blais, M., Galbraith, P.S., Plourde, S. and Lehoux, C. 2023. Chemical and Biological Oceanographic Conditions in the Estuary and Gulf of St. Lawrence during 2022. Can. Tech. Rep. Hydrogr. Ocean Sci. 357 : v + 70 p.

An overview of the chemical and biological oceanographic conditions in the Gulf of St. Lawrence in 2022 is presented as part of the Atlantic Zone Monitoring Program (AZMP). AZMP data and data from regional programs are presented in relation to long-term means. Oxygen levels in deep waters reached record-low saturation levels in the Estuary. Annual nutrient inventories were strongly below normal in the surface layer, and mostly above normal in the bottom layer of the Gulf. Mid-layer nutrient inventory anomalies were spatially variable. Annual inventories of vertically integrated chlorophyll *a* were above normal in most regions because of a strong long-lasting fall bloom. The spring bloom was the earliest of the time series in the northern Gulf. Bloom magnitudes and amplitudes were mostly near normal or below normal in all regions. Strong negative anomalies of the zooplankton biomass (strongly influenced by large *Calanus* abundances) were generally observed in the Gulf, including record lows in the Estuary and Northwest Gulf, while zooplankton biomass was high in the Magdalen Shallows and at record high at Shediac Valley station. Small calanoids, non-copepods and warm-water copepods generally had above normal abundances, except in the Northeast Gulf. The characterization of large *Calanus* development suggests their phenology was early at both high-frequency monitoring stations.

RÉSUMÉ

Blais, M., Galbraith, P.S., Plourde, S. and Lehoux, C. 2023. Chemical and Biological Oceanographic Conditions in the Estuary and Gulf of St. Lawrence during 2022. Can. Tech. Rep. Hydrogr. Ocean Sci. 357 : v + 70 p.

Un aperçu des conditions océanographiques chimiques et biologiques dans le golfe du Saint-Laurent en 2022 est présenté dans le cadre du Programme de Monitorage de la Zone Atlantique (PMZA). Les données du PMZA et celles de programmes de monitorage régionaux sont présentées par rapport aux moyennes à long terme. Les niveaux d'oxygène dans les eaux profondes ont atteint des minimums records dans l'estuaire. Les inventaires annuels d'éléments nutritifs étaient fortement sous la normale dans la couche de surface et au-dessus de la normale dans la couche profonde. Les anomalies d'inventaires d'éléments nutritifs dans la couche intermédiaire étaient spatialement variables. Les inventaires annuels de chlorophylle *a* intégrée verticalement étaient au-dessus de la normale dans la plupart des régions en raison d'une forte floraison automnale de longue durée. La floraison printanière a été la plus hâtive de la série temporelle dans le nord du golfe en 2022. L'amplitude et la magnitude des floraisons étaient soit près de la normale ou inférieures à celle-ci dans toutes les régions. De fortes anomalies négatives de la biomasse de zooplancton (grandement influencée par l'abondance des grands *Calanus*) ont généralement été observées dans le golfe, incluant des minimums records dans l'estuaire et le nord-ouest du golfe, alors que la biomasse de zooplancton était au-dessus de la normale sur le plateau madelinien et présentait un niveau record à la station de la vallée de Shediac. Les abondances de petits calanoïdes, de non-copépodes et de copépodes d'eaux chaudes étaient généralement au-dessus de la normale. La caractérisation du développement des grands *Calanus* suggère que leur phénologie était la plus hâtive de toute la série temporelle aux deux stations de monitorage à haute fréquence.

1. INTRODUCTION

The Atlantic Zone Monitoring Program (AZMP) was implemented in 1998 (Therriault et al. 1998) with the aim of 1) increasing Fisheries and Oceans Canada's (DFO) capacity to understand, describe, and forecast the state of the marine ecosystem, and 2) quantifying the changes in the ocean's physical, chemical, and biological properties and the predator-prey relationships of marine resources. AZMP provides data to support the sound development of ocean activities. A critical element of the AZMP observational program is the annual assessment of the distribution and variability of physical, chemical and biological properties of the water column. This report focuses on oxygen, nutrients, and plankton communities.

A description of the spatiotemporal distribution of dissolved oxygen, nutrient (nitrate, silicate, and phosphate), and chlorophyll *a* (chl *a*) concentrations provides important information on water mass movements and on the location, timing, and magnitude of biological production cycles. A description of the phytoplankton and zooplankton communities, distributions and phenology provide important information on the organisms forming the base of the marine food web. Understanding plankton production cycles is essential for an ecosystem approach to fisheries management.

The AZMP derives its information on the state of the marine ecosystem from a combination of satellite remote sensing and *in situ* data collected at a network of sampling locations (high-frequency monitoring stations, cross-shelf sections) in each DFO region (Québec, Gulf, Maritimes, Newfoundland and Labrador; see Figure 1 for section locations in the St. Lawrence Gulf and Estuary) occupied at a frequency of weekly to once annually. The sampling design provides valuable information on the natural variability in physical, chemical, and biological properties of the Northwest Atlantic continental shelf. Ecosystem trawl survey and cross-shelf sections provide a broad-scale overview of the conditions but are limited in their seasonal coverage while strategically located high-frequency monitoring stations complement the sampling by providing more detailed information on seasonal-scale changes in ecosystem properties. In recent years, Viking oceanographic buoy sensors have also complemented the core observations with high temporal resolution data.

In this document, we review the chemical and biological oceanographic (lower trophic levels) conditions in the Gulf of St. Lawrence in 2022. Changes in the physical pelagic environment influence both plankton community composition and annual biological production cycles, with implications for energy transfer to higher trophic-level production. Readers should refer to Galbraith et al. (2023) for a complete description of the physical conditions that prevailed in the Gulf in 2022.

2. METHODS

2.1 SAMPLING

All sample collection and processing steps meet the standards of the AZMP protocol (Mitchell et al. 2002). Field measurements included in this report were made during dedicated AZMP surveys carried out in winter, early summer, and fall (generally in March, June, and October) of each year and at two high-frequency monitoring stations (Figure 1). Oceanographic measurements made during multidisciplinary surveys (August and September; hereafter referred to as late summer surveys) and during the mackerel egg survey (June; zooplankton samples only) have been included for all years (2006–2022) for which these data are available.

In this document, stations were grouped into four main regions for which biochemical indices are presented (Figure 1):

(1) Estuary and Northwest Gulf: this region is generally deep (> 200 m) and cold in summer. It is strongly influenced by freshwater runoff from the St. Lawrence River at the surface, and by dense waters from the Laurentian Channel in deeper waters;

(2) Northeast Gulf: this region, with deep channels and a relatively wide shelf (shallower than 100 m), is characterized by high surface salinity and is influenced by the intrusion of water from the Labrador Shelf through the Strait of Belle Isle along the northern coast;

(3) Central Gulf and Cabot Strait: this region is generally deep (> 200 m) and is directly influenced by deep water masses that mix at the continental slope (warm North Atlantic Central Water that has a Gulf Stream signature and cold Labrador Current Water) and enter the Gulf through Cabot Strait;

(4) Magdalen Shallows: this region is shallow (< 100 m) and warm at the surface in summer. It is largely influenced by the Gaspé Current.

These regions match the regions used in the Gulf for the recently implemented DFO Ecosystem Approach to Fisheries Management. Since there are few biochemical data collected in Mécatina and Northumberland (Figure 1), indices will not be reported for those regions.

Table 1 provides details about the 2022 sampling surveys and Figure 2 and Figure 3 summarize the sampling effort during the seasonal surveys and at the high-frequency monitoring stations, respectively. Rimouski station (depth 320 m) has been sampled since 1991—about weekly throughout the summer, once or twice a month in early spring and late fall, and rarely in winter (except during the winter survey) due to the presence of sea ice. It is representative of conditions in the Estuary and Northwest Gulf. Shediac Valley station (depth 84 m) is representative of conditions on the Magdalen Shallows and of the Estuary outflow. Shediac Valley station is at best sampled monthly between May and November with decreasing coverage from January through April. Shediac Valley station was occupied on nine occasions in 2022, but four of those occupations occurred within a few days, at the end of May to early June. In addition to the occupations at the high-frequency monitoring stations, Viking oceanographic buoys equipped with temperature, salinity, and fluorescence surface sensors (data collected every 30 minutes) have been deployed at the high-frequency stations since 2002 and 2004 at Rimouski and Shediac Valley stations, respectively. Deployment of the Viking buoys typically occurs in late April or early May and the recovery of the buoys is usually done in late October or early November.

Sampling on the oceanographic sections and at the high-frequency monitoring stations includes a CTD profile (temperature, salinity, fluorescence, dissolved oxygen) as well as water sampling using Niskin bottles (surface, 10 m, 15 m, 25 m, 50 m, 100 m, 200 m, 300 m, 400 m, bottom). Water from the Niskin bottles is collected for the analysis of dissolved oxygen (Winkler method), nutrients (Seal Analytical AutoAnalyzer 3 or Alpkem AutoAnalyzer), chl a (fluorometer), and phytoplankton enumeration (inverted microscopy) (Mitchell et al. 2002). Finally, mesozooplankton (< 1 cm, hereafter referred to as zooplankton) is collected with bottom-to-surface vertical ring net tows (75 cm diameter, 200 µm mesh) for most surveys. Taxonomists are responsible for the identification, enumeration, and bulk biomass measurements of zooplankton samples collected during regular AZMP surveys (early summer and fall surveys) whereas samples collected during the late summer multidisciplinary survey and during the mackerel egg survey are analyzed using a semi-automated procedure developed with the ZooImage 5.5.2 software package (Grosjean et al. 2018; https://CRAN.R-project.org/package=zooimage) following the methodology described in Plourde et al. (2019)

and Blais et al. (2023). Since methods are different, and considering the larger size of net mesh used during the mackerel egg survey (333 µm mesh), large calanoid taxa indices developed with the ZooImage analysis only include copepodite stages CIV–CVI, and these data are not included in the annual abundance estimates.

2.2 IN SITU METRICS

2.2.1 Oxygen

Oxygen concentration at 300 m is used as an indicator of hypoxic conditions in the Gulf. Oxygen concentration was measured using an oxygen probe (Sea-Bird SBE43) mounted on the CTD; the probe was calibrated against collected seawater samples from every cast which were analyzed by Winkler titration (for the calibration procedure, see Sea-Bird application notes 61-1, -2, -3). Annual average time series are based on gridded (2 km^2) inverse-distance-weighted interpolation, spatially averaged over every region. Oxygen saturation level is calculated using the equation

$$O_2Sat = [O_2] / SolO_2 \times 100,$$

where $[O_2]$ is the oxygen concentration (µM) and SolO2 is the oxygen solubility (µM) at normal atmospheric pressure given *in situ* temperature and salinity.

2.2.2 Nutrients and phytoplankton

Nutrient and chl *a* concentrations (a proxy for phytoplankton biomass) collected along the AZMP sections and at the high-frequency monitoring stations were integrated over various depth intervals (i.e., 0–100 m for chl *a*; 0–50 m, 50–150 m, and 150 m–bottom for nutrients) using trapezoidal numerical integration. In 2016 and 2017, winter vertical profiles of nutrients performed all over the Gulf revealed that nutrient concentrations were relatively homogeneous in the upper 50 m of the water column during that season. Thus, for typical years when vertical nutrient profiles are not available, including 2022, integrated nutrient values for the winter survey were calculated using surface concentrations, assuming homogeneity of nutrient concentrations in the winter mixed layer. Phytoplankton taxonomic identification is performed for the high-frequency monitoring stations only. The ratio between diatoms and flagellates, or between diatoms and dinoflagellates, is used to provide information on the phytoplankton community size structure. Spring nutrient drawdown was estimated using the difference between the March and June nitrate inventories (0–50 m) and is used as a proxy for phytoplankton spring production since the early summer sampling occurs after the spring bloom.

2.2.3 Zooplankton

Since zooplankton samples are generally collected over the entire water column (0–50 m during the mackerel egg survey), zooplankton indices included in this report represent depth-integrated metrics. Only samples collected during regular AZMP surveys (early summer and fall) and analyzed by taxonomists were included in the calculation of regional zooplankton annual anomalies. A detailed list of species included in each copepod index is presented in Appendix 1. Since 2018, the results of a genetic study based on prosome length have been used to properly identify *Calanus finmarchicus* and *Calanus glacialis* (Parent et al. 2011).

We use the time series at Rimouski station to describe *C. finmarchicus* phenology and its evolution as adequate sampling and stage identification started more than 25 years ago at that station. However, sampling methodology has changed over time: from 1994 to 2004, prior to the use of AZMP standard nets (i.e., 75 cm diameter, 200 µm mesh bottom-to-surface ring net tows; Mitchell et al. 2002), *C. finmarchicus* copepodite stage abundance was determined using samples collected with 333 µm (CIV–CVI) and 73 µm (CI–III) mesh nets, towed from bottom to surface and from 50 m to surface, respectively. Samples collected using the 73 µm mesh nets were analyzed for only six years (1994, 1996–2000) of the time series (see Plourde et al. 2009 for details). In other years, before 2004, for which samples collected using the 73 µm mesh net were not analyzed, the abundance of CI–III in the samples collected using the 333 µm mesh net was adjusted based on a comparison with samples collected using a 158 µm mesh net (S. Plourde, DFO, Mont-Joli, QC; unpublished data). The phenology of *C. finmarchicus* was described using the following steps: (1) stage-relative abundances were normalized (proportion of a copepodite stage/maximum proportion for the stage) within each year for CI–III, CIV, CV, and CVI (male and female) and (2) stage proportions were smoothed using a LOESS function.

2.3 REMOTE SENSING OF OCEAN COLOUR AND SPRING BLOOM METRICS

Satellite ocean colour data provide large-scale images of surface phytoplankton biomass (chl *a*) over the Northwest Atlantic. We used daily satellite composite images within four ocean-colour polygons (Northwest Gulf, Northeast Gulf, Magdalen Shallows, and Cabot Strait; see Figure 4 for locations) to supplement our ship-based observations, especially regarding the spring bloom phenology, and to provide seasonal coverage and a large-scale context over which to interpret our survey data. However, since ocean colour imagery does not provide information on the dynamics that take place below the surface of the water column, it should be used as complementary information to the field data.

In this report, 2003–2022 data collected by the Moderate Resolution Imaging Spectroradiometer (MODIS) "Aqua" sensor launched by National Aeronautics and Space Administration (NASA) in July 2002 (4 km spatial resolution) are used to construct a continuous time series of surface chl *a* in the four ocean-colour polygons (Figure 4). The continued calibration and data reprocessing done by NASA ensure data quality over the whole MODIS time series (Xiong et al. 2020). Composite satellite images of remote sensing reflectance sourced from NASA's Goddard Space Flight Center (https://oceancolor.gsfc.nasa.gov) were converted to chl *a* using an algorithm based on empirical orthogonal function (EOF) analysis (Laliberté et al. 2018). Daily chl *a* concentrations were averaged over each ocean-colour polygon and were extracted using the PhytoFit application v1.0.0 (Clay et al. 2021). There are typically less ocean colour data available during January, February, and December due to clouds, sea ice cover, and low sun angles.

The timing (start and duration) of the spring phytoplankton bloom was derived using a symmetric shifted Gaussian function of time (Zhai et al. 2011) that was smoothed using a LOESS function (locally estimated scatterplot smoothing) over days with a minimal polygon coverage of 20%. While the start (day when concentration reaches 20% of the maximum spring bloom amplitude) and duration of the spring bloom were derived from the smoothed Gaussian curve, the amplitude (maximum chl *a*) and magnitude (the integral of chl *a* concentration under the Gaussian curve) of the spring bloom were calculated from the daily satellite-derived chl *a* within the spring bloom period rather than from the Gaussian curve.

All ocean-colour polygons are located outside of the St. Lawrence River plume because satellite-based chl *a* estimates in such areas are unreliable due to contamination by river inputs loaded with coloured matter of terrestrial origin; polygons are not directly adjacent to the coast for the same reason. This also explains why spring bloom metrics in the Estuary cannot be derived from ocean colour data. Moreover, in the Estuary, the significance of the spring bloom for the food web remains to be determined considering that primary production is generally maintained throughout summer and early fall due to frequent mixing episodes, in contrast with other regions where spring bloom represents the main food pulse for zooplankton. For these reasons, we do not provide estimates of spring bloom metrics for the Estuary. However, high-temporal-resolution information on the phytoplankton dynamics at the surface of the Estuary is available from the surface fluorescence sensor on the oceanographic Viking buoy located near Rimouski station and is presented in this document. To increase the accuracy of daily chl *a* estimates, data from the buoy sensor are calibrated against chl *a* concentrations measured in the water samples collected weekly at Rimouski station.

2.4 ANNUAL ANOMALY SCORECARDS

Normalized anomalies for the chemical and biological indices presented in scorecards were computed for the high-frequency monitoring station and oceanographic regions. These anomalies are calculated as the difference between the variable's average for the season or for the complete year and the variable's climatological mean (usually 1999–2020 for *in situ* metrics and 2003–2020 for remote sensing metrics); this number is then divided by the standard deviation over the climatological period.

Anomalies are presented as scorecards with positive anomalies depicted as shades of red, negatives as shades of blue, and anomalies within ± 0.5 SD as white (considered as normal conditions, i.e., similar to the climatology). A standard set of indices representing anomalies of nitrate inventories in the mid-layer (50–150 m), phytoplankton biomass and bloom dynamics, mesozooplankton biomass, and the abundance of dominant mesozooplankton species and groups (*C. finmarchicus, Pseudocalanus* spp., total copepods, and total non-copepods) are produced for each AZMP region (Casault et al. 2023; Maillet et al., 2022). To visualize Northwest Atlantic shelf-scale patterns of environmental variation, a zonal scorecard including observations from all AZMP regions is presented in DFO (2023).

Annual nutrient, phytoplankton, and zooplankton index anomalies are based on the mean annual concentration (mmol m^{-2} for nutrients, mg chl *a* m^{-2} for phytoplankton biomass) or density (cells L^{-1} for phytoplankton abundance, individuals m^{-2} for zooplankton abundance and g m^{-2} for zooplankton biomass) estimated at each high-frequency monitoring station and each Gulf region. These annual estimates are derived from general linear models (GLM) of the form

$\text{Log}_{10}(\textit{Density}) = \alpha + \beta_{\textit{YEAR}} + \delta_{\textit{MONTH}} + \varepsilon$ for the high-frequency monitoring stations and
$\text{Log}_{10}(\textit{Density}) = \alpha + \beta_{\textit{YEAR}} + \delta_{\text{STATION}} + \gamma_{\text{SEASON}} + \varepsilon$ for the regions,

where α is the intercept, and ε is the error. The GLM is applied to each region separately. For the high-frequency monitoring stations, β and δ are constants representing the categorical effects for year and month, respectively. For the regions, β, δ, and γ are the categorical effects of year, station, and season, respectively. We log-transformed concentrations and density values before computing anomalies to compensate for the skewed distribution of observations. We added one unit to *Density* terms for the abundance indices (phytoplankton and zooplankton counts) to include observations with values of zero. An estimate of the least-square means based on type III sums of squares is used as an estimate of annual average. Results of the GLM (significance of each factor and adjusted R squared of the regression) are presented in

Appendices 2 to 6. Four seasons (winter, early summer, late summer, and fall) are included in the GLM for estimating the annual average of surface nutrient inventories; three seasons are used to estimate the annual average of deeper nutrient inventories and phytoplankton indices (no data collection during winter); and two seasons (early summer and fall) are used to calculate annual estimates of zooplankton indices (samples analyzed via ZooImage are presented separately and their time series are based on seasonal arithmetic means).

3. OBSERVATIONS

3.1 PHYSICAL ENVIRONMENT

Stratification is one of the key physical parameters controlling primary production. For this reason, we present the upper water column stratification, calculated as the density difference between 50 m and the surface, at the high-frequency monitoring stations (Figure 5). The near-normal freshwater discharge into the Estuary during springtime (Galbraith et al. 2023) led to near-normal stratification in terms of seasonality and strength at Rimouski station. At Shediac Valley station, stratification was also close to normal with exceptions in June and August. In the Gulf, stratification was generally close to the climatology in March and above normal from August onwards (Figure 6).

3.2 DEEP OXYGEN

Oxygen saturation levels below 10% were found throughout fall in the bottom waters at Rimouski station in 2022 (Figure 7). This is the first time that such low saturation levels have persisted over several months. In the Gulf, hypoxic waters could be found from the Estuary to the deep waters south of Anticosti Island (Figure 8). In comparison, climatological oxygen saturation of waters at 200 m is above the hypoxic level everywhere in the Estuary and Gulf. The lowest levels of dissolved oxygen (below 15% saturation in recent years) are found in the deep waters at the head of the Laurentian Channel in the Estuary (Figure 8). In 2022, concentrations of dissolved oxygen at 200 m, 250 m and 300 m were again well below normal everywhere along the Laurentian Channel (Figure 8). Record-low saturation levels were observed at all depths at Rimouski station and in the Estuary, and in all regions at 200 m, particularly in Cabot Strait (Figure 9). The dissolved oxygen concentration annual average in the Estuary at 300 m was 36 µM in 2022, corresponding to ca. 12% saturation (Figure 9).

3.3 NUTRIENTS

Distributions of dissolved inorganic nutrients (nitrate, silicate, phosphate) strongly co-vary in space and time (Brickman and Petrie 2003). For this reason and because nitrogen availability controls phytoplankton growth in coastal waters of the Gulf, emphasis in this document is given to the variability in nitrate concentrations and inventories, even though the distributions of other nutrients are also briefly discussed. In this document, we use the term “nitrate” (NO_3 in figure labels) to refer to the sum of nitrate and nitrite ($NO_3^-+NO_2^-$).

3.3.1 High-frequency monitoring stations

The two high-frequency monitoring stations typically exhibit a biologically mediated reduction in surface nitrate inventories in spring/summer, a minimum during summer, and a subsequent

increase during fall/winter once water column mixing intensifies due to cooling processes and wind forcing (Figure 10 A, B). Surface nitrate inventories are typically two to three times higher at Rimouski station than at Shediac Valley station (Figure 10 A, B). In 2022, nitrate inventories in the surface layer were close to normal in March and well below normal afterwards setting new record lows for the average annual inventory at both stations (Figure 10 A, B). For Rimouski station, this is the second year in a row with historical minimums of the surface layer nitrate inventory. Nitrate inventories in the mid-layer (50–150 m) and bottom layer (50–84 m) of Rimouski and Shediac Valley stations, respectively, were also at record lows in 2022. The deep layer at Rimouski exhibited a similar pattern with below-normal nitrate inventory (Figure 10 scorecard). The vertical nitrate profiles at Rimouski show that nitrate was nearly depleted near 50 m throughout the year which is atypical (Figure 11).

3.3.2 Gulf regions

The spatial distribution of nitrate in the surface layer during winter 2022 was similar to the climatology with maximal concentrations in the Estuary and around Gaspé peninsula, but the inventories were below normal across the Gulf (Figure 12). The estimated nitrate drawdown during spring was generally close to normal, which could suggest near-normal phytoplankton spring bloom intensity (Figure 12). Surface layer nitrate inventory stayed below normal during the entire year, except for small positive anomalies in Cabot Strait and central Gulf during late summer (Figure 13, 14, 15). Nitrate inventory anomalies for the mid (50–150 m) and deep (150 m–bottom) layers indicated similar spatial patterns across the region (Figure 13, 14, 15). The Northwest and Northeast Gulf were mostly associated with negative nitrate anomaly, while positive anomalies were present near Cabot Strait and in the centre Gulf, extending further to the northeast in the bottom layer (Figure 13, 14, 15).

Similar to the high-frequency monitoring stations, annual averages of the surface layer nutrient inventory were strongly below normal in all Gulf regions and several record lows were set (Figure 16). Linear regression of the surface layer nitrate annual average by year suggests a significant ($p < 0.001$) decrease of ca. 20% in the Gulf over the past 20 years. The northern Gulf regions also showed negative anomalies of mid-layer nutrient annual inventories, while they were near-normal on the Magdalen Shallows and above normal in the Central Gulf/Cabot Strait region (Figure 17). In the deep layer, nutrient annual inventories mostly showed strong positive anomalies in all Gulf regions (Figure 18), contrasting with the negative anomaly of deep nitrate inventory at Rimouski station (Figure 10). Positive anomalies of deep nitrates have regularly been found in Central Gulf/Cabot Strait since 2012 and over the past four years in the northern regions (Figure 18).

The Redfield-Brzezinski C:Si:N:P ratio, which presumes equilibrium between phytoplankton composition and the deep-ocean nutrient inventory, is 106:15:16:1 (Brzezinski 1985; Redfield 1958). In the deep waters of the Gulf, the N:P ratio is lower than the target of 16 and ranges from 11.1 to 12.4 while the Si:N ratio tends to be higher than the target of 0.94, ranging between 1.2 and 1.8 (Figure 18). N:P (Si:N) ratio is highest (lowest) at the entrance of the Laurentian Chanel and decreases (increases) as water progresses up the deep channel from Cabot Strait to the Estuary (not shown). In 2022, the deep layer N:P ratios were below normal in all regions while Si:N ratios were above normal, including record low and record high in the Estuary/Northwest Gulf region, respectively. Interestingly, these patterns of lower (N:P) and higher (Si:N) than normal values have been consistent over the last six/seven years in the northern Gulf (Figure 18).

3.4 PHYTOPLANKTON

3.4.1 High-frequency monitoring stations

The seasonal cycles of chl *a* inventories are different at the two high-frequency monitoring stations. At Rimouski station, the inventory typically reaches a maximum during early summer and stays at a relatively high level until late summer/early fall. At Shediac station, the maximum is presumably reached (but outside of the station's seasonal coverage) in early spring before rapidly diminishing and staying stable during the remainder of the year (Figure 10). Following the spring bloom, chl *a* inventories are typically two to three times higher at Rimouski station than at Shediac Valley station (Figure 10 C, D). In 2022, a high chl *a* inventory was observed in late April at Rimouski station, suggesting an early spring bloom (Figure 10 C). There were successive pulses of chl *a* throughout the summer, preceded by small increases in the nitrate inventory, and the phytoplankton biomass stayed largely above the climatology from October onwards (Figure 10 A, C). Overall, the annual average of the chl *a* inventory was above normal at Rimouski station (Figure 10 scorecard). At Shediac Valley station, the chl *a* inventory was either below normal or near normal during the months when sampling occurred except in November when phytoplankton biomass was about 6 times higher than the climatology (Figure 10 D). The annual average inventory was below normal (Figure 10 scorecard).

The phytoplankton abundance at Rimouski station was mainly near normal in 2022. At the end of June, very high abundances of *Skeletonema costatum*, a common North Atlantic centric diatom, brought the total phytoplankton abundance to values between 5 and 8 times higher than the climatology (Figure 19 A). The proportion of diatoms was much higher than the climatology in April and December but the proportion of each main phytoplankton taxonomic group was similar to the climatology the rest of the year (Figure 19 B, C). The high proportion of diatoms in April supports the hypothesis of an early spring bloom in the Estuary. Overall, the annual average diatom abundance showed a positive anomaly while all other phytoplankton taxonomic indices were near or below normal (Figure 20). Mostly negative anomalies for dinoflagellates and positive anomalies of the diatom:dinoflagellate ratio have often been observed at Rimouski station since 2014 and 2016, respectively (Figure 20).

At Shediac Valley station, phytoplankton abundance was generally slightly below normal in 2022 (Figure 21A). Moreover, the proportion of small phytoplankton taxa (ciliates, flagellates, dinoflagellates) was much higher than normal between May and November, at the expense of diatoms. The taxonomic composition of the phytoplankton community was normal again in November and coincided with the above-normal total phytoplankton abundance (Figure 21). Consequently, annual abundance of diatoms showed a negative anomaly while that of smaller taxa showed positive anomalies. This continues a pattern observed since 2014 (Figure 20).

3.4.2 Gulf regions

In early and late summer 2022, chl *a* inventories (0–100 m) were mostly below or near normal across the Gulf (Figure 22). However, during fall, very high inventories were observed in most of the Gulf, especially in the Northwest Gulf and around the Gaspé peninsula (Figure 22). The annual phytoplankton biomass was slightly above normal in most regions of the Gulf owing to the occurrence of a strong fall bloom (Figure 23). The Northeast Gulf was the only exception with a slightly negative anomaly of annual phytoplankton biomass and a large fraction of this region showing negative anomalies of chl *a* during fall. The fall bloom that took place in most of the Gulf set new historical chl *a* maxima in the Estuary/Northwest Gulf and on the Magdalen Shallows and was the second highest of the time series in central Gulf/Cabot Strait (Figure 23). This is in agreement with the high chl *a* inventories observed at both high-frequency monitoring stations during fall (Figure 10 C, D). It is the fifth year in a row that a larger-than-normal fall

bloom is observed in the Estuary/Northwest Gulf. Removing the effect of the fall AZMP survey timing by selecting only field data collected within a two-week period (Oct 27–Nov 6), linear regressions suggest that the increase in phytoplankton biomass during fall is significant over the time series in the Estuary/Northwest Gulf and the central Gulf/Cabot Strait ($p < 0.001$). In these two regions, it corresponds to an average increase of fall phytoplankton biomass of roughly 125% and 60%, respectively, when comparing the beginning and the end of the time series.

Similar observations were made from ocean colour observations. During most of the year, chl *a* concentrations at the sea surface were close to or below normal. However, chl *a* concentrations were much higher than the climatology in October and November in all ocean colour polygons except the one located in the Northeast Gulf (Figure 24, 26). The western side of the Magdalen Shallows and the Northwest Gulf showed particularly strong positive anomalies in late October/early November (Figure 26). Chlorophyll *a* concentrations were also much higher than usual in mid-March in the polygons located in the northern Gulf, suggesting an early spring bloom timing in these locations. High surface chl *a* concentrations were also observed during January on the Magdalen Shallows suggesting that the phytoplankton community was still active during early winter (Figure 24). Overall, annual averages suggest that phytoplankton biomass at the surface was below or near normal except on the Magdalen Shallows where the small annual positive anomaly was attributable to the record high fall average (Figure 27).

The most striking feature of the 2022 spring bloom is its early occurrence—about a month earlier—in the northern regions of the Gulf (Figure 27). This early timing was associated with a longer duration in these two polygons but spring bloom magnitude and amplitude were smaller than normal in Northwest Gulf and relatively close to normal in Northeast Gulf. On the Magdalen Shallows, spring bloom was fairly normal for most metrics. In Cabot Strait, the Gaussian fit suggests that the bloom was slightly delayed, being also shorter than normal with near-normal amplitude (Figure 27). However, only few ocean colour observations were available during the spring bloom in this particular polygon (Appendix 7) and the spring bloom metrics should thus be interpreted with caution. Bloom fits for 2022 are available in the Appendix 7.

3.5 ZOOPLANKTON

3.5.1 High-frequency monitoring stations

In 2022, the zooplankton biomass at Rimouski station was largely below the climatology from May onwards, contrasting with observations at Shediac Valley station where zooplankton biomass was either close to or above normal (Figure 28). Copepod abundance, however, was mostly above normal at Rimouski station, with a higher-than-normal proportion of *Microcalanus* spp. and a lower-than-normal proportion of large *Calanus* species (Figure 29). At Shediac Valley station, copepod abundance was generally close to normal and the taxonomic composition of the copepod community was similar to the climatology with the exception of September when the total copepod abundance was higher than normal owing to the larger-than-normal abundance of *Temora longicornis* (Figure 30).

The abundance of *C. finmarchicus* was generally below normal at Rimouski station and mostly near normal at Shediac Valley station (Figure 31). The peak of CI-CIII copepodite stages was observed in May 2022 instead of June as in the climatology which suggests that *C. finmarchicus* phenology was earlier than usual at Rimouski station (Figure 31). Similarly, at Shediac Valley station, the end of CI-CIII peak was seen in June instead of July as in the climatology, also

suggesting an earlier phenology at that station (Figure 31). However, the absence of sampling in April at both stations prevents a complete description of the phenology pattern. There was a second pulse of early copepodite stages at Rimouski station in August and a large one at Shediac Valley station in November (Figure 31).

Similar to the biomass, the abundance of *C. hyperboreus* was below normal at Rimouski station and near normal at Shediac Valley station during the months when sampling occurred (Figure 32). The large proportion of CIV copepodite stage in May in comparison with the climatology (50% in 2022 versus 40% in the climatology for Rimouski station, and 40% in 2022 versus 20% in the climatology for Shediac Valley station) also suggests an earlier-than-normal development for this species at both stations (Figure 32). In contrast with the pattern of the large *Calanus* at Rimouski station, the abundance of *Pseudocalanus* spp. was generally above normal at this station and its phenology was similar to the climatology (Figure 33). The abundance of *Pseudocalanus* spp. was near normal at Shediac Valley station.

Changes in the timing of zooplankton development are further described using the detailed seasonal pattern of the relative abundance of copepodite stages of *C. finmarchicus* at Rimouski station from 1994 to 2022 (Figure 34). A scorecard showing the anomaly of the first day when the normalized proportion of CIV was higher than 0.35 and the day of the maximal normalized proportion of CIV (visually defining the end of early stage peaks CI–CIII) was also added to provide an objective tool to describe *C. finmarchicus* phenology. Overall, there is a trend towards an earlier population development, with anomalies for both indices being nearly always negative since 2012. This trend was reinforced by the two consecutive record lows of 2021 and 2022 for the first day index. From 2010 to 2014, there was a second distinct pulse of early stages in late summer and a similar pattern was also clearly seen in 2021 and 2022 (Figure 34).

3.5.2 Gulf regions

Zooplankton biomass is usually concentrated in the deep channels of the Estuary and Gulf, where higher abundances of *C. hyperboreus* typically occur; consequently zooplankton biomass tends to be lower on coastal portions of sections and on the Magdalen Shallows. Although this general pattern could be seen in 2022 during fall, high zooplankton biomass was observed on the Magdalen Shallows during early summer (Figure 35). This is the only region that showed above-normal zooplankton biomass for both seasons in 2022; zooplankton biomass was instead below normal in the other regions in both seasons and record lows were set in the Estuary/Northwest Gulf and central Gulf/Cabot Strait regions in early summer (Figure 35). The same observations were made for the distribution of *C. hyperboreus* abundance in 2022 for which record lows were also set in the same regions during early summer (Figure 36).

The abundance of *C. Finmarchicus* was close to normal in all regions during early summer 2022 (Figure 37). The highest abundances were found on the Magdalen Shallows and in Cabot Strait during fall when abundances were above normal. In the Northeast Gulf, *C. finmarchicus* abundance was strongly below normal during fall (Figure 37). The pattern of abundance for *Pseudocalanus* spp. was highly variable across seasons and regions with the highest abundances observed on the western side of the Cabot Strait section during both seasons (Figure 38).

The 2022 seasonal averages for zooplankton indices from the mackerel egg survey on the Magdalen Shallows and from the northern Gulf late-summer survey (ZooImage) generally agree with these findings (Figure 39). The abundance of large calanoids was near normal on the

Magdalen Shallows during early summer and it reached the lowest level of the time series in the northern Gulf during late summer due to record-low abundances of *C. hyperboreus*. Small calanoids were close to normal during both surveys (Figure 39).

3.5.3 Scorecards

The time series of annual zooplankton biomass anomalies highlight recent major changes in the community, with mostly near-normal to negative anomalies across the Gulf since 2009 (Figure 40). Over the time series, there is a significant decrease of zooplankton biomass ($p < 0.05$) in all regions except the Northeast Gulf. Between the beginning and the end of the time series, this represents a biomass loss of about 25% in the northwestern Gulf and on the Magdalen Shallows, and about 45% in the central Gulf/Cabot Strait. In 2022, zooplankton biomass anomalies were strongly negative in most of the Gulf regions, except on the Magdalen Shallows (including Shediac Valley station where it was a record high). The lowest biomass for the entire time series was recorded at Rimouski station and in the Estuary/Northwest Gulf region in 2022. The central Gulf/Cabot Strait and Northeast Gulf regions also indicated near record low anomalies respectively (Figure 40). Zooplankton biomass is strongly influenced by the abundance of large *Calanus* spp. While *C. finmarchicus* annual abundances were near-normal in most regions (Figure 41), *C. hyperboreus* mostly showed strong negative anomalies, except on the Magdalen Shallows, including unprecedented low abundances in the Estuary/Northwest Gulf and second-lowest abundances of the time series at Rimouski station and in central Gulf/Cabot Strait (Figure 42). This represents the second year of large and widespread negative anomalies for *C. hyperboreus*. As a consequence, the large calanoid index was either normal or below normal at all locations except Shediac Valley station where it was slightly positive. Near-normal to negative anomalies for this index have been observed regularly since 2010 (Figure 42).

The general decrease in zooplankton biomass over time is consistent with the increase in the abundance of *Pseudocalanus* spp., non-copepods, small calanoids, cyclopoids, and the total copepod abundance, for which positive anomalies have been regularly observed since around 2014 (Figure 41, 42; see Appendix 1 for a detailed list of species included in each of these indices). These groups presented relatively similar anomaly patterns in 2022. Their anomalies were generally positive at high-frequency monitoring stations and in the Estuary/Northwest Gulf, near-normal on the Magdalen Shallows, and they were negative in the Northeast Gulf (Figure 41). In the latter region, all zooplankton indices presented negative anomalies except for warm and cold-water copepods (Figure 40–42; see Appendix 1 for a detailed list of species included in these indices). At Rimouski station, *Pseudocalanus* spp., non-copepods and small calanoids were at record high levels and the total abundance of copepods was the second highest on record (Figure 41).

The abundance of warm-water copepods has also increased since 2011. This was observed again in 2022, with positive anomalies over most of the Gulf except for Shediac Valley station. In central Gulf/Cabot Strait region, it was the highest abundance of the time series. *Centropages* spp. and *Metridia lucens* were both responsible for these high abundances (not shown). Interestingly, cold-water copepods have also regularly shown positive anomalies in most regions over the past recent years, including 2022 (Figure 42). It is mostly *M. longa* abundance, not *C. glacialis*, that accounts for these positive anomalies (not shown).

In general, annual anomalies were coherent among the high-frequency monitoring stations and their associated Gulf region (Figure 40–42). This suggests a high reliability of our annual estimates throughout the Gulf even though data collection is limited to early summer and fall surveys for zooplankton indices.

4. DISCUSSION

4.1 ENVIRONMENTAL CONDITIONS

The timing of the onset and extent of water column stratification plays a role in defining spring bloom phenology, phytoplankton production, species succession, and trophic interactions over the complete growth season (Levasseur et al. 1984). In 2022, the timing and strength of upper water column stratification were similar to the climatology at both high-frequency monitoring stations, but the strength of stratification during late summer and fall was much higher than normal across the Gulf, perhaps due to the strong warming of the upper water column during summer (Galbraith et al. 2023). In addition to the effect of water column stratification on phytoplankton dynamics, thermal properties of the surface, intermediate, and deep water masses play a role in defining zooplankton dynamics (Plourde et al. 2002). Galbraith et al. (2023) reported on the physical conditions that prevailed in the Gulf during 2022, showing warmer-than-normal conditions for most indices which likely had direct or indirect effects on the chemical and biological conditions observed in the Gulf in 2022.

In the Gulf, a dissolved oxygen value of 100 µM corresponds to approximately 30% saturation, below which the water is considered to be hypoxic and can reduce the survival of some species such as Atlantic cod (Plante et al. 1998). The combination of AZMP data with the time series published by Gilbert et al. (2005) indicates that the deep waters of the Estuary have consistently been hypoxic since 1984. Changes in dissolved oxygen of the deep waters entering the Gulf at the continental shelf are related to the varying proportions of Labrador Current water (cold/fresh, high dissolved oxygen levels) and North Atlantic Central Water (NACW; warm/salty, low dissolved oxygen levels), which together form the source of Gulf deep waters (McLellan 1957, Lauzier and Trites 1958, Gilbert et al. 2005). In recent years, the contribution of NACW to the deep Gulf waters has increased (Gilbert et al. 2005, Galbraith et al. 2023) and is now nearly 100% (Jutras et al. 2023). Given the inherent properties of the Gulf source waters (North Atlantic Central Water vs. Labrador Current water; Gilbert et al. 2005), changes in their mixing ratio at Cabot Strait imply that a decrease of 1.46 µM might be expected for each 0.1 °C temperature increase. However, today's deep oxygen concentrations at Cabot Strait represent a decline of ca. 70 µM compared with their concentrations in the early 1970s (ca. 190 µM; Blais et al. 2021), for a 2.0 °C increase in temperature over the same period (Figure 48 in Galbraith et al. 2023). Considering that these deep waters travel from the mouth of the Laurentian Channel to the Estuary in roughly three to four years (Gilbert 2004), decreasing in dissolved oxygen content in response to *in situ* respiration and oxidation of organic material by microbes as they progress to the channel heads, the record low saturation level measured at Cabot Strait at 200 m in 2022 suggests that the hypoxic conditions of the Estuary are likely to worsen in a near future. Moreover, the inflow of warmer waters to the Estuary is expected to exacerbate the hypoxic conditions since these waters are typically poor in dissolved oxygen (McLellan 1957, Lauzier and Trites 1958, Gilbert et al. 2005). Deep water temperature has increased by 2.03 °C at 300 m between the early 1970s and 2022 (Figure 48 in Galbraith et al. 2023) while oxygen concentration has decreased from ca. 105 µM (Blais et al. 2021) to 34.5 µM over the same period in the Estuary. This is over twice as much as what could be expected from temperature only according to the mixing ratio of source waters. Thus, warming of bottom water and reduced initial oxygen saturation levels through changes in the mixing ratio of source waters are not the only factors contributing to the decrease in oxygen concentrations in the Gulf. Other factors that can cause variability in oxygen concentration of deep waters include interannual changes in the vertical flux of organic matter, modification to microbial metabolic processes such as increased respiration in warmer waters, and a reduction of bottom waters ventilation via increased stratification.

Winter mixing is a critical process for bringing nutrient-rich deep water to the surface. In the Gulf, winter convection is partly driven by buoyancy loss of surface waters attributable to cooling and reduced freshwater runoff, brine rejection associated with sea ice formation, and wind-driven mixing prior to ice formation (Galbraith 2006). Warmer-than-normal surface waters throughout the winter, minimal sea ice formation, and reduced volume of winter mixed-layer can be associated with low winter convection and may reduce the amount of nutrients available for spring primary production. The CIL represents the winter surface mixed layer that has been insulated from the atmosphere by near-surface stratification and whose nutrient inventory will supply primary producers during the growth season through vertical mixing. Negative nutrient anomalies in the surface layer have been regularly encountered in the Gulf since 2010, a period over which several temperature and ice-cover indices have shown clear warming of the Gulf (Galbraith et al. 2023), and they represent a significant decrease in the nitrate content of the surface layer over the time series. Thus, low winter convection and strengthening of the stratification later during the year in association with global warming could have limited the nutrient flux to the surface layer in recent years. However, in 2022, the sea ice volume and the CIL winter mixed-layer volume suggest a relatively normal, albeit slightly smaller, winter convection. The freshwater inflow, which accounts for up to 35% of nutrient input to the Estuary (Lavoie et al. 2021), was also near-normal. The stratification index also suggested near-normal conditions during wintertime but stronger-than-normal stratification from August onwards. Consequently, the mean annual surface nutrient inventories that showed strong negative anomalies in most regions in 2022, including nitrate record lows in the Northeast Gulf and on the Magdalen Shallows, have possibly been driven to a certain extent by biological factors during winter and emphasized by stratification later during summer. Delay in sea ice formation (Galbraith et al. 2023) may have maintained phytoplankton production over a longer period of time, as suggested by high chl *a* concentration in January 2022 on the Magdalen Shallows (remote sensing), which could have led to a higher nutrient consumption from the surface layer.

Positive anomalies in deep-water (300 m) nitrates have been regularly observed since 2012 in the central Gulf and Cabot Strait in association with a water mass composition that has a greater contribution of NACW than Labrador Shelf water (Gilbert et al. 2005, Galbraith et al. 2023, Jutras et al. 2023). Moreover, reduction of exchanges between the upper and the cold intermediate layer associated with a generally increased stratification might further increase the deep nutrient pool. A positive, although small, deep nitrate anomaly was also observed in the Estuary for a third consecutive year. This suggests that waters with a larger proportion of NACW have reached the Estuary, as indicated by increased bottom water temperature in the Estuary (Galbraith et al. 2023). The year 2022 marks the sixth consecutive year of rather strong nutrient ratio anomalies in the deep waters of the Gulf (negative anomalies for N:P and positive anomalies for Si:N). While different nutrient ratios of the source deep water masses along with the change in their mixing proportion at Cabot Strait may partly explain these observations, microbial processes involved in N cycling could also be at play, such as decreased nitrification or increased denitrification (typically occurring in hypoxic to anoxic conditions). The change in nutrient ratio (further nitrate depletion) as water progresses from Cabot Strait to the Estuary also supports this hypothesis. Nitrification was recently identified as a key process in the accurate modelling of nitrogen fluxes in the Gulf (Lavoie et al. 2021). Moreover, the routine measurement of NH_4 concentrations has recently been added to AZMP sampling in the Gulf and will eventually be helpful in verifying the latter hypothesis.

4.2 PHYTOPLANKTON

Except at Rimouski station, where sampling regularly covers the spring bloom period, phytoplankton production during the spring bloom must be inferred either from indirect indices, such as the difference in the nutrient inventory of the surface mixed layer between the winter and the early summer surveys, or from satellite observations. The estimate of nutrient drawdown during spring suggests that bloom production in 2022 was generally near, or slightly below normal, in agreement with satellite observations. The intensity (magnitude) of the spring bloom is a combined index of its duration and amplitude (maximum chl *a* concentration reached). While duration tends to be negatively correlated with the start of the spring bloom, which depends on the onset of the water column stratification, the amplitude is mostly determined by the availability of nitrogen. Thus, low nitrate availability in March likely played a key role in preventing the formation of a strong spring bloom. Interestingly, field observations at Rimouski station in April (high proportion of diatoms and high biomass) along with satellite observations indicate that the bloom timing in the Estuary and the northern Gulf was the earliest of the time series. However, there are no indications of change in the timing of the water column stratification, nor change in the timing of last occurrence of sea ice in 2022 (Galbraith et al. 2023).

No distinct trends in spring bloom metrics can be identified over the time series. Under global warming scenarios, an earlier onset of stratification is expected to trigger an early spring bloom. However, the expected concomitant large freshet (due to an increase in precipitation) may prevent the accumulation of phytoplankton biomass in the water column in regions under the influence of freshwater, which may instead delay detection of the bloom start in these regions (Zakardjian et al. 2000). Densities of overwintering copepods, which were generally low in the Gulf for 2016–2018 and 2021–2022 (low annual biomass), also impact spring bloom intensity and other bloom metrics through grazing (Sommer and Lengfellner 2008). Along with winter convection and nutrient availability, they largely influence bloom metrics and likely account for the large interannual variability seen in these metrics.

For all seasons except spring, ocean colour data is complemented by field data. These two data sources have regularly offered different conclusions in terms of anomalies in the seasonal phytoplankton biomass. Over the past four years, ocean colour data often suggested below-normal chl *a* concentrations in the thin surface layer during fall while field data have regularly suggested positive phytoplankton biomass anomalies in recent years. Divergences, when occurring, can be explained by several factors including the vertical structure of phytoplankton in the water column, the way seasonal anomalies are computed (three-month periods in each ocean-colour polygon versus a few days in each Gulf region for *in situ* sampling—timing of sampling of each dedicated AZMP surveys is indicated in Figure 24), field sampling timing in relation with phytoplankton phenology, and cloud cover. However, surface chl *a* concentrations estimated from remote sensing were quite consistent with *in situ* observations in 2022 and these two sources of observations both suggested that phytoplankton biomass was above normal in most regions during fall 2022, with possible implications for higher trophic levels. An increased occurrence of fall storms, as frequently observed in recent years (Galbraith et al. 2023), promotes ideal growth conditions for phytoplankton, especially if combined with a reduction of grazing pressure due to the diminution of grazer abundances. This was likely the case in December at Rimouski station when chl *a* concentration was about 6-fold the climatology and zooplankton abundance was nearly 3-fold lower than the climatology.

4.3 ZOOPLANKTON

Zooplankton biomass has generally been below normal in recent years, with several record-low levels in 2016–2017 and in 2021–2022, resulting in a significant decreasing trend over time in the Gulf. Lower biomass is typically associated with a decrease in the abundance of large zooplankton species. The mean weight of large calanoids (e.g., *C. hyperboreus*: 3.5 mg per adult female) is between one and two orders of magnitude greater than that of small calanoids (e.g., *Pseudocalanus* spp.: 0.02 mg per adult female) (Conover and Huntley 1991, Plourde et al. 2003). Thus, low abundance of large calanoid has a greater impact on zooplankton biomass than is generally offset by high *Pseudocalanus* spp. Abundances for instance, as has been regularly observed over recent years. The increase in small calanoids seems to be coupled with an increase in non-copepod abundance, mostly larvae of benthic organisms. Suitability of environmental conditions, competition for food, the availability of large versus small phytoplankton cells, and/or differential predation pressure might favour the dominance of either one of these communities, i.e., one dominated by large calanoids versus one dominated by a combination of small calanoids and non-copepods (Hall et al. 1976; Daewel et al. 2014), with potential implications for the pelagic food web and pelago–benthic coupling.

Life cycle strategies vary among large copepod species, and so do the environmental drivers influencing their phenology. For instance, interannual variations in the abundance of *C. hyperboreus* and its overwintering stage structure is known to be mostly influenced by spring conditions, including timing of sea ice retreat and temperature (Plourde et al. 2003, Lehoux et al. 2021), while fall environmental conditions also influence the phenology of *C. finmarchicus*. Moreover, the timing of reproduction of each taxon relative to the freshet—considering its influence on water mass circulation and transport in regions that are under the influence of freshwater (Runge et al. 1999)—can largely influence zooplankton spatial distribution and result in dissimilarities in the spatial pattern of different species.

In 2022, the strong negative anomalies of zooplankton biomass and *C. hyperboreus* abundances in all regions where deep channels are a dominant bathymetric feature likely resulted from environmental conditions. The early phenology of the spring bloom possibly resulted in the early development of the large *Calanus* species, as seen at the high-frequency monitoring stations. The peak of *C. hyperboreus* early copepodite stages likely occurred in April (no data in April) in Rimouski, coinciding with the maximal spring freshet (Galbraith et al. 2023) and increasing their export to the Magdalen Shallows. The high proportion *C. hyperboreus* diapausing CIV in early summer most likely favoured their retention in this region (Brennan et al. 2019). Even though earlier than usual, it seems that the timing of the peak of *C. finmarchicus* early copepodite stages (May) at Rimouski station did not result in a massive export to the Magdalen Shallows as it did for *C. hyperboreus*. Under favourable conditions, and quite often since 2010, *C. finmarchicus* sometimes produces a second cohort that typically occurs in late summer. In 2022, this occurred at Rimouski station in August and at Shediac Valley in November, clearly coinciding with the fall bloom.

The Northeast Gulf and the central Gulf/Cabot Strait regions are less influenced by freshwater; environmental conditions modifying the zooplankton community in these regions might instead include CIL conditions, the volume and temperature of cold and saline Labrador Shelf water that flows into Northeast Gulf through the Strait of Belle Isle or the mixing ratio of source waters that enters the deep Laurentian Chanel through Cabot Strait. Differences in these environmental drivers might explain why these two regions often show distinct anomaly patterns for the zooplankton assemblage compared to what is observed elsewhere, like the contrasted abundance pattern that was seen for *Pseudocalanus* spp. in 2022.

4.4 PERSPECTIVES

Questions that may arise from these indications of changes in nutrient inventories, phytoplankton biomass, and zooplankton community composition and size structure are related to the underlying explanatory drivers and how they are expected to change in the near future. While the roles of predation and of changing predator stocks in the observed trends have yet to be determined, it is possible to get some insight regarding the effect of environmental variables using a simple correlation matrix (Figure 43). Among other things, this matrix shows that a cold CIL—which would imply higher winter convection and a later onset of stratification—promotes a late bloom start and high nitrate inventories. Interestingly, high nitrate inventories in the surface layer are well correlated with higher zooplankton biomass. The latter is strongly positively correlated to a community dominated by large copepods and inversely correlated with small calanoids and non-copepods as would be expected. While nutrients likely have little direct effect on the zooplankton community composition, thermal properties of the water column and spring bloom—especially its timing—could be major drivers of zooplankton assemblage. Indeed, it seems that a cold CIL favours high zooplankton biomass (dry weight; negative correlation) while a cold deep layer reduces the abundance of non-copepods (positive correlation). Phytoplankton community composition and changes in species succession may also be important drivers for the zooplankton assemblage, but they were not included in this correlation matrix since information is only available at the high-frequency monitoring stations. These environmental drivers may also trigger changes in the developmental timing of zooplankton taxa (not illustrated on the figure), such as the earlier development of *C. finmarchicus* at Rimouski station in recent years, especially in 2022. Overall, these preliminary analyses highlight the importance of bottom-up controls in shaping zooplankton communities, although the relative importance of these processes is not yet well understood.

5. SUMMARY

This document reports on the chemical and biological (plankton) conditions in the Gulf of St. Lawrence observed in 2022 in the context of warmer-than-normal conditions prevailing since 2010.

- Concentrations of dissolved oxygen at 200 m, 250 m, and 300 m reached record-low levels at Rimouski station and in the Estuary. Lowest saturation levels of the time series were also recorded at 200 m in all regions but the record low was particularly striking at Cabot Strait for a second year in a row. Average annual saturation levels at 300 m in the Estuary and at Rimouski station are now 12% and 11%, respectively.
- Nutrient inventories were strongly below normal in the surface layer of the Gulf, and above normal in the deep layer. Positive deep nitrate anomalies have been frequently observed since 2012 in Cabot Strait and the central Gulf associated with the change in the mixing ratio of source waters entering the Gulf through Cabot Strait. Since 2017, the positive anomalies of deep nutrient content are associated with negative anomalies of the N:P ratio and positive anomalies of the Si:N ratio.
- Except in the Northeast Gulf, annual averages of *in situ* chl *a* inventory in the other regions of the Gulf were slightly above normal, due to the occurrence of strong fall blooms.
- Ocean colour data showed near-normal annual surface chl *a* concentrations and indicated that spring phytoplankton biomass was slightly lower than normal across the Gulf but strongly above normal during fall in all regions but the Northeast Gulf.
- Spring bloom metrics indicated that the timing of the spring bloom was the earliest of the time series in the northern Gulf, but relatively close to normal in the southern regions. Spring bloom amplitude and magnitude suggested a slightly weaker to near-normal spring bloom in all regions.
- Diatom annual average abundance was at record high at Rimouski station in 2022. At Shediac Valley station, there is instead a general decline in the abundance of diatoms since 2010, and 2022 was a continuation of this pattern.
- Zooplankton biomass reached the lowest level on record in the Estuary/Northwest Gulf region, and second lowest in the central Gulf/Cabot Strait region. In parallel, very low abundances of *C. hyperboreus* were generally observed in the Gulf, but especially in the Estuary/Northwest Gulf where record-low abundances were observed. The Magdalen Shallows region is the only exception to this general pattern with positive anomalies for these two indices in 2022.
- The phenology of large *Calanus* at the high-frequency station was a few weeks earlier than usual and the earliest of the time series at Rimouski station for *C. finmarchicus*.
- The community size-structure shift towards a higher proportion of small copepods continued in 2022 with several positive anomalies for *Pseudocalanus* spp., small calanoids, cyclopoids and non-copepods, especially in the regions under the influence of freshwater (i.e., Estuary/Northwest Gulf, Magdalen Shallows, and the high-frequency monitoring stations).
- The abundance of warm-water copepods was above normal across the Gulf in 2022 and continuing the trend observed since 2010. Record-high levels of warm-water copepods were observed in the central Gulf/Cabot Strait.

ACKNOWLEDGEMENTS

The data used in this report would not be available without the amazing work of the AZMP team (Félix St-Pierre, David Leblanc, Caroline Lafleur, Anthony Ouellet, Nicolas Coulombe, Sylvain Dubé, Guillaume Mercier, Myranda Blouin, Michel Rousseau, Véronique Desborbes, Marie-Noëlle Bourassa and Hélèna Talbot) in organizing and carrying out AZMP surveys, analyzing samples, and ensuring quality control of the data. We thank Jean-Yves Couture, Marie-France Beaulieu, Caroline Lebel and Christian Turcotte for preparation and standardization of the phytoplankton and zooplankton data; Jeff Spry, Kevin Pauley, Jay Bugden and Lindsay Beazley for providing data from Shediac Valley station; and Emmanuel Devred and Stephanie Clay for their large contribution and support in providing ocean colour data. We are grateful to Charles Tilsney and Benoît Casault for their critical reviews.

REFERENCES

Blais, M., Galbraith, P.S., Plourde, S., Devine, L. and Lehoux, C. 2021. Chemical and Biological Oceanographic Conditions in the Estuary and Gulf of St. Lawrence during 2019. DFO Can. Sci. Advis. Sec. Res. Doc. 2021/002. iv + 66 p.

Blais, M., Galbraith, P.S., Plourde, S., Devine, L. and Lehoux, C. 2023. Chemical and Biological Oceanographic Conditions in the Estuary and Gulf of St. Lawrence during 2021. DFO Can. Sci. Advis. Sec. Res. Doc. 2023/045. iv + 74 p.

Brennan, C.E., Maps, F., Gentleman, W.C., Plourde, S., Lavoie, D., Chassé, J., Lehoux, C., Krumhansl, K.A., and Johnson, C.L. 2019. How transport shapes copepod distributions in relation to whale feeding habitat : Demonstration of a new modelling framework. Prog. Oceanogr. 171: 1–21. Elsevier. doi:10.1016/j.pocean.2018.12.005.

Brickman, D., and Petrie, B. 2003. Nitrate, silicate and phosphate atlas for the Gulf of St. Lawrence. Can. Tech. Rep. Hydrogr. Ocean Sci. 231: xi + 152 pp.

Brzezinski, M. A. 1985. The Si:C:N ratio of marine diatoms: interspecific variability and the effect of some environmental variables. J. Phycol. 21: 347-357.

Casault, B., Johnson, C., Devred, E., Head, E. and Beazley, L. 2023. Optical, Chemical, and Biological Oceanographic Conditions on the Scotian Shelf and in the eastern Gulf of Maine during 2021. DFO Can. Sci. Advis. Sec. Res. Doc. 2023/016. v + 74 p.

Clay, S., Layton, C., and Devred, E. 2021. BIO-RSG/PhytoFit: First release (Version v1.0.0). Zenodo. https://doi.org/10.5281/zenodo.4770754

Conover, R. J., and Huntley, M. 1991. Copepods in ice-covered seas - Distribution, adaptations to seasonally limited food, metabolism, growth patterns and life cycle strategies in polar seas. J. Mar. Syst. 2: 1–41.

Daewel, U., Hjøllo, S.S., Huret, M., Ji, R., Maar, M., Niiranen, S., Travers-Trolet, M., Peck, M.A., and van de Wolfshaar, K. E. 2014. Predation control of zooplankton dynamics: a review of observations and models. ICES J. Mar. Sci. 71(2): 254–271.

DFO. 2023. Oceanographic conditions in the Atlantic zone in 2022. DFO Can. Sci. Advis. Sec. Sci. Advis. Rep. 2023/019. 34 p.

Galbraith, P. S. 2006. Winter water masses in the Gulf of St. Lawrence. J. Geophys. Res. 111, C06022, doi: 10.1029/2005JC003159.

Galbraith, P.S., Chassé, J., Shaw, J.-L., Dumas, J., Lefaivre, D., and Lafleur, C. 2023. Physical oceanographic conditions in the Gulf of St. Lawrence during 2022. Can, Tech. Rep. Hydrogr. Ocean Sci. 354: v + 88 p.

Gilbert, D. 2004. Propagation of temperature signals from the northwest Atlantic continental shelf edge into the Laurentian Channel. ICES CM, 2004/N: 7, 12 pp.

Gilbert, D., Sundby, B., Gobeil, C., Mucci, A., and Tremblay, G.-H. 2005. A seventy-two-year record of diminishing deep-water oxygen in the St. Lawrence estuary: The Northwest Atlantic connection. Limnol. Oceanogr., 50(5): 1654–1666.

Grosjean, P., Denis K., and Wacquet G. 2018. ZooImage: Analysis of numerical plankton images. R package version 5.5.2. https://CRAN.R-project.org/package=zooimage

Hall, D.J., Threlkeld, S.T., Burns, C.W., and Crowley, P.H. 1976. The size-efficiency hypothesis and the size structure of zooplankton communities. Annu. Rev. Ecol. Evol. Syst. 7: 177–208.

Jutras, M., Mucci, A., Chaillou, G., Nesbitt, W.A., and Wallace D.W.R. 2023. Temporal and spatial evolution of bottom-water hypoxia in the St. Lawrence estuarine system. Biogeosciences. 20: 839-849.

Laliberté, J., Larouche, P., Devred, E., and Craig, S. 2018. Chlorophyll-a concentration retrieval in the optically complex waters of the St. Lawrence Estuary and Gulf using principal component analysis. Remote Sens. 10, 265, doi: 10.3390/rs10020265.

Lavoie, D., Lambert, N., Starr, M., Chassé, J., Riche, O., Le Clainche, Y., Azetsu-Scott, K., Béjaoui, B., Christian, J.R., and Gilbert, D. 2021 The Gulf of St. Lawrence biogeochemical model: A modelling tool for Fisheries and Ocean management. Front. Mar. Sci. 8:732269, doi: 10.3389/fmars.2021.732269

Lauzier, L.M., and Trites, R.W. 1958. The deep waters of the Laurentian Channel. J. Fish. Res. Board Can. 15: 1247–1257.

Lehoux, C., Plourde, S., Chamberland, J.-M., and Benoît, H. 2021. Linking interannual variations of capelin abundance indices in the Gulf of St. Lawrence to environmental proxies of bottom-up regulation of cohort strength. DFO Can. Sci. Advis. Sec. Res. Doc. 2021/068. iv + 51 p.

Levasseur, M., Therriault, J.-C., and Legendre, L. 1984. Hierarchical control of phytoplankton succession by physical factors. Mar. Ecol. Prog. Ser. 19: 211–222.

Maillet, G., Bélanger, D., Doyle, G., Robar, A., Rastin, S., Ramsay, D., and Pepin, P. 2022. Optical, Chemical, and Biological Oceanographic Conditions on the Newfoundland and Labrador Shelf during 2018. DFO Can. Sci. Advis. Sec. Res. Doc. 2022/075

McLellan, H.J. 1957. On the distinctness and origin of the slope water off the Scotian Shelf and its easterly flow south of the Grand Banks. J. Fish. Res. Board Can. 14: 213–239.

Mitchell, M. R., Harrison, G., Pauley, K., Gagné, A., Maillet, G., and Strain, P. 2002. Atlantic Zonal Monitoring Program sampling protocol. Can. Tech. Rep. Hydrogr. Ocean Sci. 223: iv + 23 pp.

Plante, S., Chabot, D., and Dutil, J.-D. 1998. Hypoxia tolerance in Atlantic cod. J. Fish Biol. 53: 1342–1356.

Plourde, S., Dodson, J. J., Runge, J. A., and Therriault, J.-C. 2002. Spatial and temporal variations in copepod community structure in the lower St. Lawrence Estuary, Canada. Mar. Ecol. Prog. Ser. 230: 221–224.

Plourde, S., Joly, P., Runge, J.A., Dodson, J., and Zakardjian B. 2003. Life cycle of *Calanus hyperboreus* in the lower St. Lawrence Estuary and its relationship to local environmental conditions. Mar. Ecol. Prog. Ser. 255: 219–233.

Plourde, S., Maps, F., and Joly, P. 2009. Mortality and survival in early stages control recruitment in *Calanus finmarchicus*. J. Plankton Res. 31(4): 371–388.

Plourde, S., Lehoux, C., Johnson, C. L., Perrin, G., and Lesage, V. 2019. North Atlantic right whale (*Eubalaena glacialis*) and its food: (I) a spatial climatology of *Calanus* biomass and potential foraging habitats in Canadian waters. J. Plankton Res. 41(5): 667–685.

Redfield A. C. 1958. The biological control of chemical factors in the environment. Am. Sci. 46, 205–221.

Runge, J. A., Castonguay, M., de Lafontaine, Y., Ringuette, M., and Beaulieu, J. L. 1999. Covariation of climate, zooplankton biomass and mackerel recruitment in the southern Gulf of St. Lawrence. Fish. Oceanogr. 8(2): 139–149.

Sommer, U., and Lengfellner, K. 2008. Climate change and the timing, magnitude, and composition of the phytoplankton spring bloom. Global Change Biol. 14: 1199–1208.

Therriault, J.-C., Petrie, B., Pépin, P., Gagnon, J., Gregory, D., Helbig, J., Herman, A., Lefaivre, D., Mitchell, M., Pelchat, B., Runge, J., and Sameoto, D. 1998. Proposal for a Northwest Atlantic zonal monitoring program. Can. Tech. Rep. Hydrogr. Ocean Sci. 194: vii + 57 pp.

Xiong, X., Angal, A., Chang, T., Chiang, K., Lei, N., Li, Y., Sun, J., Twedt, K., and Wu, A. 2020. MODIS and VIIRS calibration and characterization in support of producing long-term high-quality data products. Remote Sens. 12:3167; doi:10.3390/rs12193167

Zakardjian, B.A., Gratton, Y., Vézina, A.F. 2000. Late spring phytoplankton bloom in the Lower St. Lawrence Estuary: the flushing hypothesis revisited. Mar. Ecol. Prog. Ser. 192: 31–48

Zhai, L., Platt, T., Tang, C., Sathyendranath, S., and Hernández Walls, R. 2011. Phytoplankton phenology on the Scotian Shelf. ICES J. Mar. Sci. 68: 781–791, doi:10.1093/icesjms/fsq175.

TABLES

Table 1. List of oceanographic surveys with dates and sampling activities for each Gulf region/subregion. While numbers of CTD/bottle are indicated for each subregion, numbers of nets are only indicated for main regions (see region vs. subregion in Figure 1).

High Frequency monitoring stations

Dates (2022)	Vessel	Station	CTD/Bottle	Net
Mar. 4–Dec. 7	*Beluga II* (+ others)	Rimouski	24	21
Mar. 10–Nov. 6	Multiple	Shediac Valley	9	7

Surveys

Survey	Dates (2022)	Vessel	Region/subregion	CTD/Bottle	Net
Winter	Mar. 4–1	GC-945 Helicopter	Estuary	5	0
			Northwest Gulf	9	
			Northeast Gulf	22	0
			Central Gulf	9	0
			Cabot Strait	7	
			Magdalen Shallows	32	0
			Total	84	0
Early summer	May 26–Jun. 26	Teleost	Estuary	16	18
			Northwest Gulf	12	
			Northeast Gulf	12	7
			Central Gulf	17	11
			Cabot Strait	5	
			Magdalen Shallows	95	63
			Total	157	99
Late summer	Aug. 12–29 Sep.	Teleost	Estuary	12	17
			Northwest Gulf	6	
			Northeast Gulf	6	23
			Central Gulf	16	17
			Cabot Strait	3	
			Magdalen Shallows	61	1
			Total	104	58
Fall	Oct. 25–Nov. 8	Coriolis II	Estuary	14	18
			Northwest Gulf	15	
			Northeast Gulf	16	7
			Central Gulf	12	9
			Cabot Strait	5	
			Magdalen Shallows	18	12
			Total	80	46

FIGURES

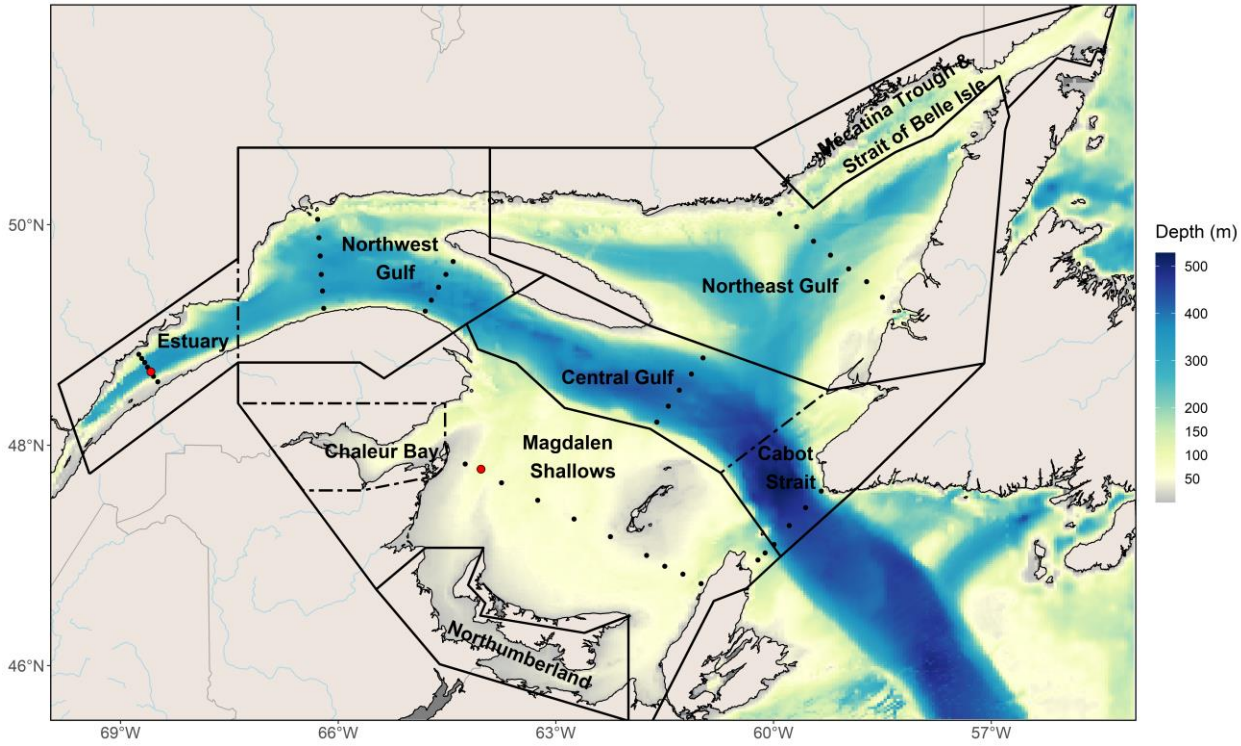

Figure 1. Bathymetric map of the Estuary and Gulf of St. Lawrence showing core AZMP sampling stations on the different sections (black dots) and high-frequency Rimouski and Shediac Valley stations (red circles). Dashed lines indicate region subdivisions. Water depth is shown by the colour axis.

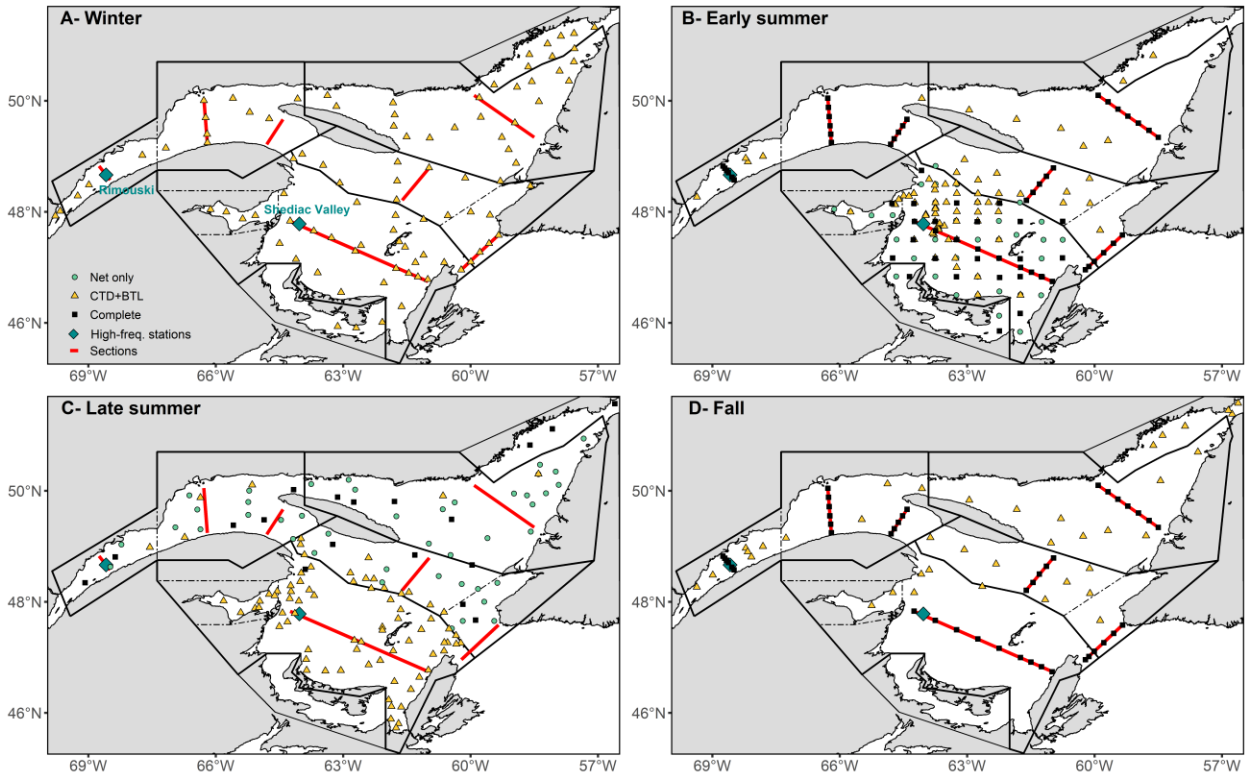

Figure 2. Locations of stations sampled (complete CTD/bottle profile) during winter (A), early summer (B), late summer (C), and fall (D) 2022 (see Figure 1 caption for region and subregion descriptions). A complete station indicates that CTD profile, water collection and zooplankton net tows were performed. Red lines show the AZMP sections.

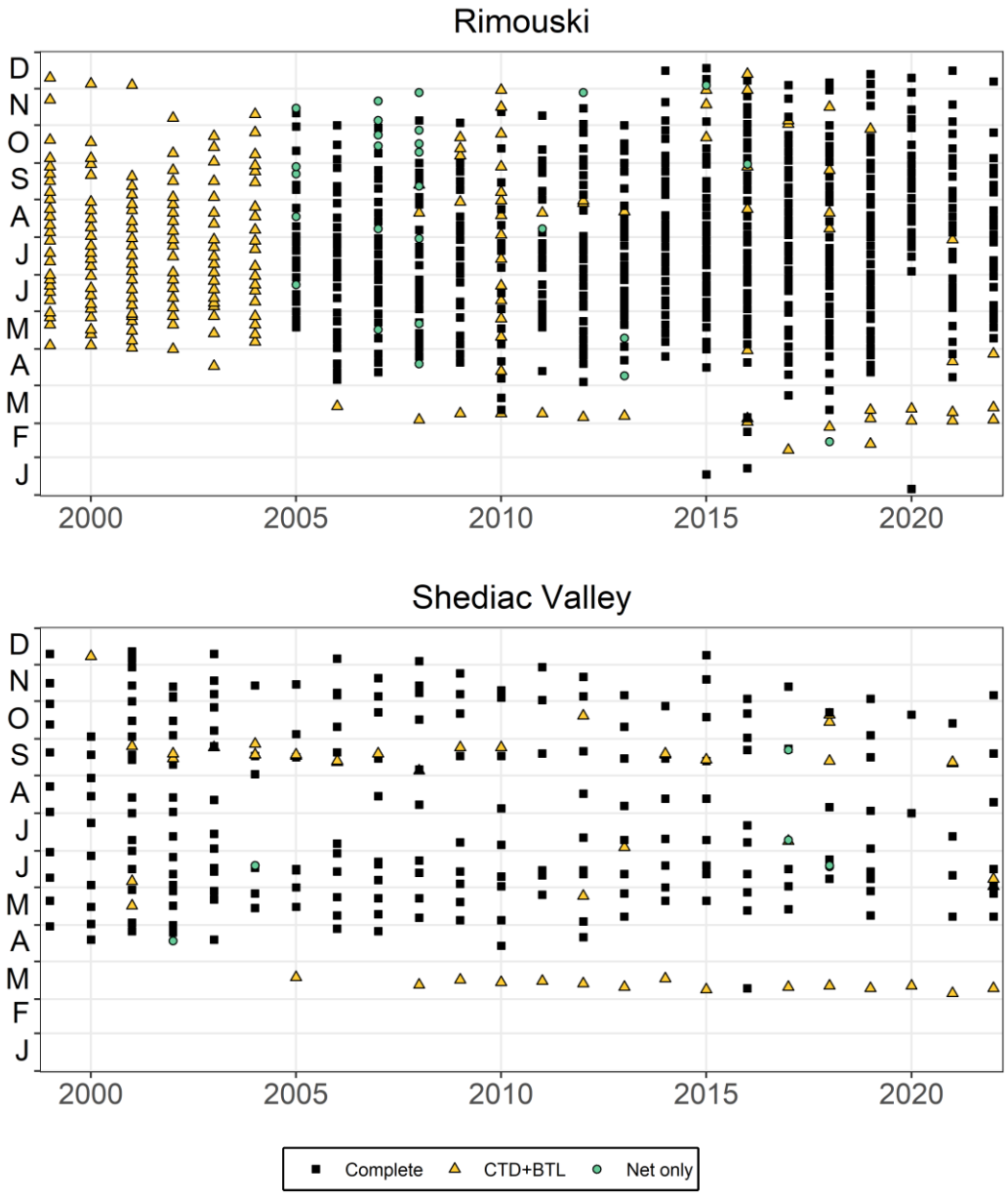

Figure 3. Sampling frequency at Rimouski and Shediac Valley stations through 2022. Sampling included CTD/bottle and plankton net tows most of the time (weather permitting).

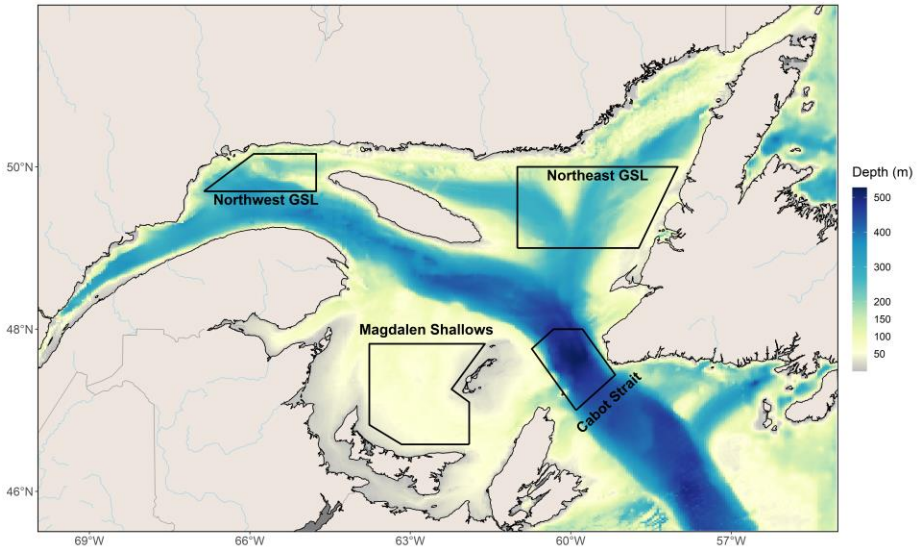

Figure 4. Bathymetric map of the Estuary and Gulf of St. Lawrence showing location of the statistical polygons identified for the spatial/temporal analysis of satellite ocean colour data. Water depth is shown by the colour axis.

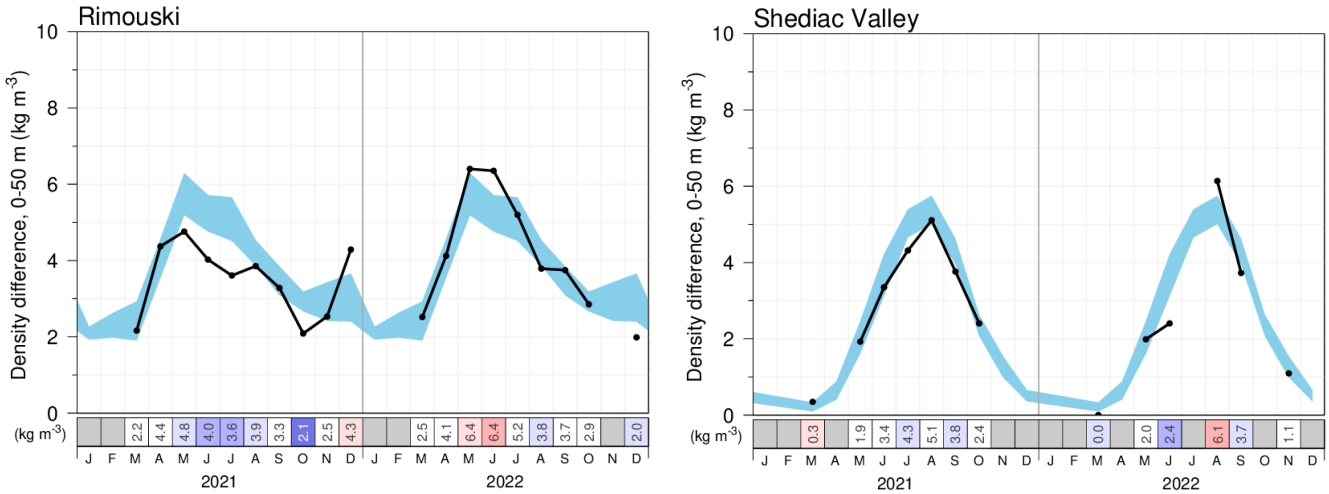

Figure 5. Seasonal stratification index during 2021 and 2022 at Rimouski and at Shediac Valley stations. The blue area represents the climatological monthly mean ± 0.5 SD (1991–2020). Numbers in the scorecard are monthly density differences in kg m^{-3}. Blue colours indicate weaker-than-normal levels (negative anomaly), red colours indicate stronger-than-normal stratification (positive anomaly), and white represents normal stratification.

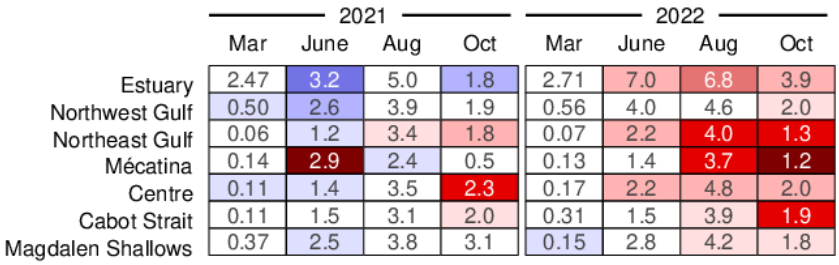

Figure 6. Monthly average stratification values (kg m^{-3}) for the Gulf-wide oceanographic surveys in 2021 and 2022. Blue colours indicate weaker-than-normal levels (negative anomaly), red colours indicate stronger-than-normal stratification (positive anomaly), and white represents normal stratification. This figure is an adaptation of Figure 56 in Galbraith et al. (2023).

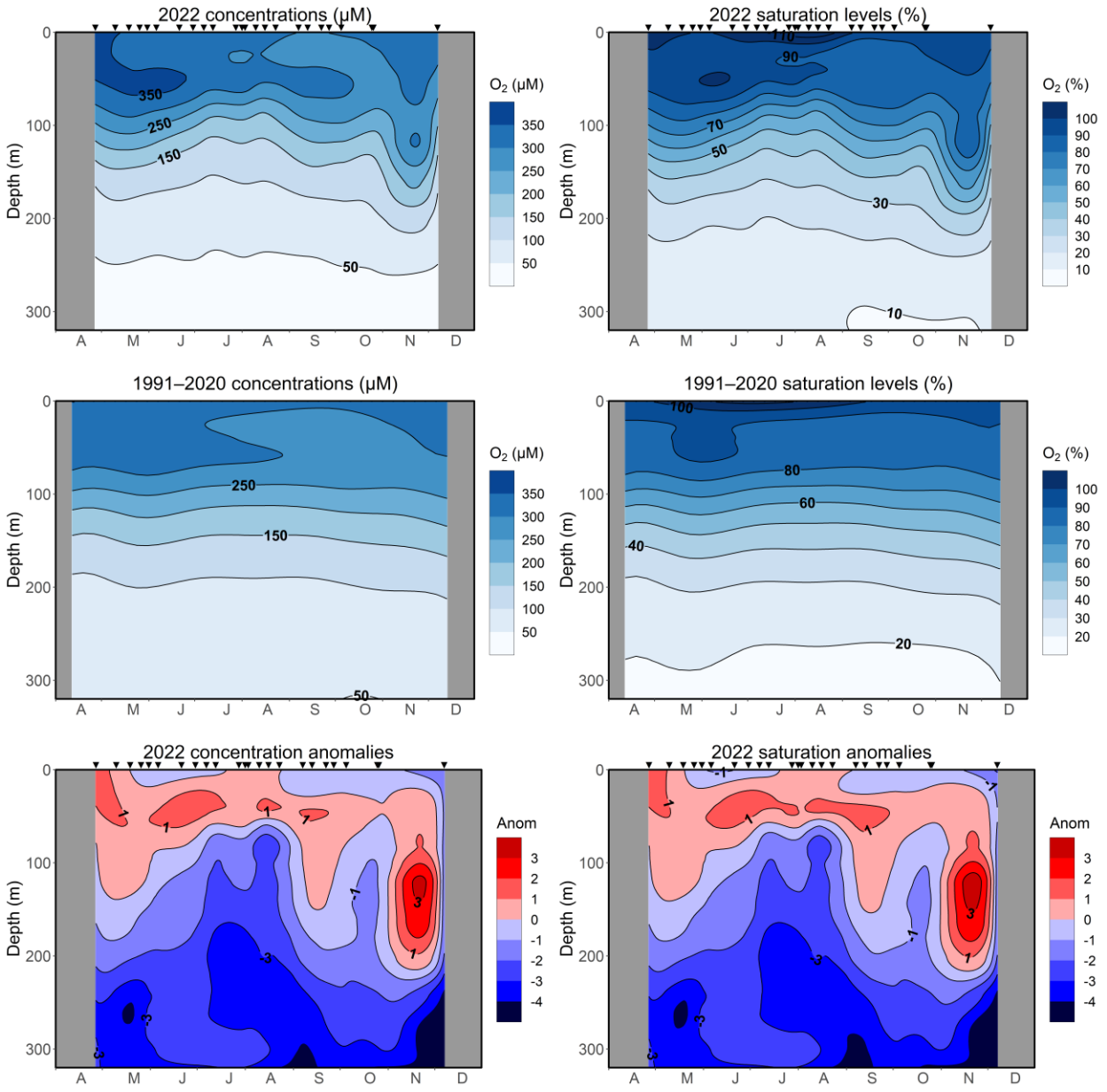

Figure 7. Vertical profiles of oxygen concentration (left panels) and saturation (right panels) at Rimouski station in 2022 (upper panels), climatology 1991–2020 (centre panels) and normalized anomaly (bottom panels). For oxygen concentration and saturation, values are shown by shades of blue and labelled contours. For anomalies, blue colours indicate below-normal levels (negative anomaly), reds are above-normal levels (positive anomaly), and white represents normal levels. Black triangles indicate timing of the station occupation.

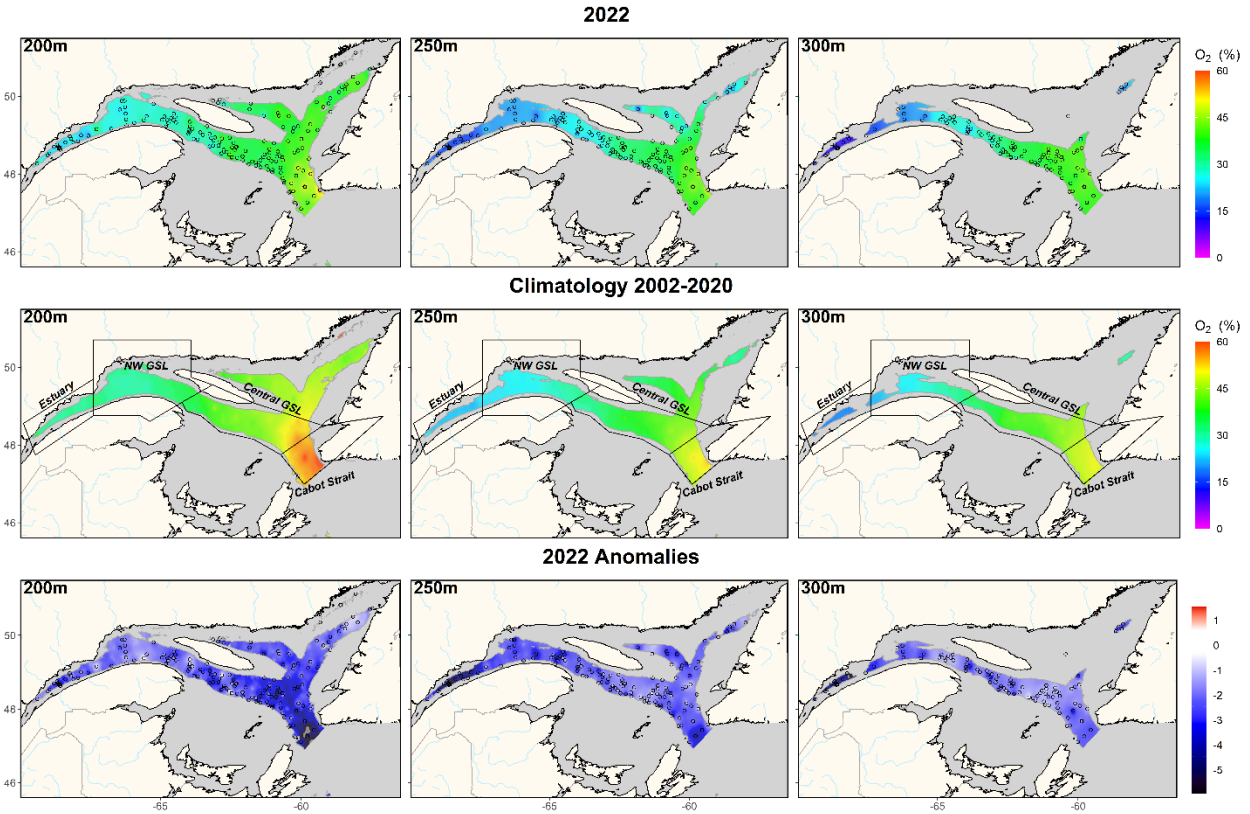

Figure 8. Annual average distribution of dissolved oxygen saturation at depths of 200 m, 250 m, and 300 m in the Estuary and Gulf of St. Lawrence during 2022 (upper panel). The climatology (2002–2020; middle panel) and anomalies (lower panel) are also shown. In the anomaly panels, blue colours indicate below-normal levels (negative anomaly), red colours are above-normal levels (positive anomaly), and white represents normal levels. Open circles show station locations in 2022.

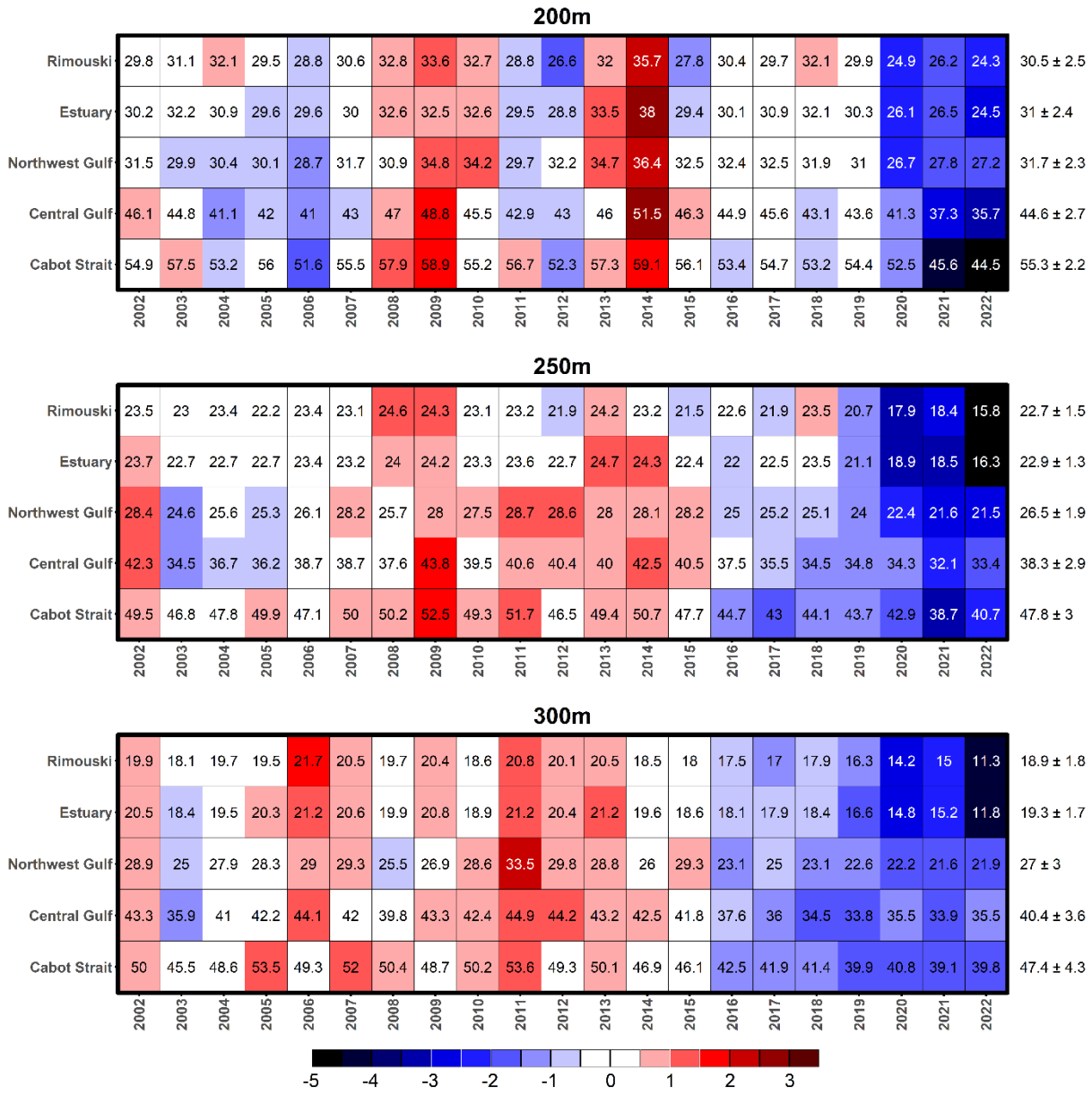

Figure 9. Time series of deep-layer dissolved oxygen saturation annual average (%) at 200 m, 250 m, and 300 m. The numbers on the right are the 2002–2020 climatological means and standard deviations, and the numbers in the boxes are the oxygen saturation levels. Blue colours indicate below-normal levels (negative anomaly), red colours are above-normal levels (positive anomaly), and white represents normal levels.

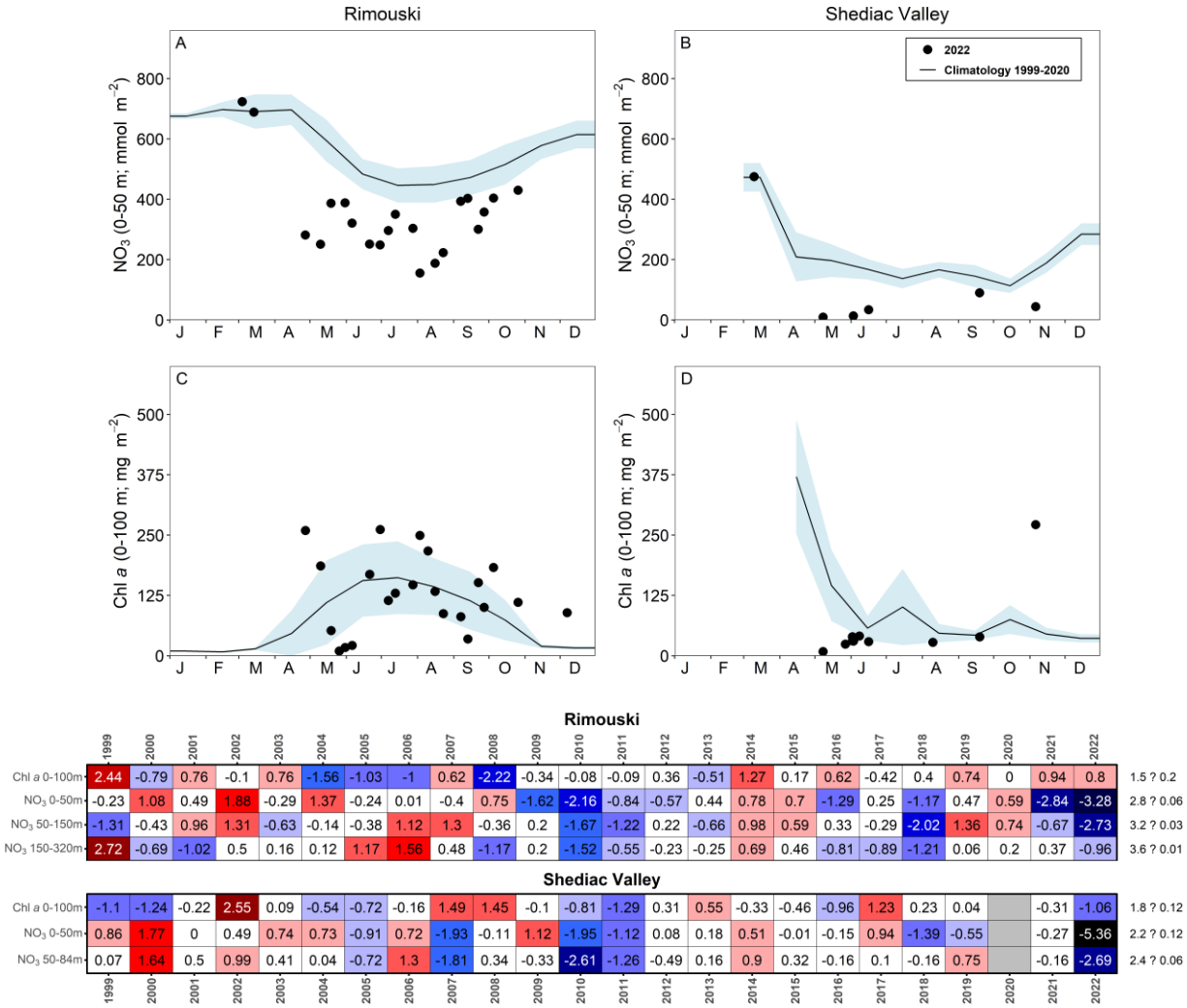

Figure 10. Nitrate inventories (0–50 m; top panels) and chlorophyll *a* inventories (0–100 m for Rimouski and 0–84 m for Shediac Valley; bottom panels) in 2022 (black circles) with monthly mean conditions (± 0.5 SD) for the 1999–2020 climatology (black line with blue shading) at Rimouski and Shediac Valley stations. Time series of normalized annual anomalies for nitrate and chlorophyll *a* inventories are also presented with the variable means and standard deviations for the 1999–2020 climatology in units of $\log_{10}$(mmol m^{-2}) and $\log_{10}$(mg chl *a* m^{-2}), respectively, to the right of the scorecard. Blue colours indicate below-normal levels (negative anomaly), reds are above-normal levels (positive anomaly), and white represents normal levels. Gray cells indicate missing data.

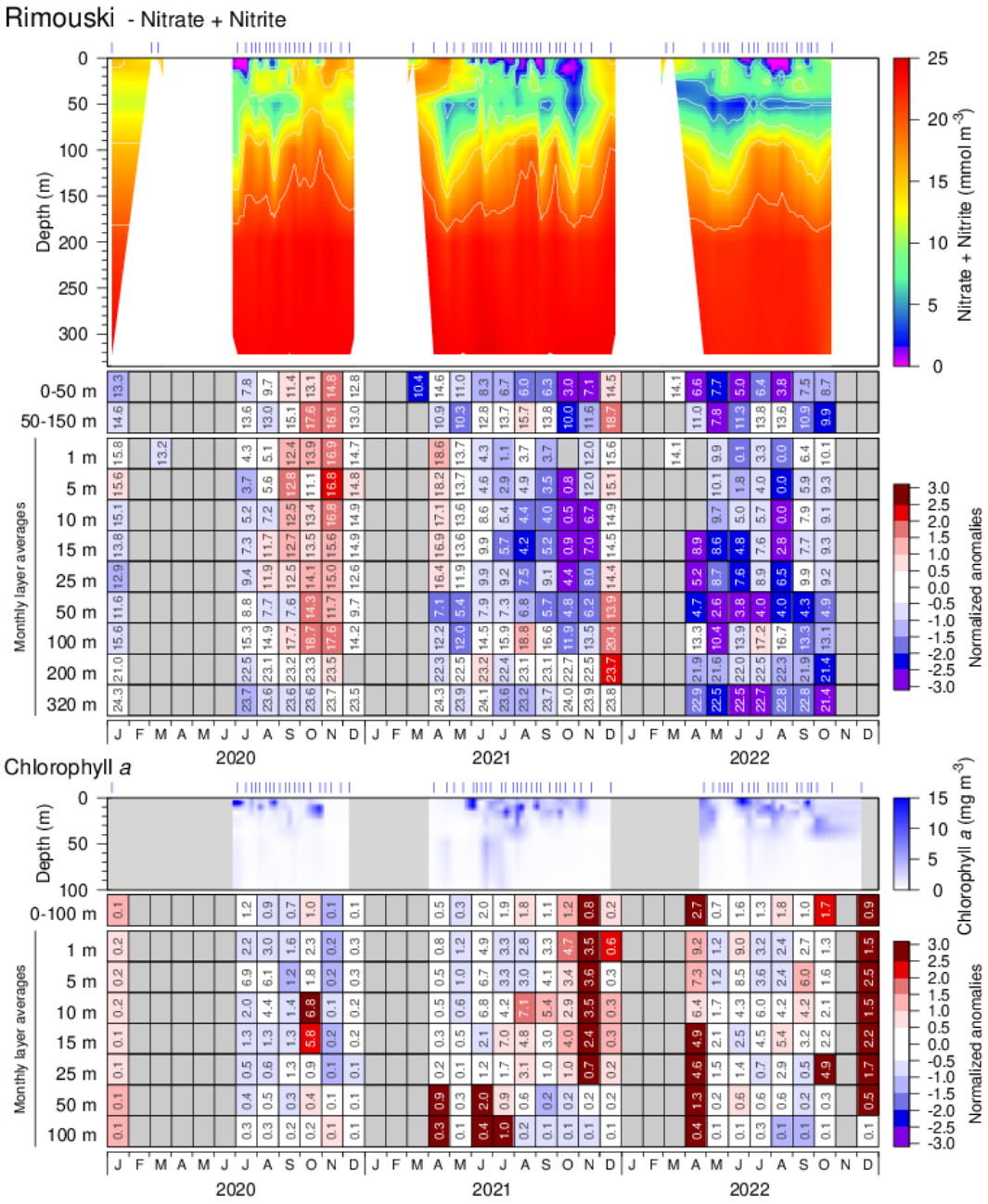

Figure 11. Nitrate (top) and chlorophyll *a* (bottom) concentrations at Rimouski station during the 2020 to 2022 sampling seasons. Contour plots use data from individual sampling events while monthly means are shown in the tables below the graphics (nitrates: mmol m^{-3}; chl *a*: mg m^{-3}). Scorecard cell colours indicate normalized anomalies based on the 1999–2020 climatology. Blue colours indicate below-normal levels (negative anomaly), reds are above-normal levels (positive anomaly), and white represents normal levels.

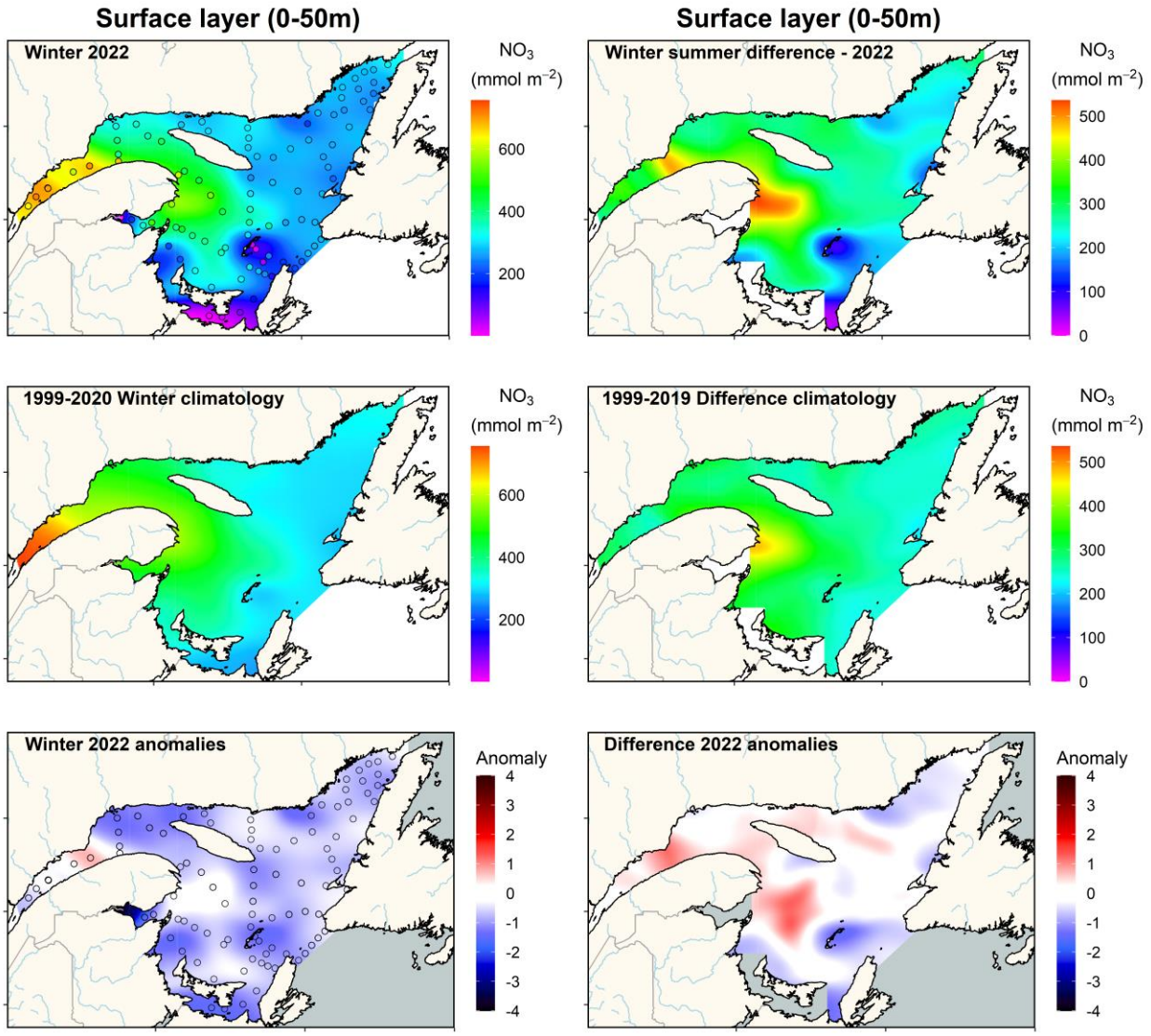

Figure 12. Nitrate inventories (mmol m^{-2}) in the surface layer (0–50 m) of the Estuary and Gulf of St. Lawrence during early March 2022 (upper left panel). Difference in nitrate inventories (mmol m^{-2}) in the surface layer of the Estuary and Gulf of St. Lawrence between winter and early summer (upper right panel). The climatology (1999–2020 for winter, 1999–2019 for difference; middle panels) and anomalies (lower panels) are shown. Blue colours indicate below-normal levels (negative anomaly), red colours are above-normal levels (positive anomaly), and white represents normal levels.

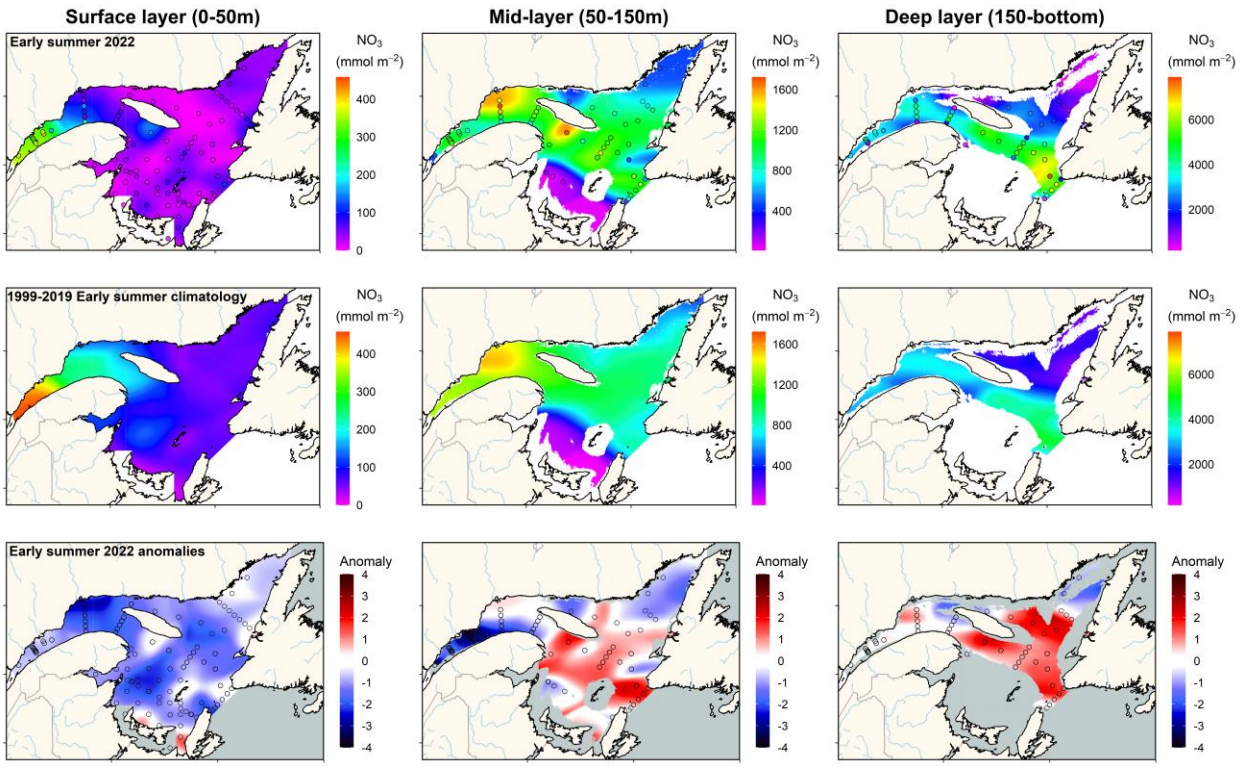

Figure 13. Nitrate inventories (mmol m^{-2}) in the surface (left panels), mid (middle panels), and deep (right panels) layers of the Estuary and Gulf of St. Lawrence during early summer 2022 (upper panels). The climatology (1999–2019; middle panels) and anomalies (lower panels) are shown for each layer. Blue colours indicate below-normal levels (negative anomaly), red colours are above-normal levels (positive anomaly), and white represents normal levels.

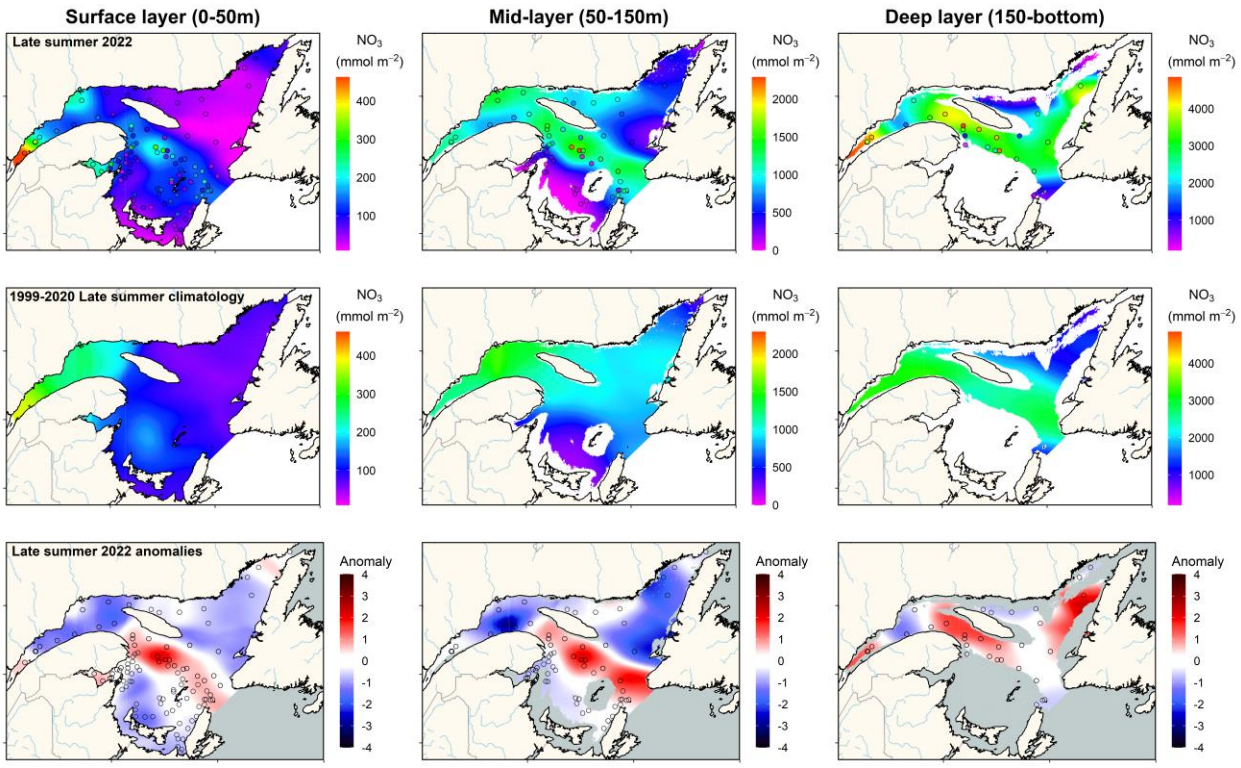

Figure 14. Nitrate inventories (mmol m^{-2}) in the surface (left panels), mid (middle panels), and deep (right panels) layers of the Estuary and Gulf of St. Lawrence during late summer 2022 (upper panels). The climatology (1999–2020; middle panels) and anomalies (lower panels) are shown for each layer. Blue colours indicate below-normal levels (negative anomaly), red colours are above-normal levels (positive anomaly), and white represents normal levels.

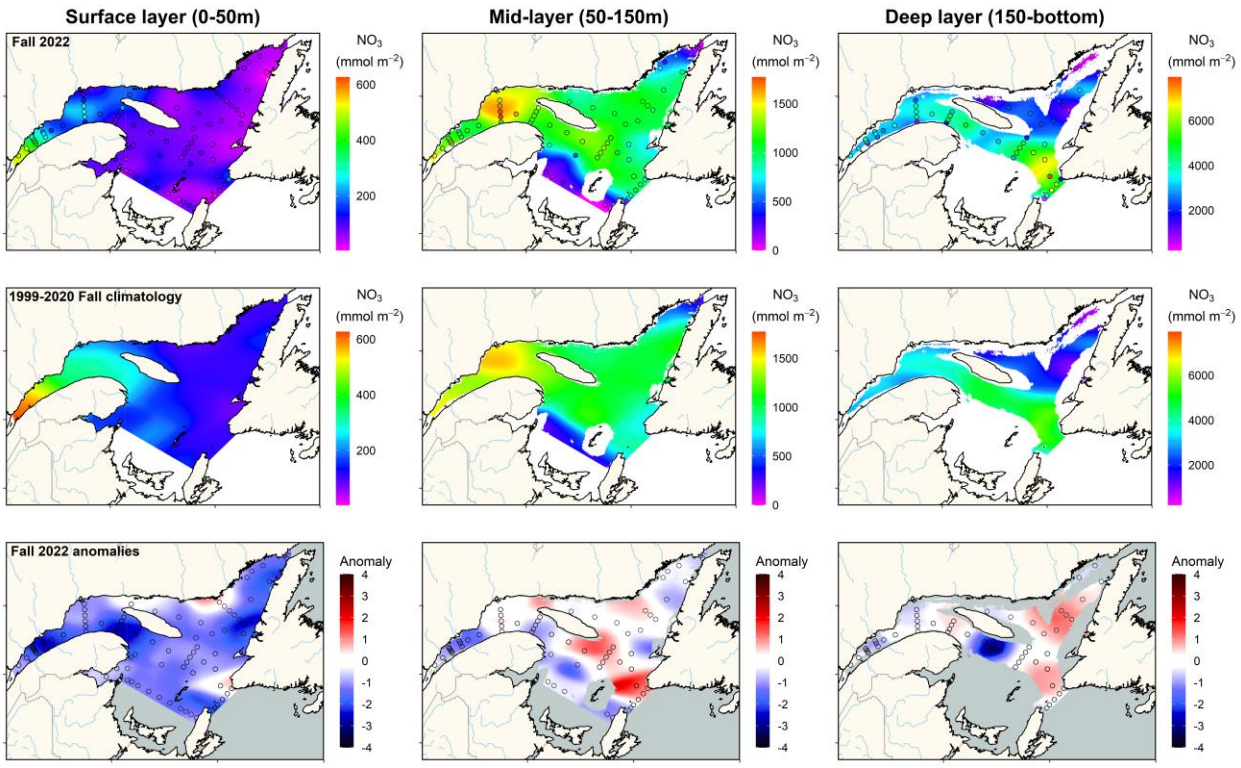

Figure 15. Nitrate inventories (mmol m^{-2}) in the surface (left panels), mid (middle panels), and deep (right panels) layers of the Estuary and Gulf of St. Lawrence during fall 2022 (upper panels). The climatology (1999–2020; middle panels) and anomalies (lower panels) are shown for each layer. Blue colours indicate below-normal levels (negative anomaly), red colours are above-normal levels (positive anomaly), and white represents normal levels.

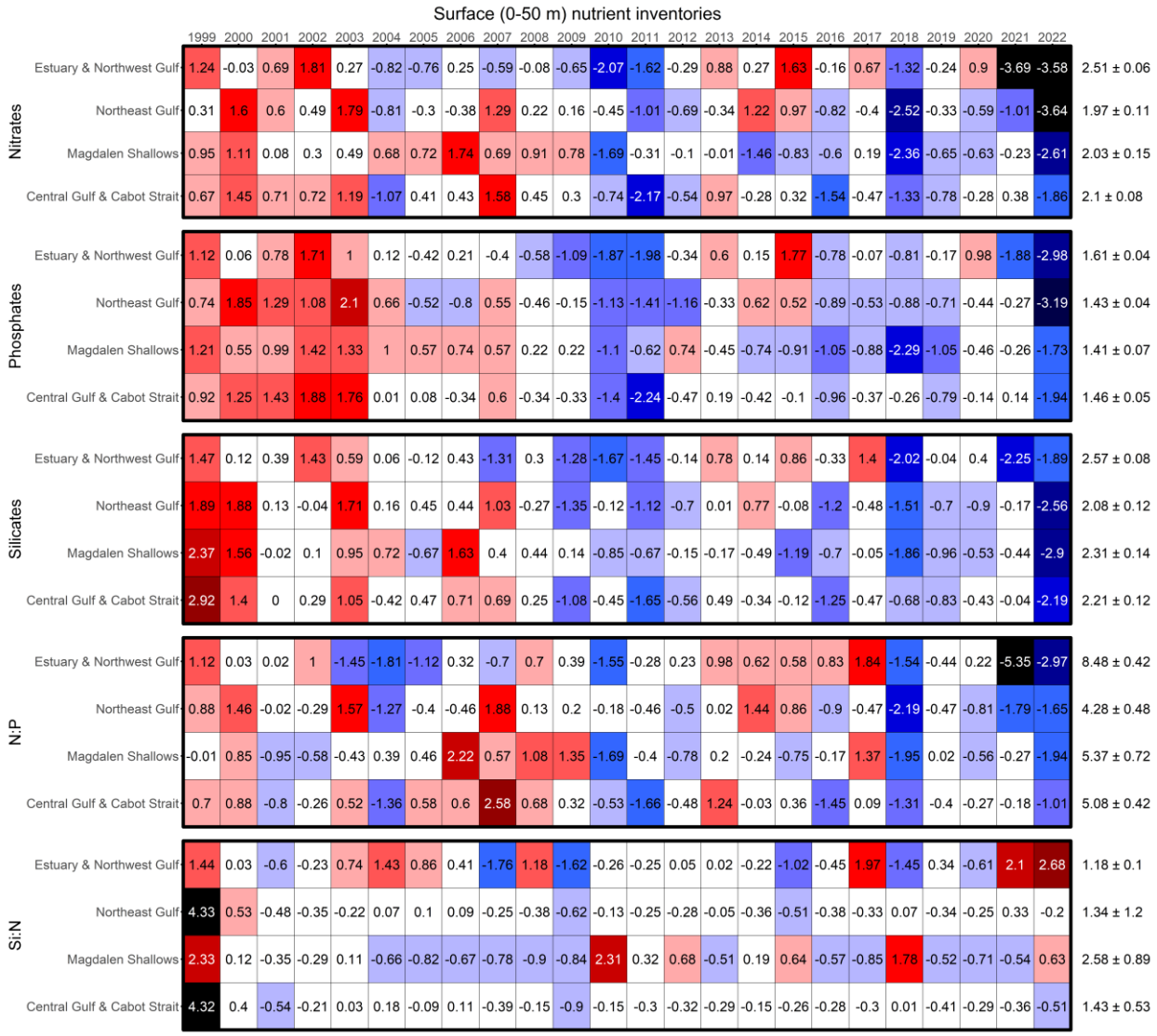

Figure 16. Time series of normalized annual anomalies for nutrient inventories and ratios in the surface layer (0–50 m) for Gulf regions. The numbers on the right are the 1999–2020 climatological means and standard deviations in units of $\log_{10}$(mmol m^{-2}) for nutrient inventories; nutrient ratios are dimensionless and have not been log-transformed. Blue colours indicate below-normal levels (negative anomaly), red colours are above-normal levels (positive anomaly), and white represents normal levels.

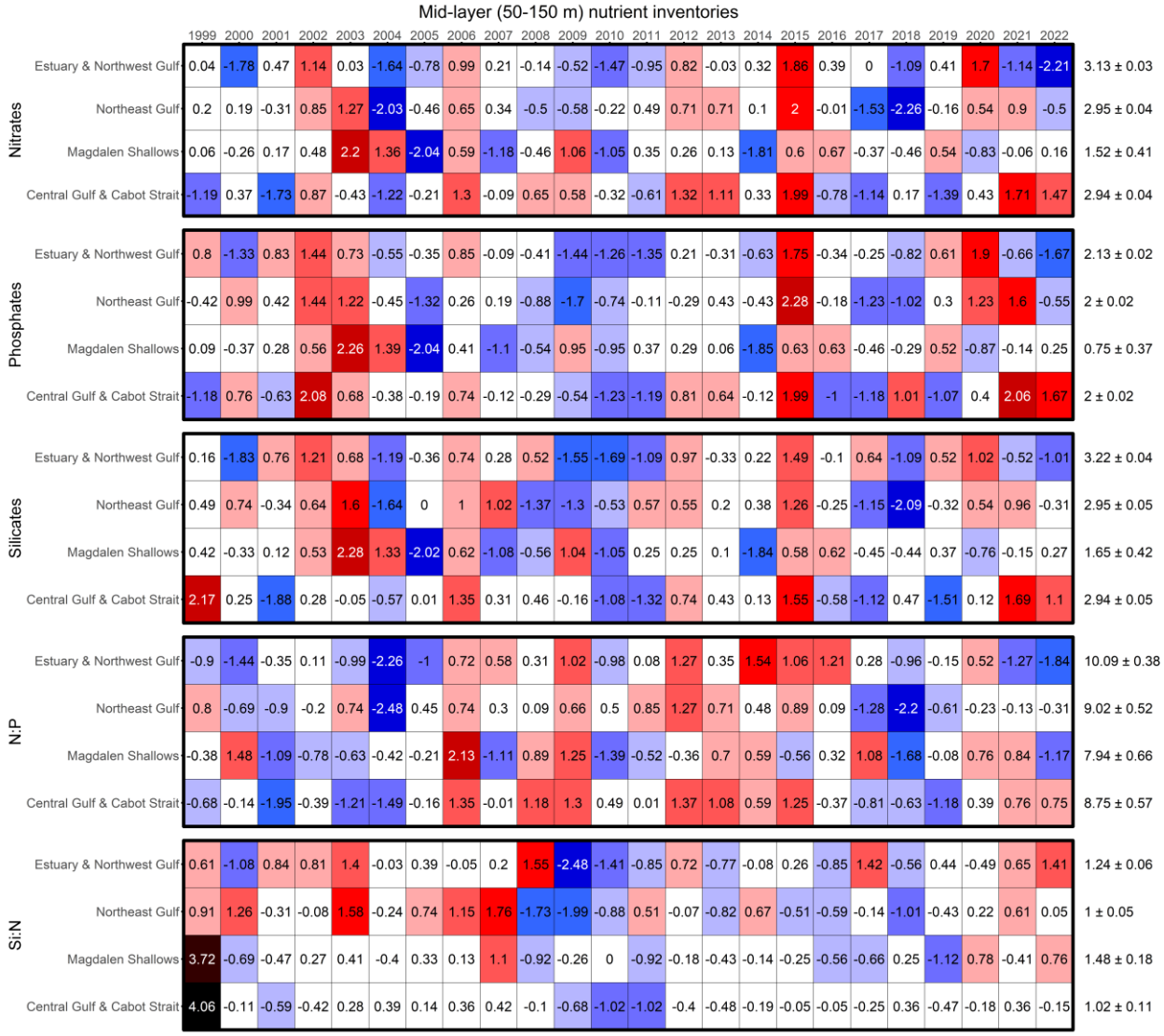

Figure 17. Time series of normalized annual anomalies for nutrient inventories and ratios in the mid-layer (50–150 m) for Gulf regions. The numbers on the right are the 1999–2020 climatological means and standard deviations in units of $\log_{10}$(mmol m^{-2}) for nutrient inventories; nutrient ratios are dimensionless and have not been log-transformed. Blue colours indicate below-normal levels (negative anomaly), red colours are above-normal levels (positive anomaly), and white represents normal levels.

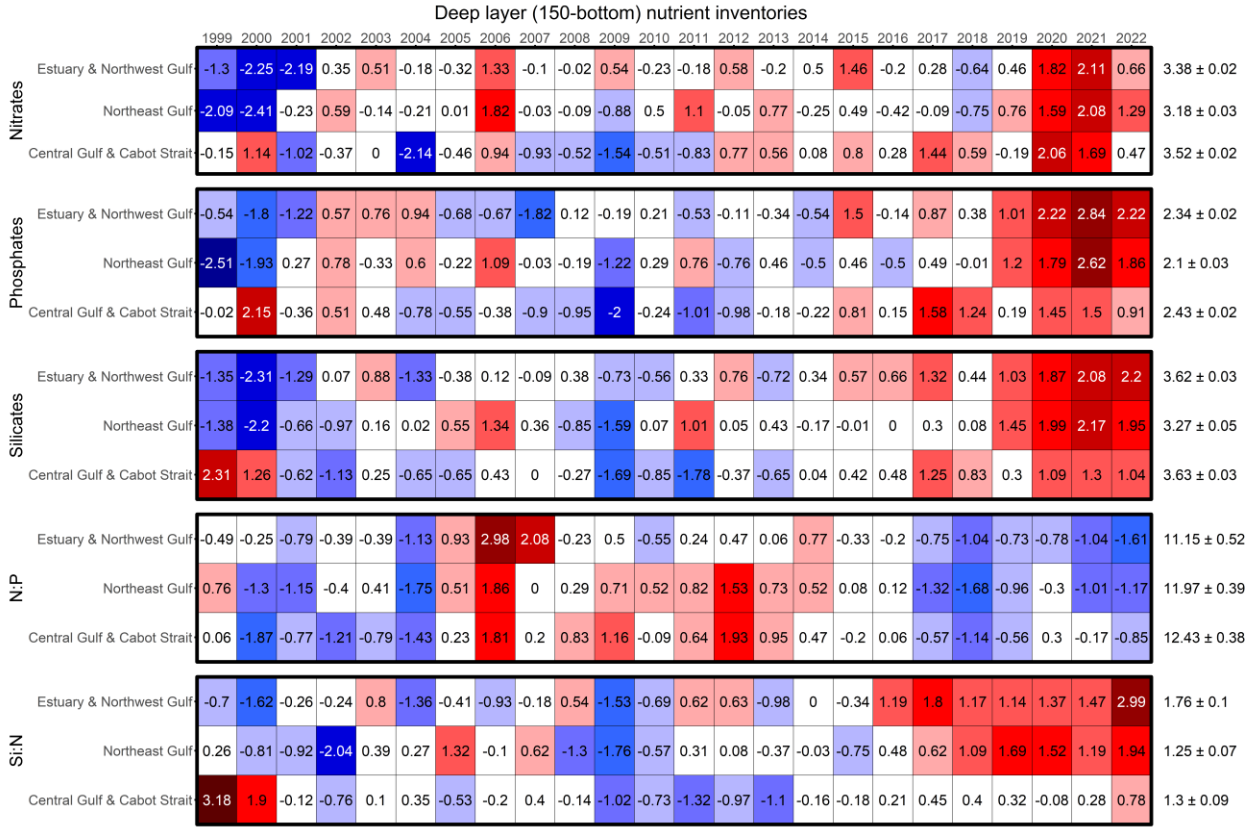

Figure 18. Time series of normalized annual anomalies for nutrient inventories and ratios in the deep layer (150–bottom) for Gulf regions. The numbers on the right are the 1999–2020 climatological means and standard deviations in units of $\log_{10}$(mmol m^{-2}) for nutrient inventories; nutrient ratios are dimensionless and have not been log-transformed. Blue colours indicate below-normal levels (negative anomaly), red colours are above-normal levels (positive anomaly), and white represents normal levels.

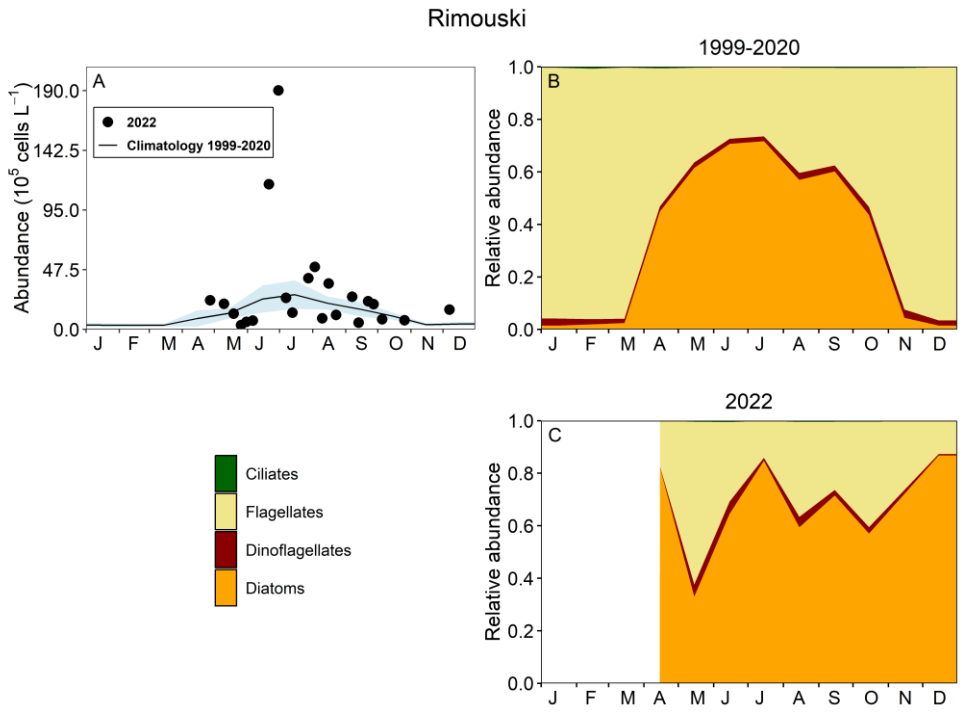

Figure 19. Phytoplankton abundance (A) and community composition at Rimouski station for the 1999–2020 climatology (B) and for 2022 (C). The blue shading on panel (A) represents ± 0.5 SD of the monthly mean phytoplankton abundance for the climatology. While ciliate abundances were included in the graphics, they are not visible because they represent < 1% of phytoplankton cells each month for the climatology.

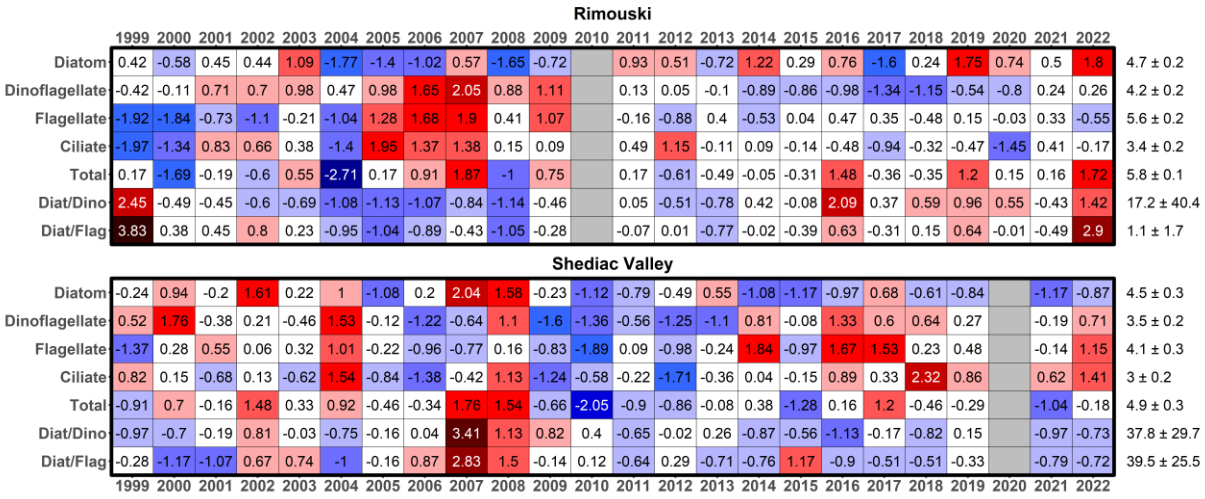

Figure 20. Time series of normalized annual (April–December) anomalies for the abundance of the main phytoplankton taxonomic groups and total phytoplankton abundance, and for the diatom/dinoflagellate and diatom/flagellate ratios at Rimouski and Shediac Valley stations. The numbers on the right are the 1999–2020 climatological means and standard deviations in units of $\log_{10}$(cells L^{-1}) for abundance indices (no data transformation for ratios). Blue colours indicate below-normal levels (negative anomaly), red colours are above-normal levels (positive anomaly), and white represents normal levels. Gray cells indicate missing data.

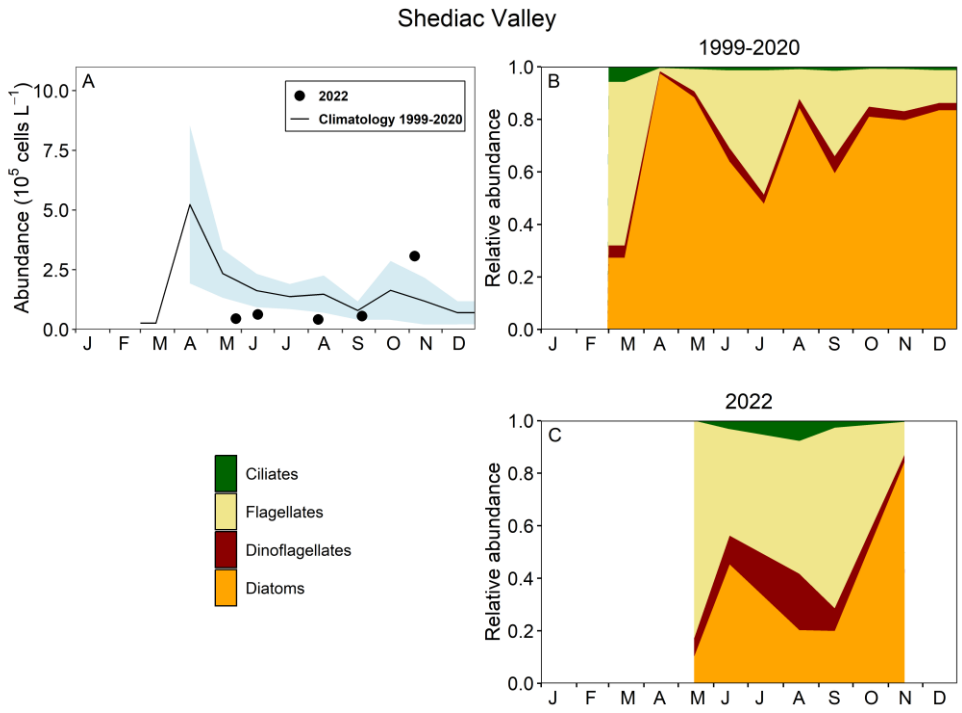

Figure 21. Phytoplankton abundance (A) and community composition at Shediac Valley station for the 1999–2020 climatology (B) and for 2022 (C). The blue shading on panel (A) represents ± 0.5 SD of the monthly mean phytoplankton abundance for the climatology.

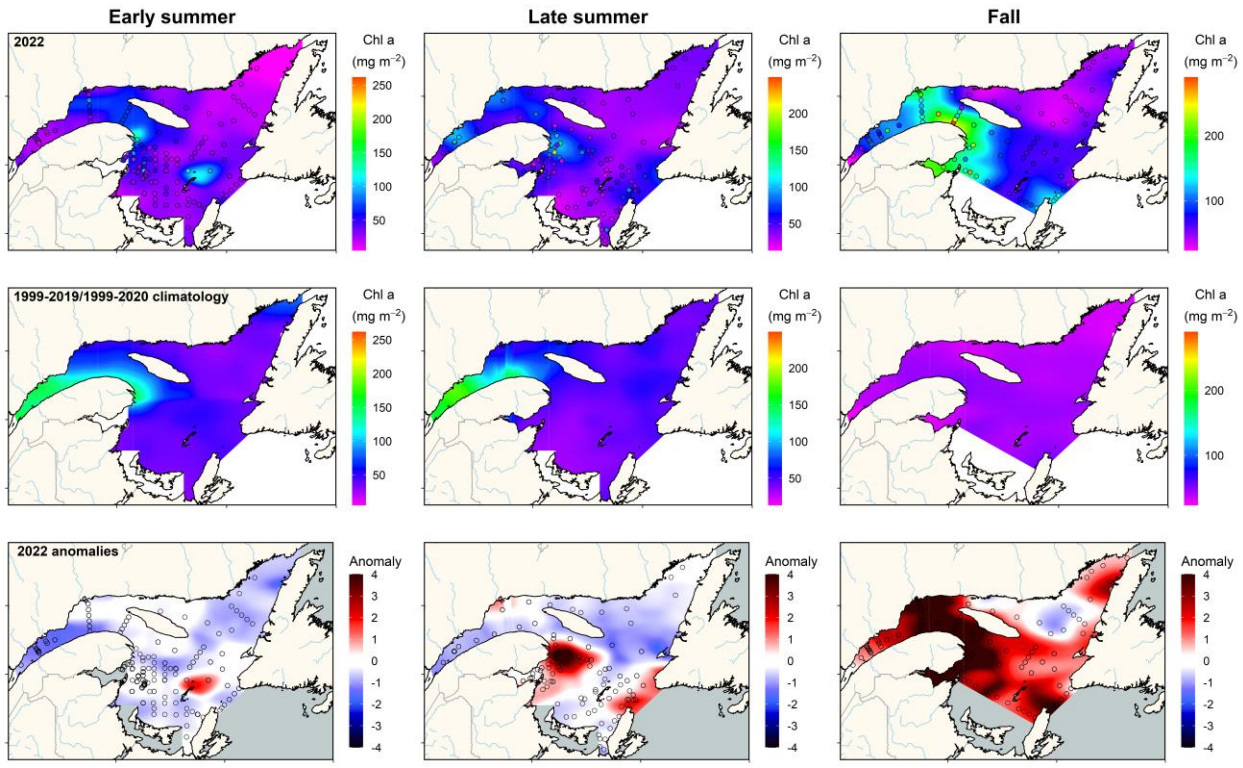

Figure 22. Vertically integrated (0–100 m) chlorophyll *a* inventory (mg m^{-2}) in the Estuary and Gulf of St. Lawrence during early summer (left panels), late summer (middle panels), and fall (right panels) 2022. The climatology (1999–2019 for early summer and 1999–2020 for other seasons; middle panels) and anomalies (lower panels) are shown for each season. In the anomaly panels, blue colours indicate below-normal levels (negative anomaly), red colours are above-normal levels (positive anomaly), and white represents normal levels.

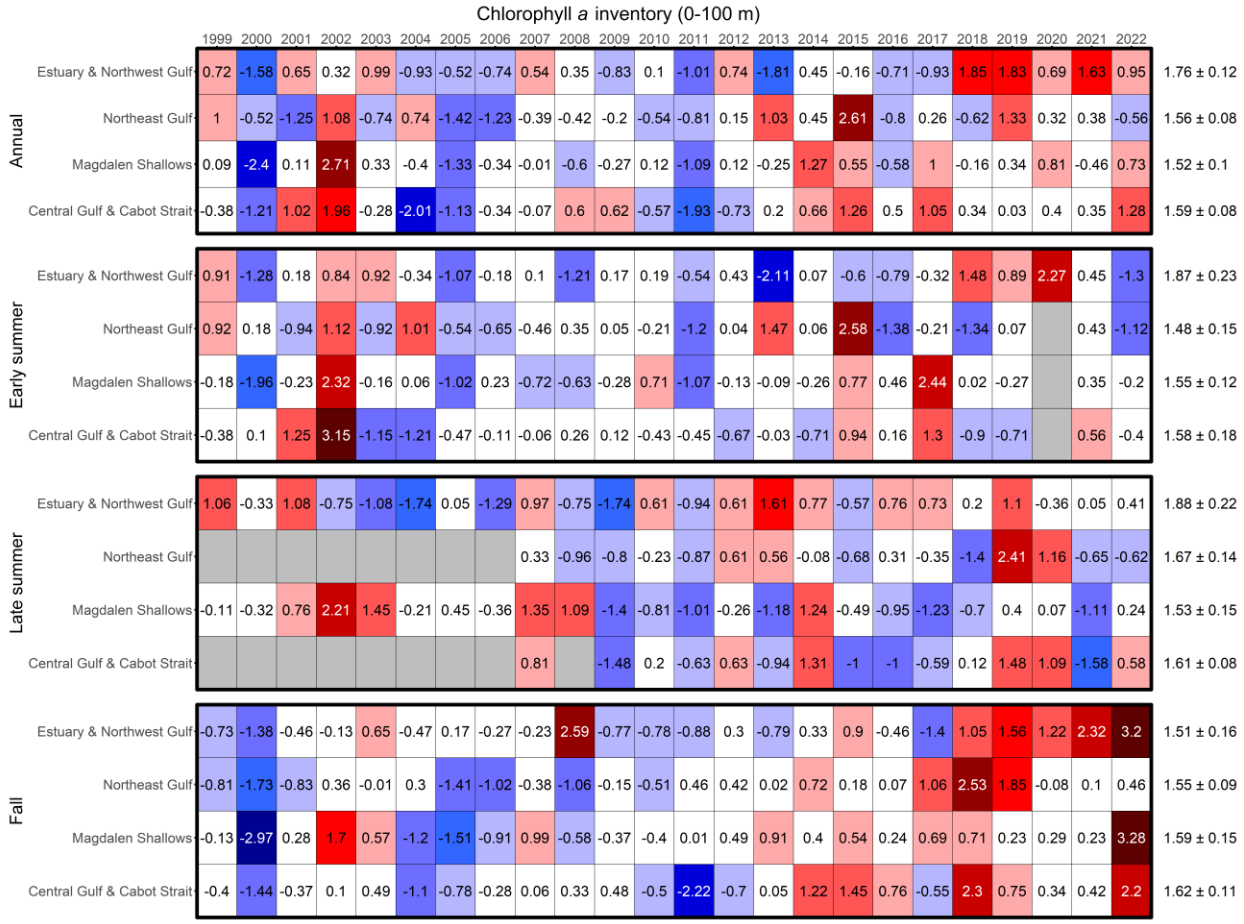

Figure 23. Time series of normalized annual and seasonal anomalies for chlorophyll *a* inventories (0–100 m) for Gulf regions. The numbers on the right are the 1999–2020 (1999–2019 for early summer) climatological means and standard deviations in units of $\log_{10}(\text{mg m}^{-2})$. Blue colours indicate below-normal levels (negative anomaly), reds are above-normal levels (positive anomaly), and white represents normal levels. Gray cells indicate missing data.

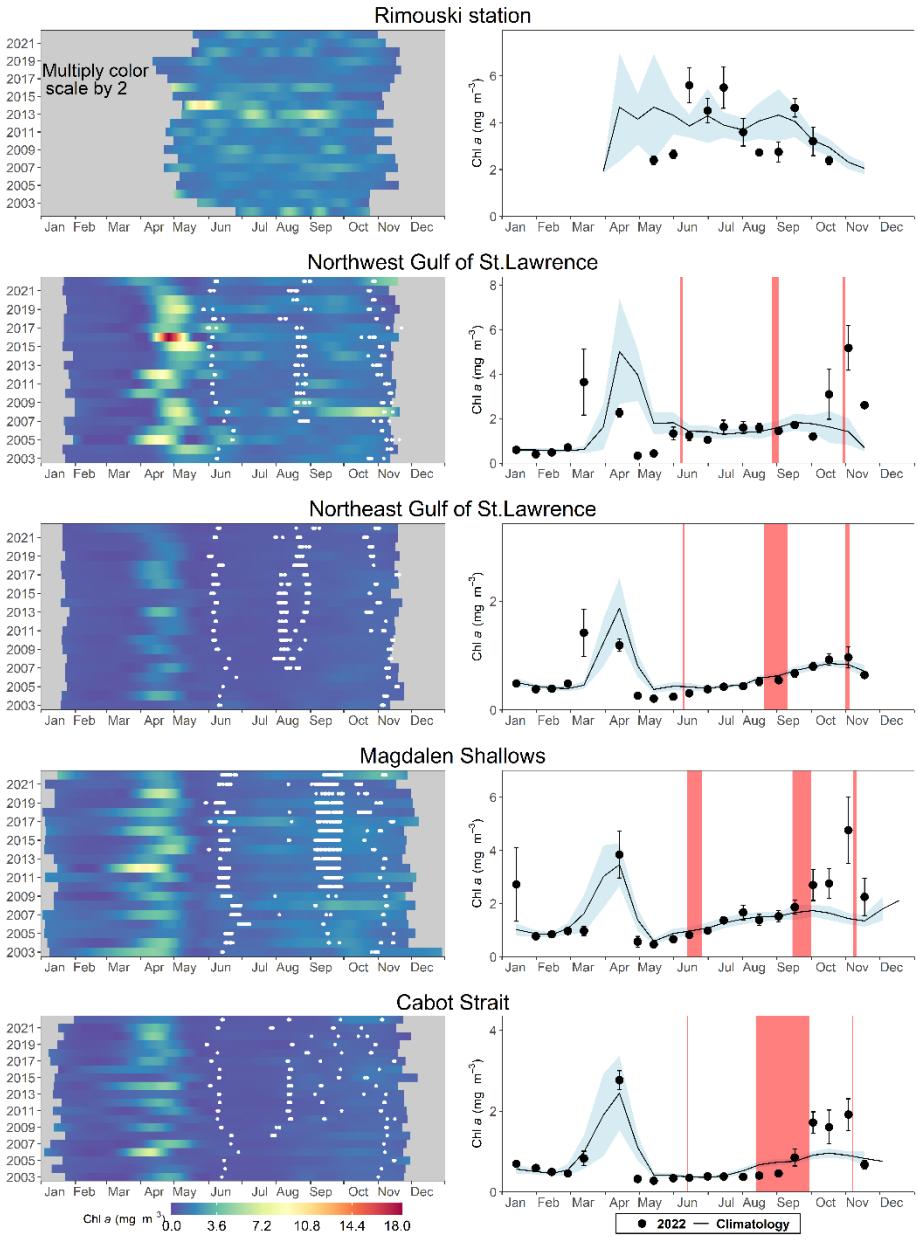

Figure 24. Left panels: LOESS-smoothed time series of daily surface chlorophyll *a* concentrations derived from data produced by a fluorescence sensor fixed on the Viking buoy at Rimouski station (1st row panels) and from MODIS ocean-colour data in the ocean colour polygons (see Figure 4 for polygon locations). White dots indicate sampling times of the main surveys. Right panels: comparison of the semimonthly mean (± 0.5 SD) of surface chlorophyll *a* estimates in 2022 (black circles) with average (± 0.5 SD) conditions from the 2003–2020 climatology (2002–2020 for Rimouski station; solid line with blue shading) for the same ocean-colour polygons. Red shadings indicate sampling times of the main surveys.

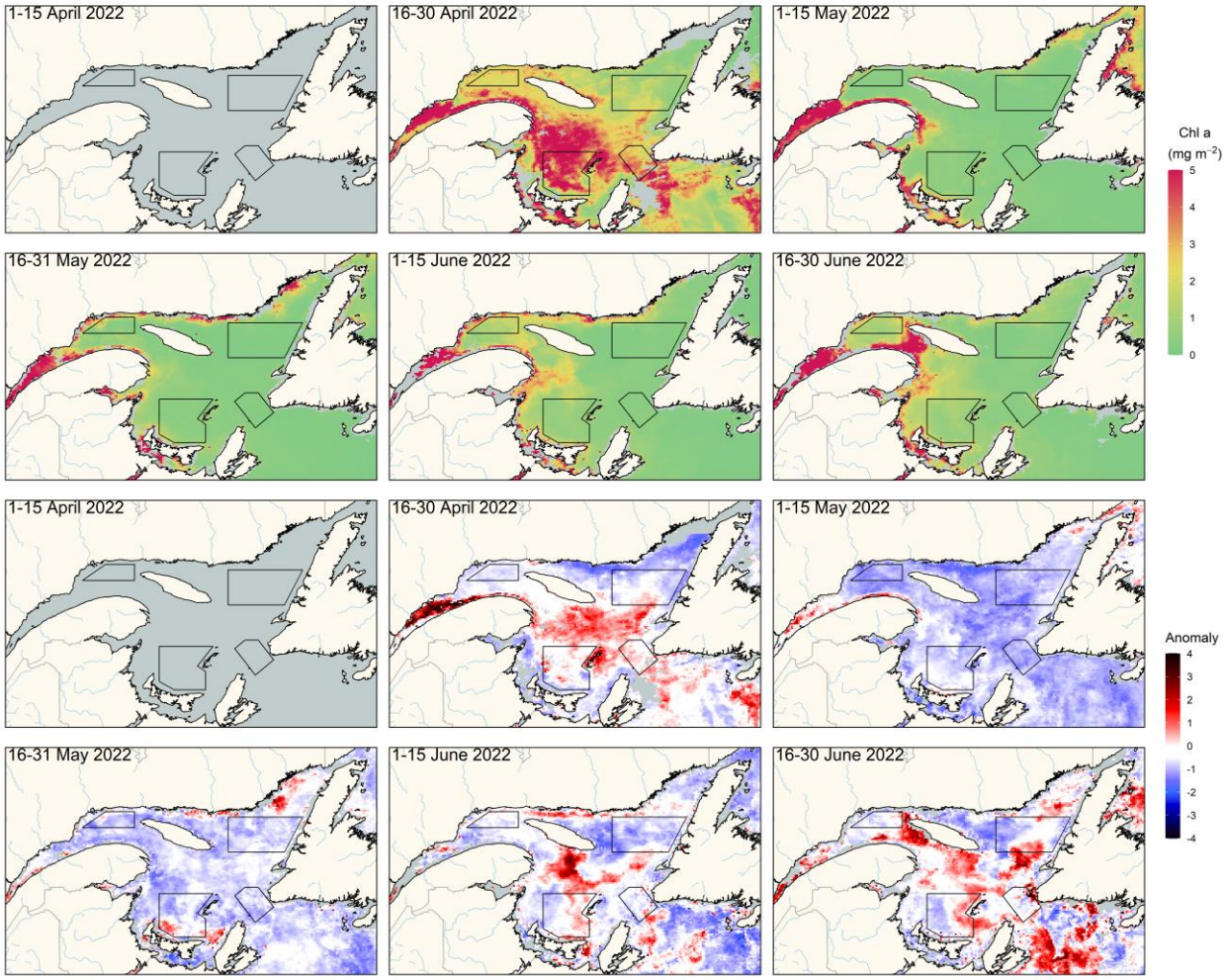

Figure 25. MODIS composite images of surface chlorophyll *a* (mg m^{-3}; upper panels) and chlorophyll *a* normalized anomaly based on the 2003–2020 climatology (lower panels) in the Gulf of St. Lawrence during spring/early summer 2022. Grey colour indicates the absence of data. Blue colours indicate below-normal levels (negative anomaly), red colours are above-normal levels (positive anomaly), and white represents normal levels.

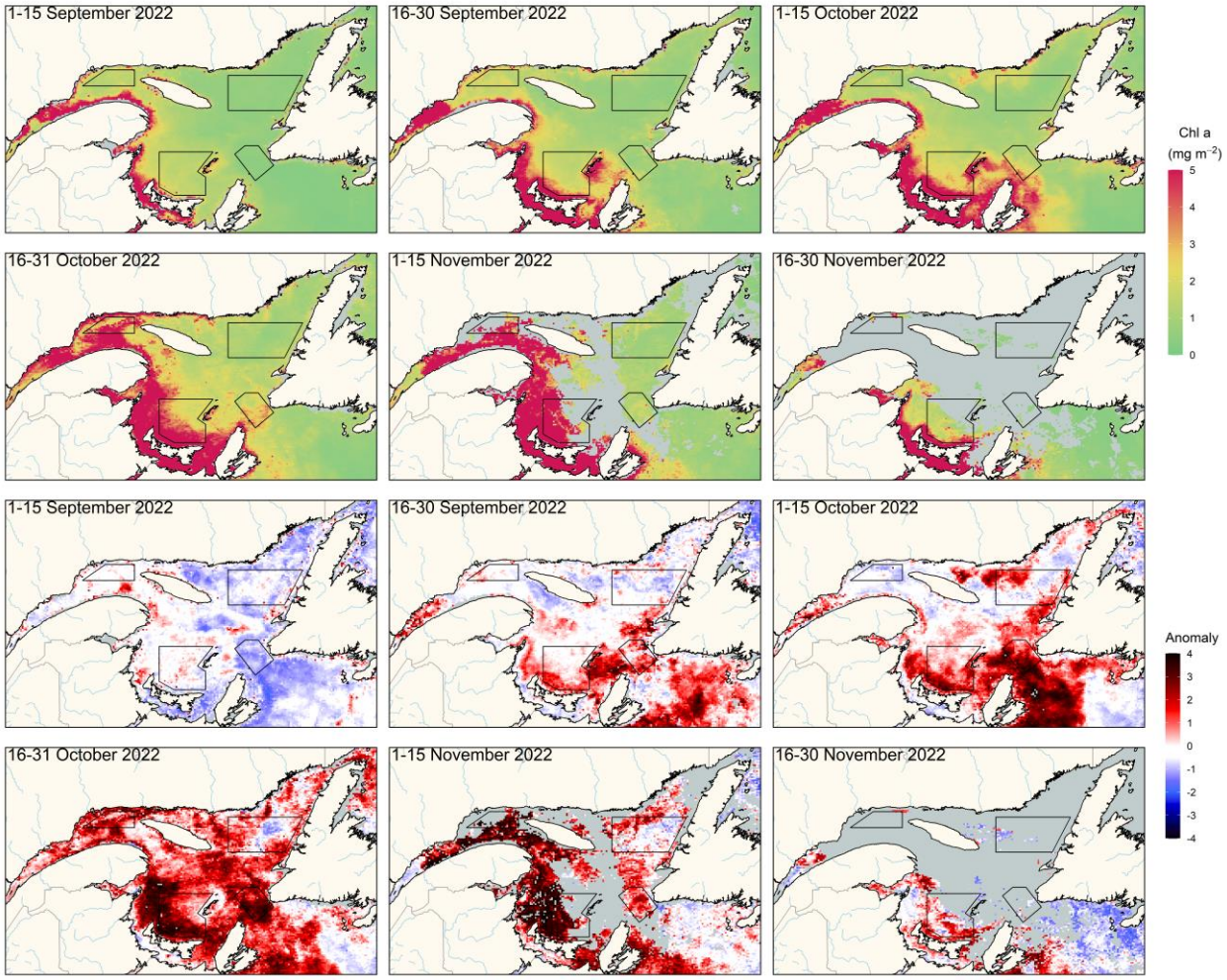

Figure 26. MODIS composite images of surface chlorophyll *a* (mg m^{-3}; upper panels) and chlorophyll *a* normalized anomaly based on the 2003–2020 climatology (lower panels) in the Gulf of St. Lawrence during fall 2022. Grey colour indicates the absence of data. Blue colours indicate below-normal levels (negative anomaly), red colours are above-normal levels (positive anomaly), and white represents normal levels.

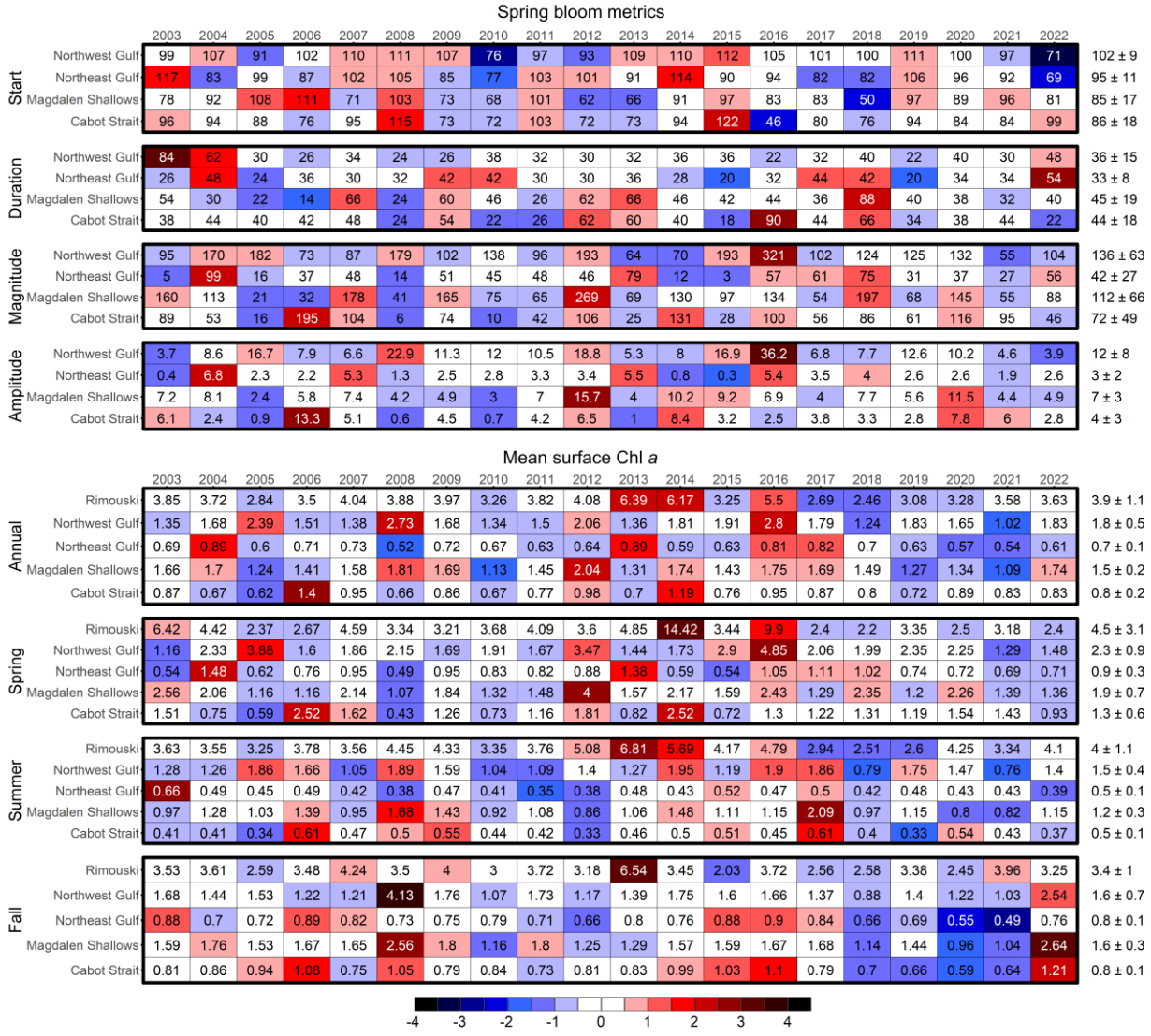

Figure 27. Time series of spring bloom metrics (upper section) and annual/seasonal mean surface chlorophyll *a* (lower section; mg m^{-3}) estimated from satellite ocean colour data (MODIS: 2003–present) in the Gulf of St. Lawrence ocean-colour polygons (see Figure 4) and from Viking buoy surface sensor at Rimouski station. The spring bloom indices are start (day of the year), duration (days), magnitude (mg chl *a* m^{-3} day^{-1}), and amplitude (mg *a* chl m^{-3}). Variable means and standard deviations for the 2003–2020 climatology are shown to the right of the scorecard. Blue colours indicate below-normal levels (negative anomaly), red colours are above-normal levels (positive anomaly), and white represents normal levels. Spring is from March to May, summer from June to August, and fall from September to November.

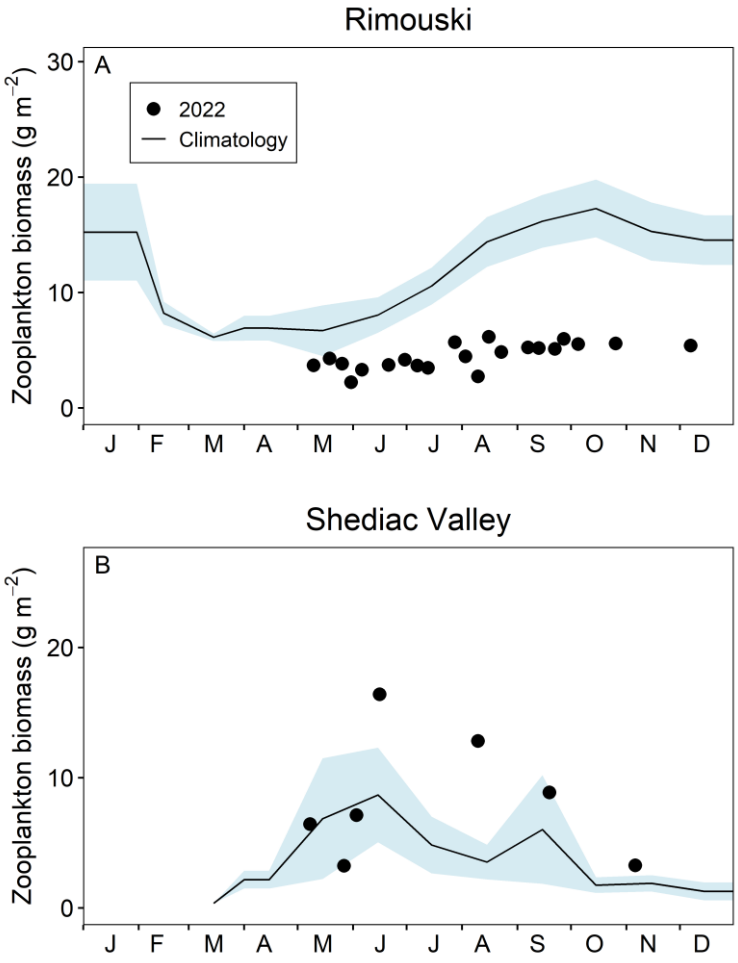

Figure 28. Comparison of total zooplankton biomass (dry weight) in 2022 (circles) with the monthly climatology from (A) Rimouski (2005–2020) and (B) Shediac Valley (1999–2020) stations (black line with blue shading). Blue shading represents ± 0.5 SD of the monthly means.

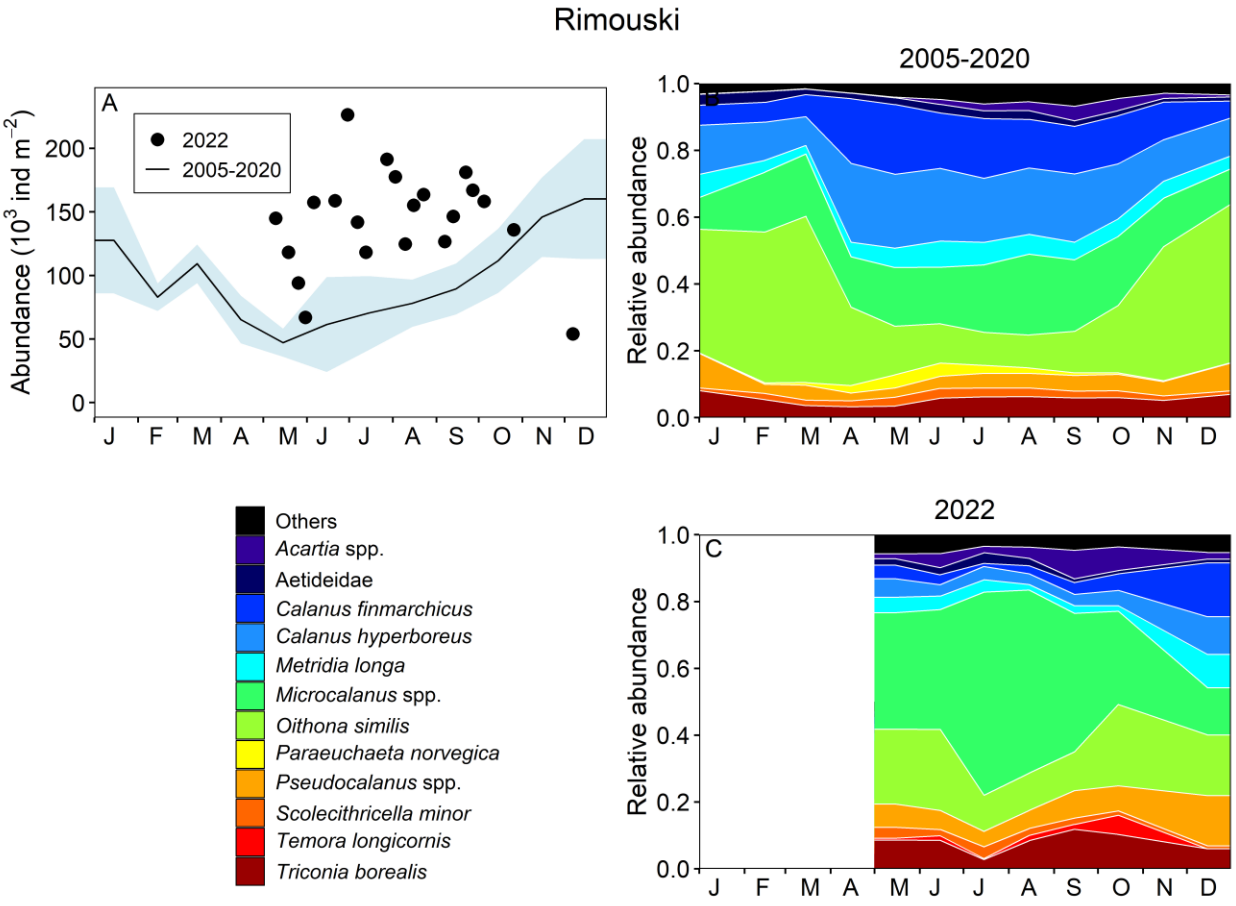

Figure 29. Seasonal variability of dominant copepods at Rimouski station. Climatology of copepod copepodite abundance (black line with blue shading indicating ± 0.5 SD) and in 2022 (circles) (A); climatology of the relative abundance of the identified copepod taxa representing 95% of total copepod abundance during the 2005–2020 period (B) and in 2022 (C).

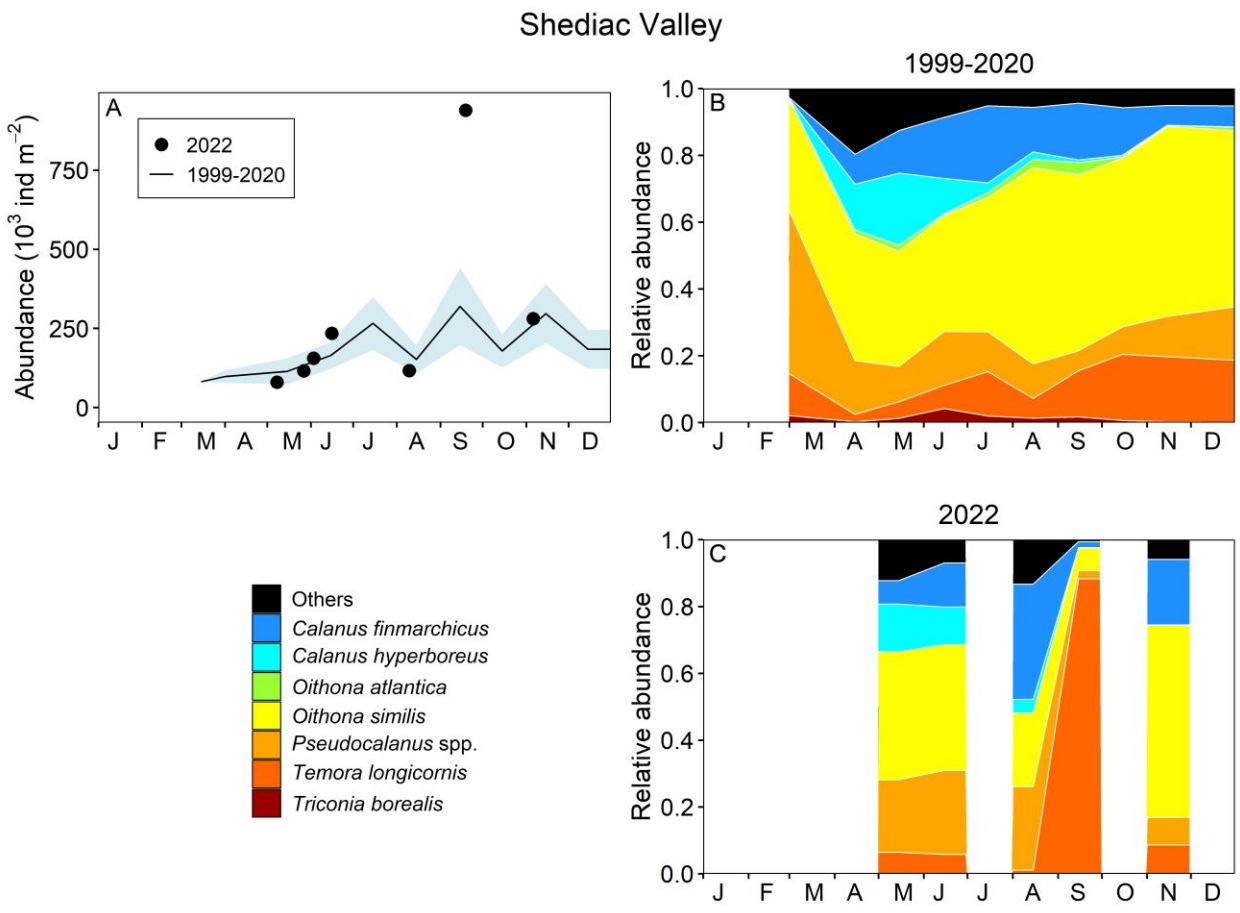

Figure 30. Seasonal variability of dominant copepods at Shediac Valley station. Climatology of copepod copepodite abundance (black line with blue shading indicating ± 0.5 SD) and in 2022 (circles) (A); climatology of the relative abundance of the identified copepod taxa representing 95% of total copepod abundance during the 1999–2020 period (B) and in 2022 (C).

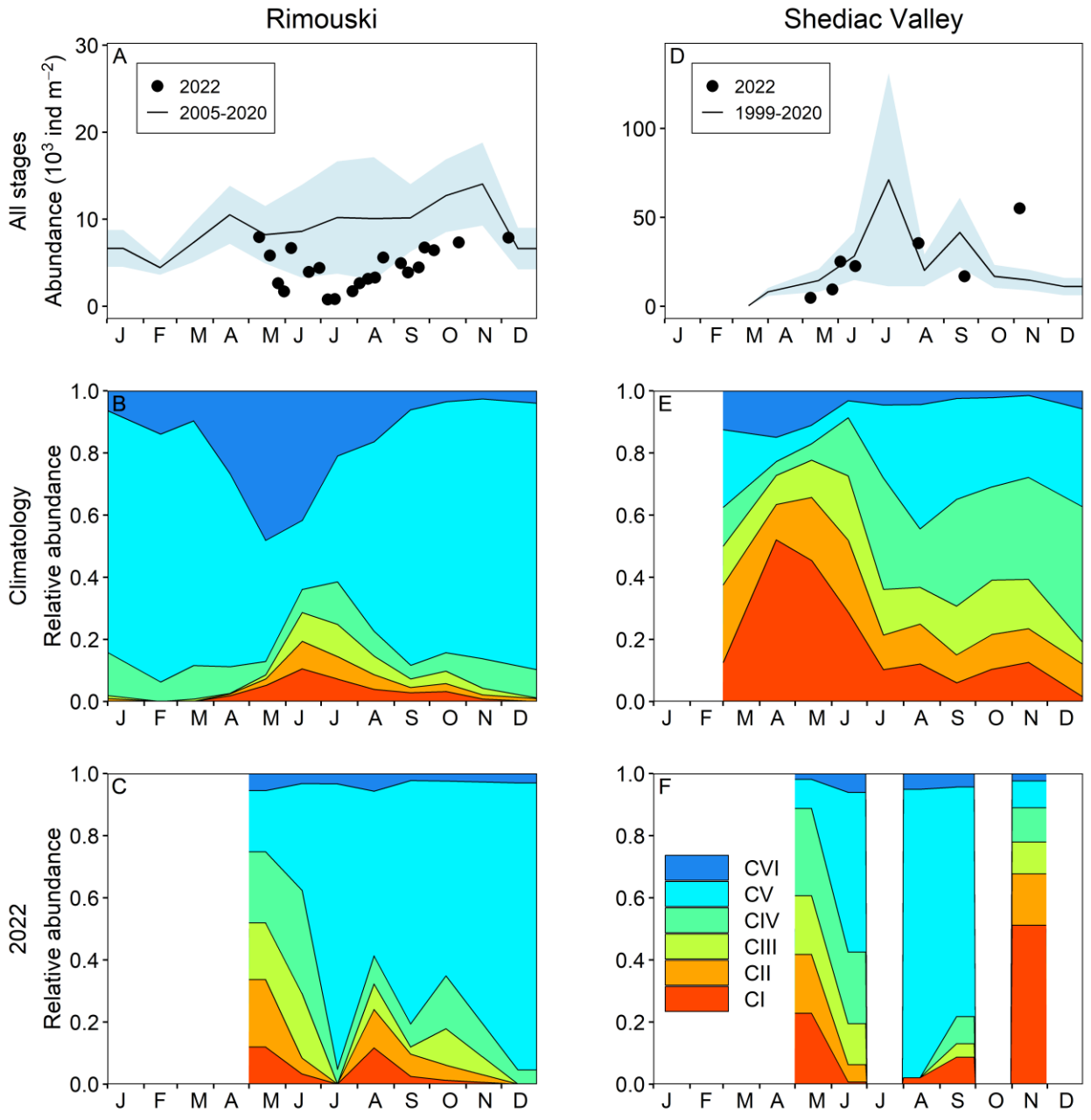

Figure 31. Seasonal variability in *Calanus finmarchicus* copepodite abundance and stage distribution at Rimouski (A–C) and Shediac Valley (D–F) stations. Climatology of *C. finmarchicus* abundance (black line with blue shading indicating ± 0.5 SD) with data from 2022 (circles) (A, D). Climatology of individual copepodite stages (B, E) and data for 2022 (C, F).

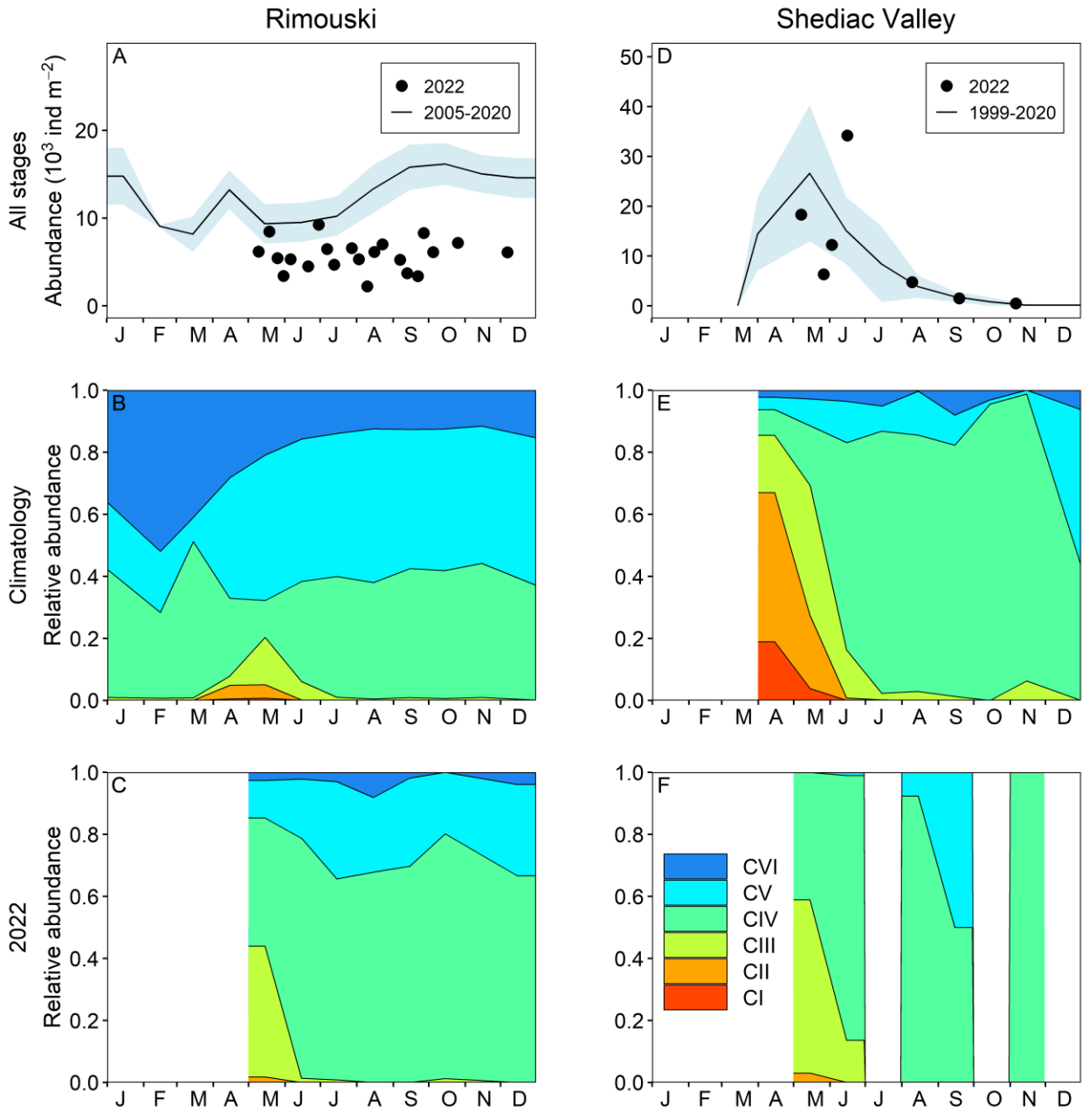

Figure 32. Seasonal variability in *Calanus hyperboreus* copepodite abundance and stage distribution at Rimouski (A–C) and Shediac Valley (D–F) stations. Climatology of *C. hyperboreus* abundance (black line with blue shading indicating ± 0.5 SD) with data from 2022 (circles) (A, D). Climatology of individual copepodite stages (B, E) and data for 2022 (C, F).

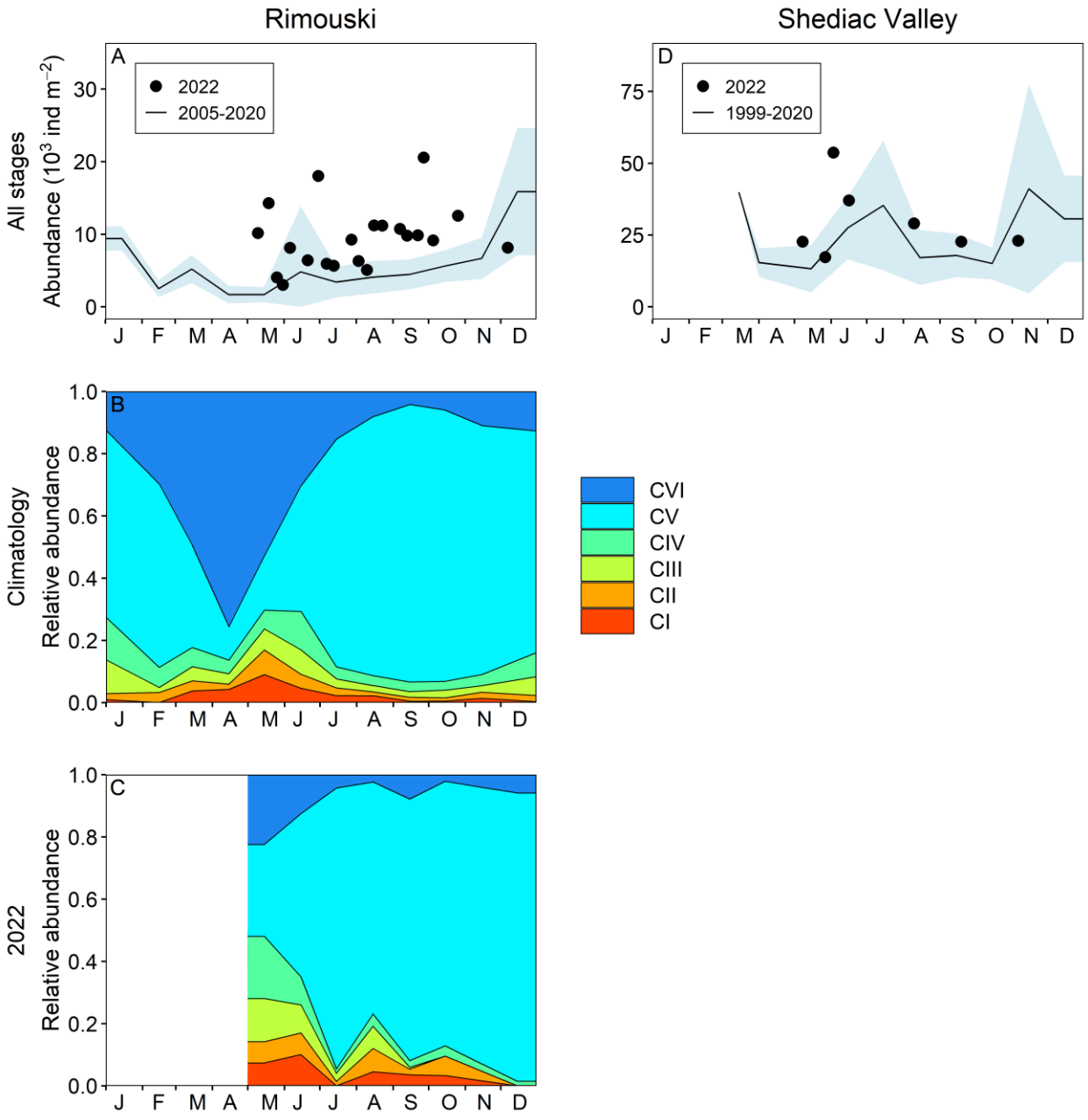

Figure 33. Seasonal variability in *Pseudocalanus* spp. Copepodite abundance and stage distribution at Rimouski (A–C) and Shediac Valley (D) stations. Climatology of *Pseudocalanus* spp. Abundance (black line with blue shading indicating ± 0.5 SD) with data from 2022 (circles) (A). Climatology of individual copepodite stages (B) and data for 2022 (C). Stage information is not available for Shediac Valley.

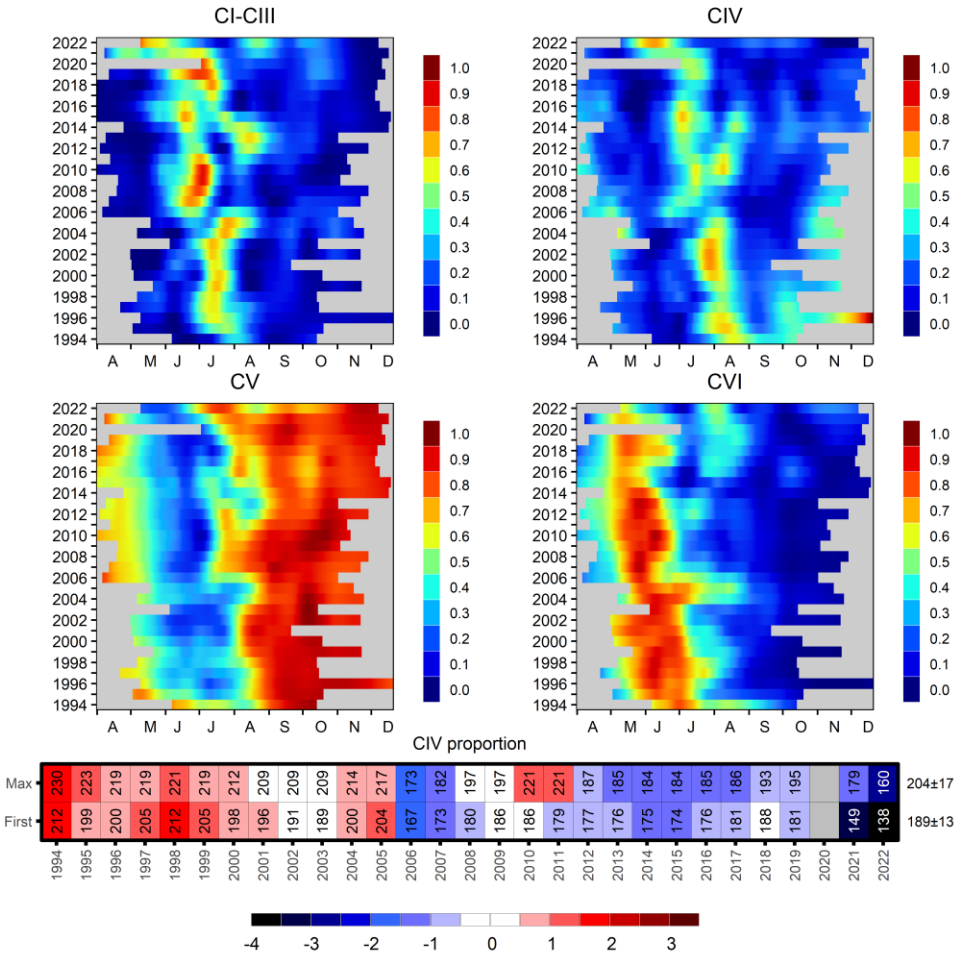

Figure 34. Time series of the seasonal cycle of relative proportion for *Calanus finmarchicus* copepodite stages at Rimouski station. Proportions are normalized by their annual maximum and smoothed using a LOESS regression. Bottom scorecard shows the anomaly time series (climatology 1994–2020) associated with the first day when the normalized proportion of CIV copepodite stage was higher than 0.35 and the day of maximum CIV proportion. Variable means and standard deviations (in units of day) for the 2003–2020 climatology are shown to the right of the scorecard. Blue colours indicate below-normal levels (negative anomaly), red colours are above-normal levels (positive anomaly), and white represents normal levels. Gray cells indicate missing data.

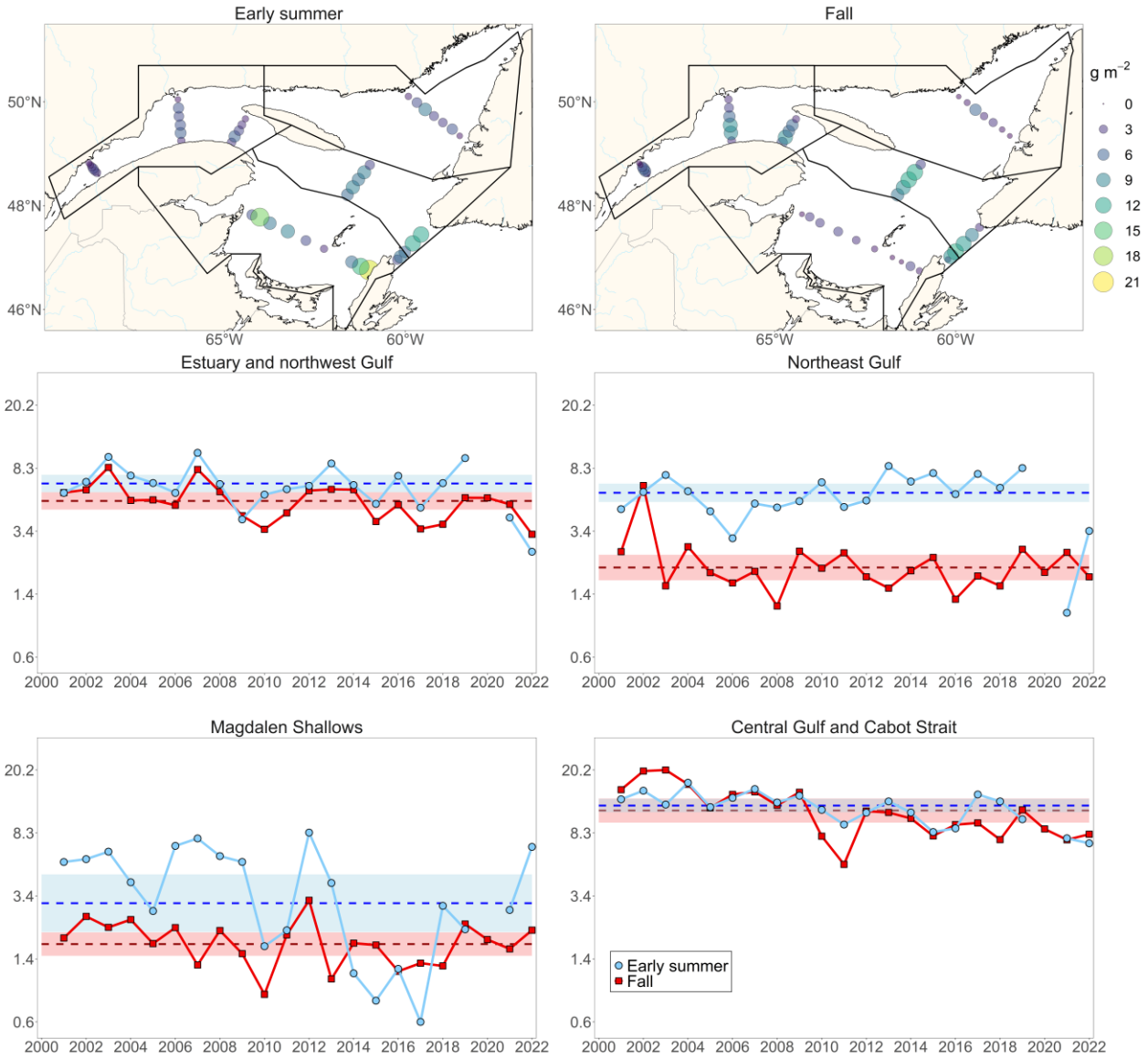

Figure 35. Zooplankton biomass (dry weight; g m^{-2}) spatial distribution during early summer and fall 2022 (upper panels) and regional seasonal time series of mean total zooplankton biomass (g m^{-2}; middle and bottom panels). Dashed blue and red lines represent the climatological (2001–2020) averages (shading represents ± 0.5 SD) for early summer and fall, respectively.

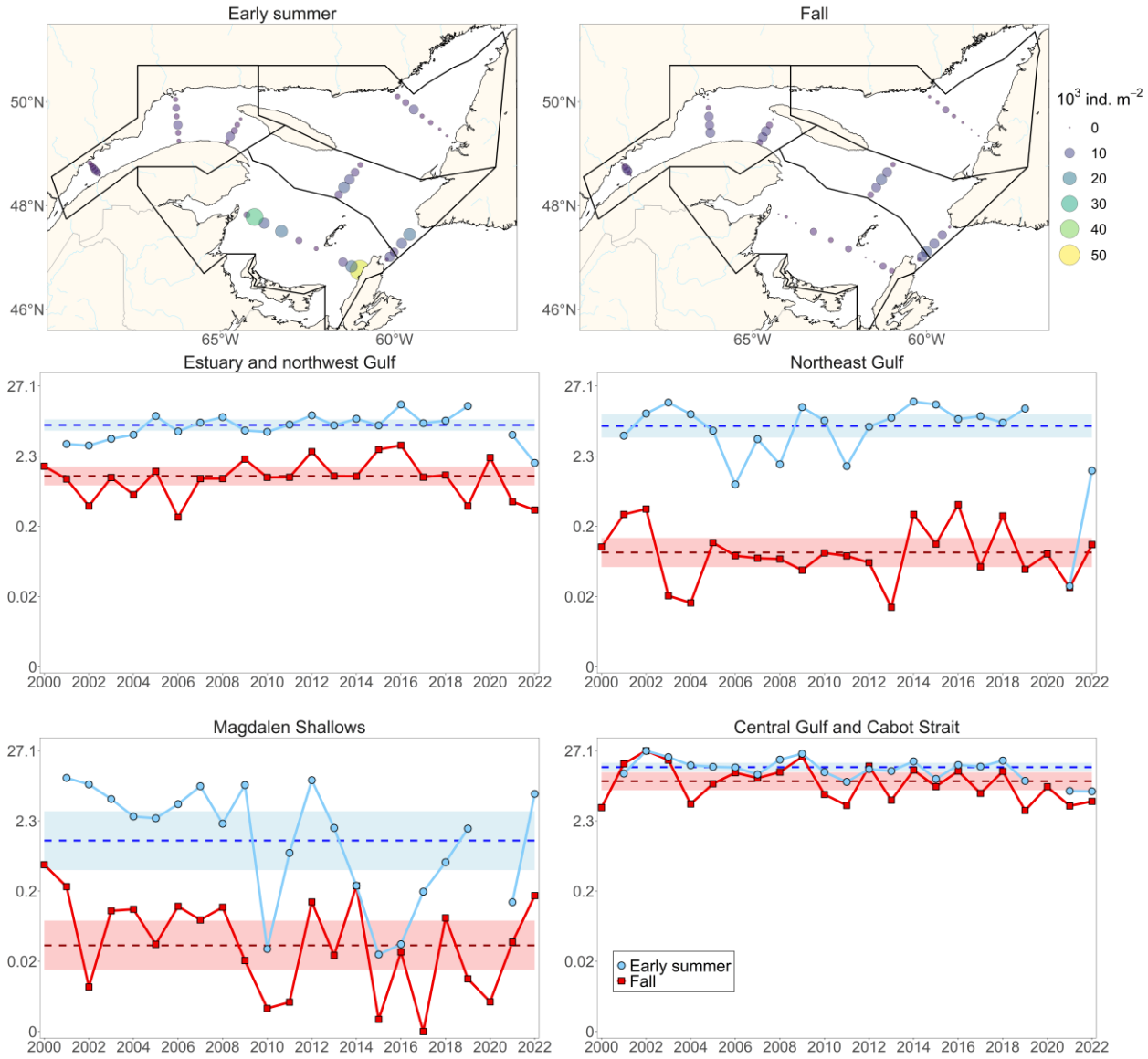

Figure 36. *Calanus hyperboreus* abundance (10^3 ind m^{-2}) spatial distribution during early summer and fall 2022 (upper panels) and regional seasonal time series of mean total C. hyperboreus abundance (10^3 ind m^{-2}; middle and bottom panels). Dashed blue and red lines represent the climatological (2000–2020) averages (shading represents ± 0.5 SD) for early summer and fall, respectively.

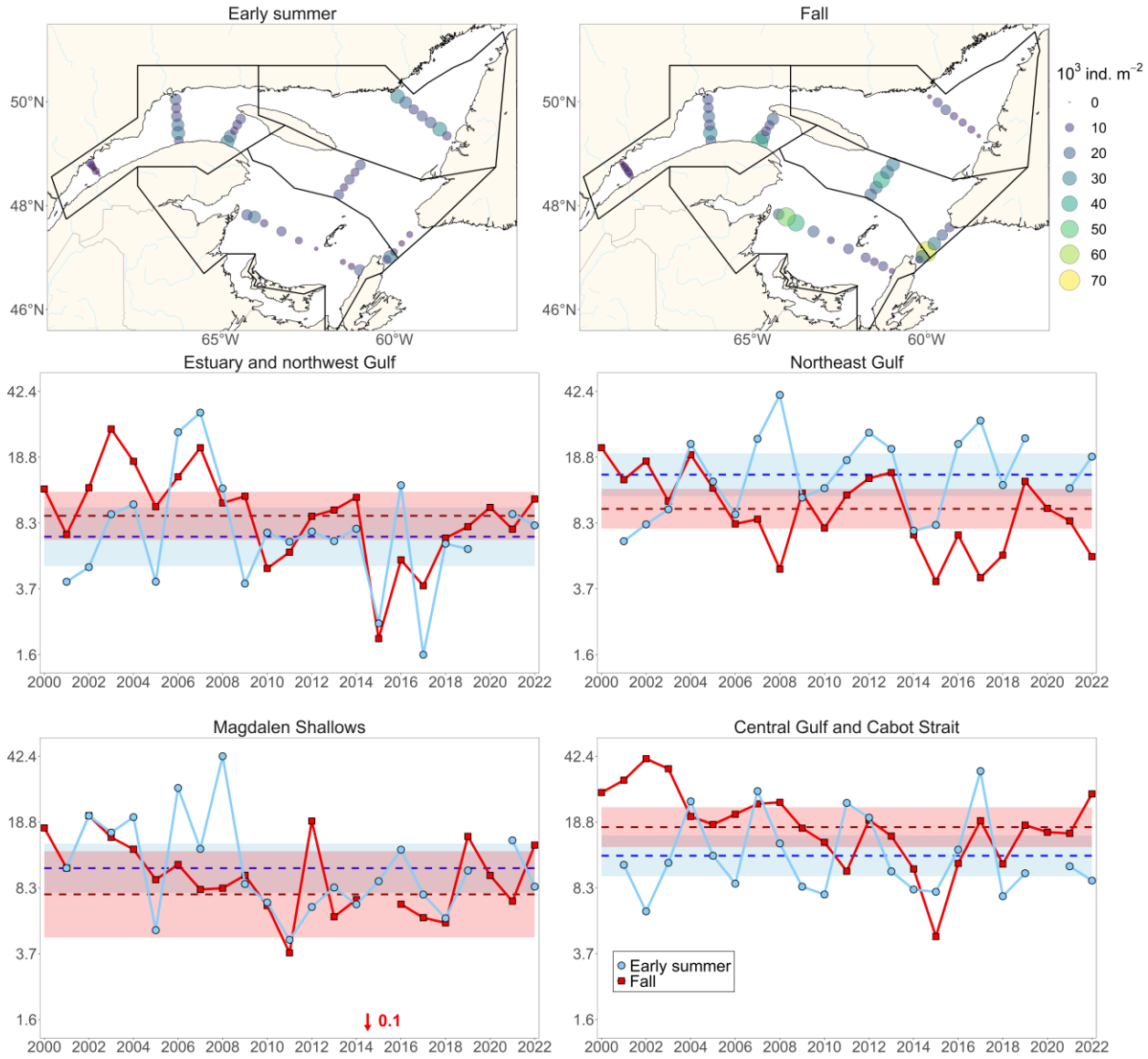

Figure 37. *Calanus finmarchicus* abundance (10^3 ind m^{-2}) spatial distribution during early summer and fall 2022 (upper panels) and regional seasonal time series of mean total C. hyperboreus abundance (10^3 ind m^{-2}; middle and bottom panels). Dashed blue and red lines represent the climatological (2000–2020) averages (shading represents ± 0.5 SD) for early summer and fall, respectively.

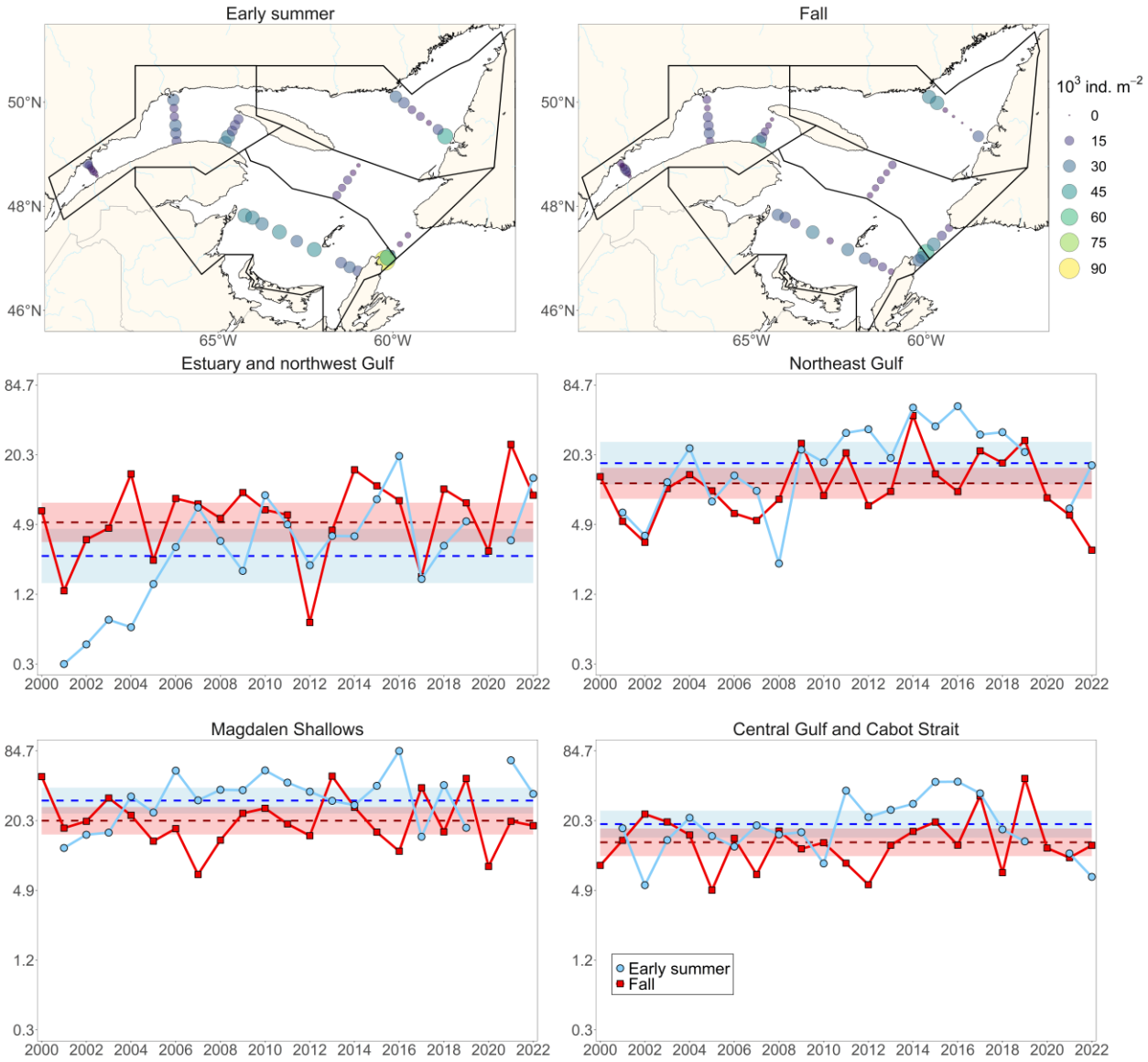

Figure 38. *Pseudocalanus* spp. abundance (10^3 ind m^{-2}) spatial distribution during early summer and fall 2022 (upper panels) and regional seasonal time series of mean total *Pseudocalanus* spp. abundance (10^3 ind m^{-2}; middle and bottom panels). Dashed blue and red lines represent the climatological (2000–2020) averages (shading represents ± 0.5 SD) for early summer and fall, respectively.

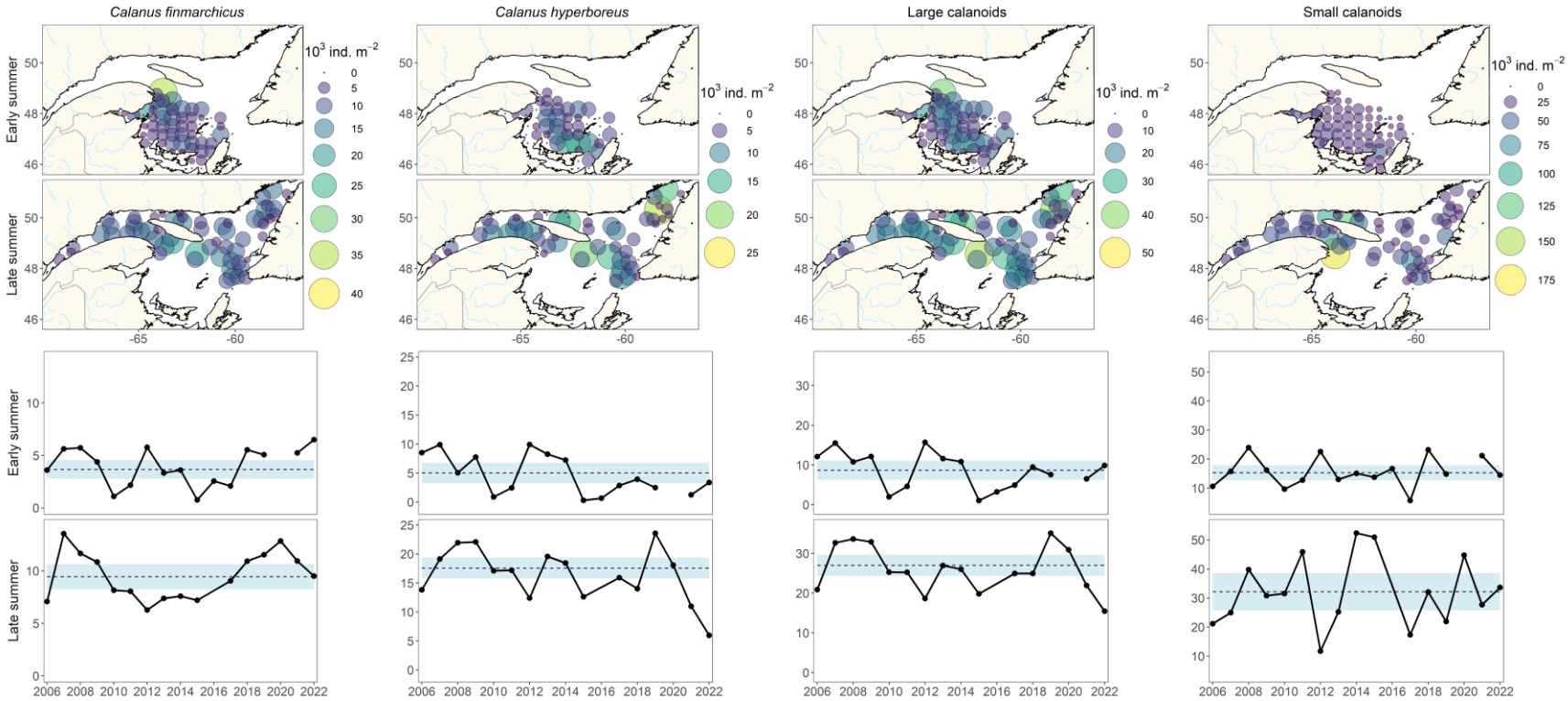

Figure 39. Abundances (10^3 ind m^{-2}) of main taxa identified through automated numerical zooplankton images analysis (ZooImage) at each sampling station during early summer on the Magdalen Shallows and late summer 2022 in the northern Gulf (upper panels). The seasonal time series of mean total abundances are also shown for these taxa (10^3 ind m^{-2}; bottom panels). Dashed lines represent the climatology (2006–2020) averages (shading represents ± 0.5 SD). The abundances of *C. finmarchicus* and *C. hyperboreus* include copepodite stages CIV–CVI only. ZooImage does not distinguish between *C. finmarchicus* and *C. glacialis*; thus both species are included in the *C. finmarchicus* index. Large calanoid abundances correspond to the sum of these *C. finmarchicus* and *C. hyperboreus* indices; and small calanoid abundances correspond to the sum of the following taxa: *Temora* spp., *Eurytemora* spp., *Pseudocalanus* spp., *Microcalanus* spp. and *Scolecithricella* spp.

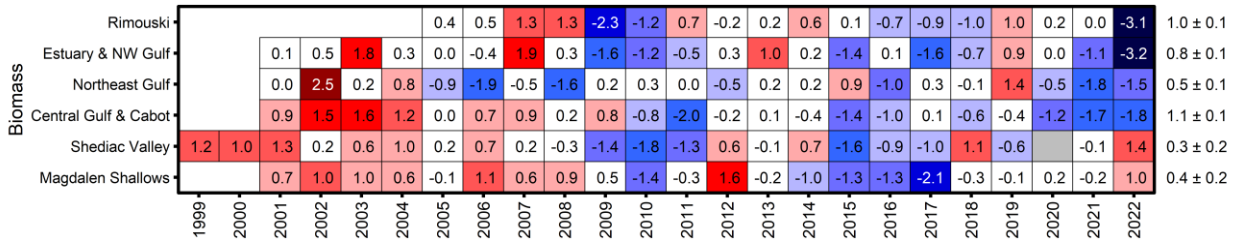

Figure 40. Time series of normalized annual anomalies of zooplankton biomass (dry weight) for the high-frequency monitoring stations and the regions of the Gulf of St. Lawrence. The numbers on the right are the 2001–2020 (2005–2020 for Rimouski; 1999–2020 for Shediac Valley) climatological means and standard deviations in units of $\log_{10}(g\ m^{-2})$. Blue colours indicate below-normal levels (negative anomaly), red colours are above-normal levels (positive anomaly), and white represents normal levels. Gray cells indicate missing data.

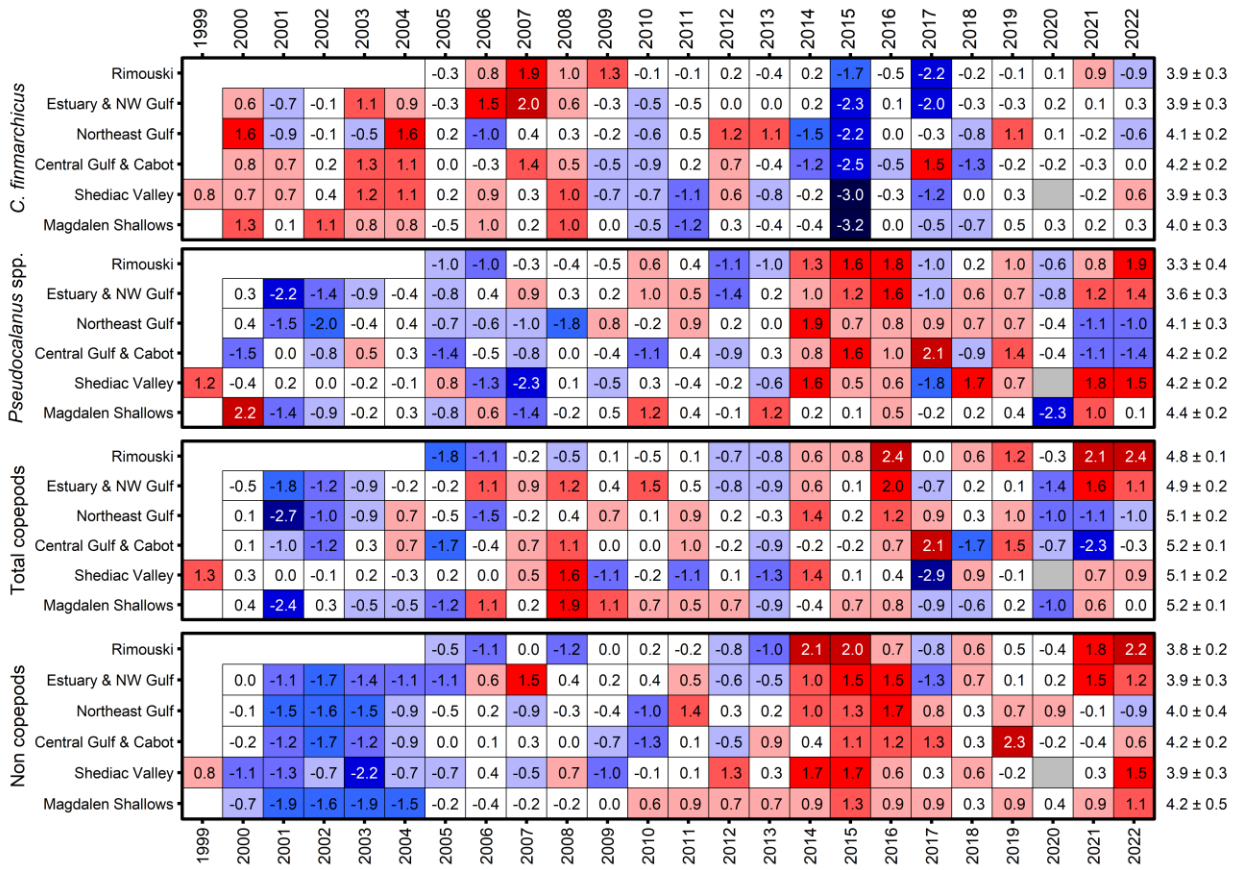

Figure 41. Time series of normalized annual anomalies for the abundance of four zooplankton categories for the high-frequency monitoring stations and regions of the Gulf of St. Lawrence. The numbers on the right are the 2000–2020 (2005–2020 for Rimouski; 1999–2020 for Shediac Valley) climatological means and standard deviations in units of $\log_{10}(ind\ m^{-2})$. Blue colours indicate below-normal levels (negative anomaly), red colours are above-normal levels (positive anomaly), and white represents normal levels. Gray cells indicate missing data.

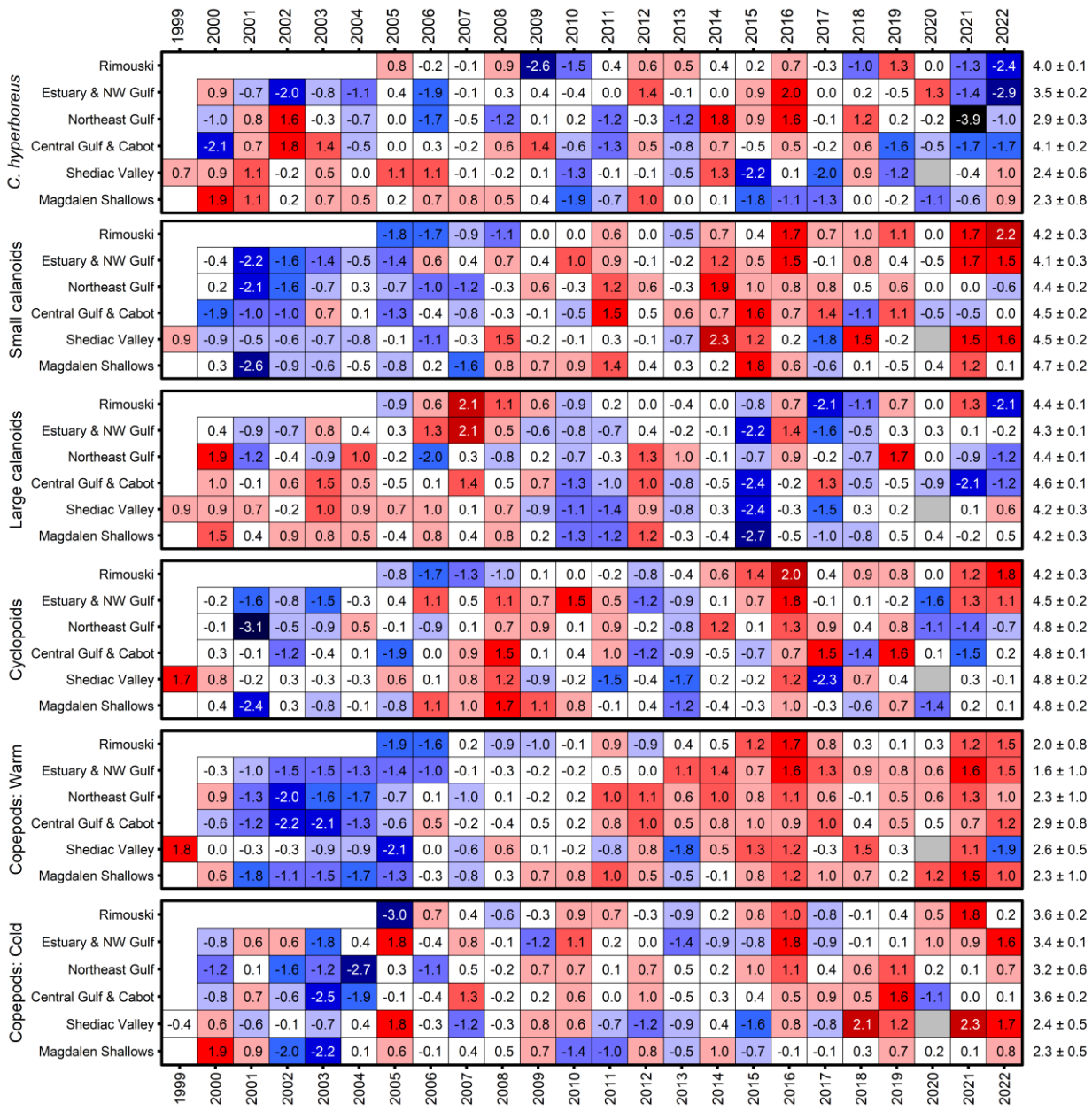

Figure 42. Time series of normalized annual anomalies for the abundance of six categories of zooplankton assemblages for the high-frequency monitoring stations and the regions of the Gulf of St. Lawrence. The numbers on the right are the 2001–2020 (2005–2020 for Rimouski station; 1999–2020 for Shediac Valley station) climatological means and standard deviations in units of $\log_{10}(\text{ind m}^{-2})$. Blue colours indicate below-normal levels (negative anomaly), red colours are above-normal levels (positive anomaly), and white represents normal levels. Gray cells indicate missing data. A detailed list of species included in each large copepod index is presented in Appendix 2.

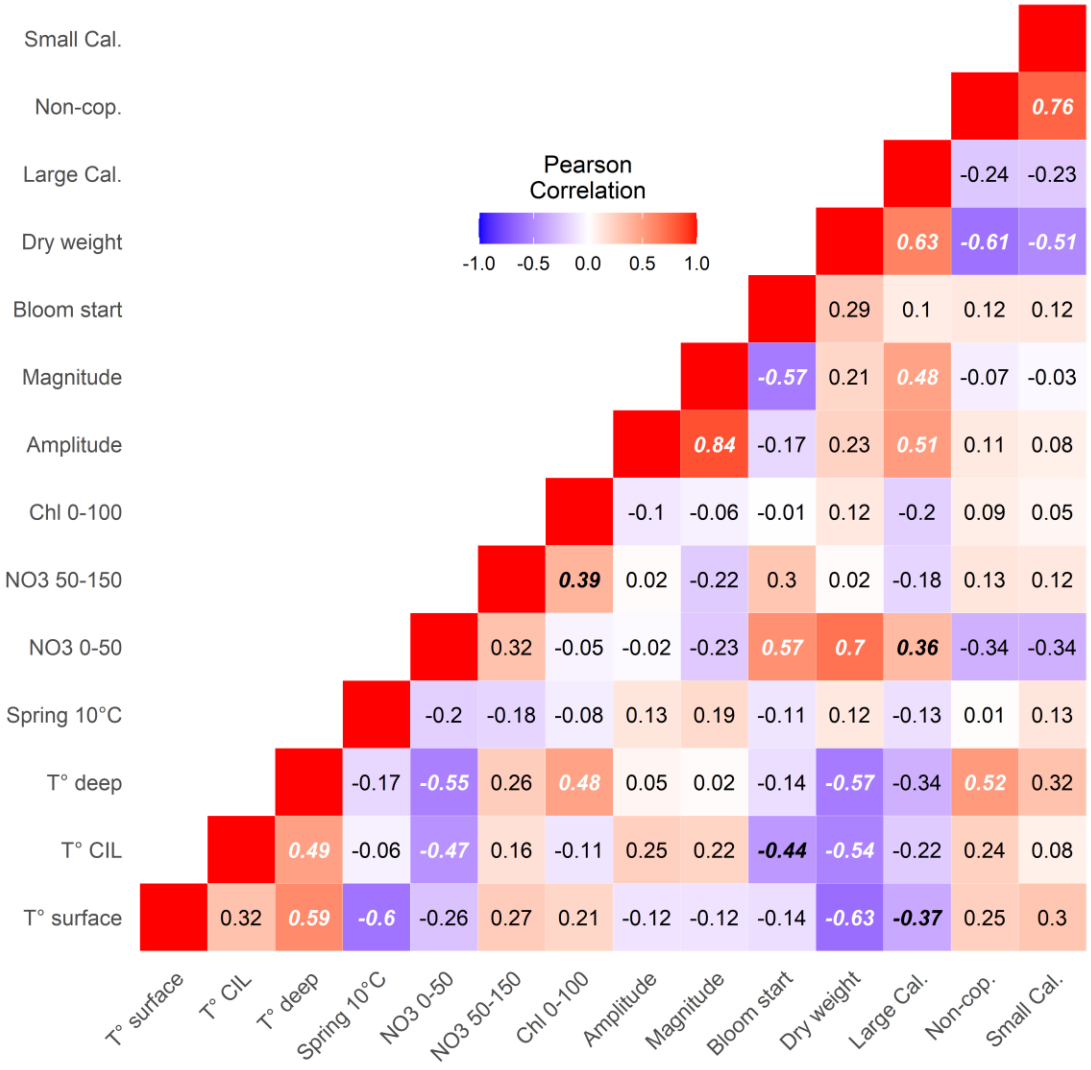

Figure 43. Correlation matrix for weighted average anomaly of key Gulf indices. Blue colours indicate negative correlations and red colours are positive correlations. Significant correlations are indicated in black bold italic ($p < 0.1$) or in white bold italic ($p < 0.05$). CIL: cold intermediate layer. Spring 10 °C is an index of spring timing based on the average Gulf temperature at the surface.

APPENDICES

Appendix 1 : List of taxa associated with each copepod index.

Small calanoids	*Acartia* spp.
	Aetideidae
	Centropages spp.
	Clausocalanus spp.
	Eurytemora spp.
	Microcalanus spp.
	Nannocalanus minor
	Paracalanus parvus
	Pseudocalanus spp.
	Scolecithricella spp.
	Spinocalanus spp.
	Temora spp.
	Tortanus spp.
Large calanoids	*Anomalocera* spp.
	Calanus finmarchicus
	Calanus glacialis
	Calanus hyperboreus
	Euchaeta spp.
	Metridia spp.
	Paraeuchaeta
	Pleuromamma borealis
	Pleuromamma robusta
Warm-water copepods	*Centropages* spp.
	Clausocalanus spp.
	Metridia lucens
	Nannocalanus minor
	Paracalanus spp.
	Pleuromamma borealis
	Pleuromamma robusta
Cyclopoids	*Oithona* spp.
	Oncaea spp.
	Triconia borealis
	Triconia conifer
	Triconia similis
Cold-water copepods	*Metridia longa*
	Calanus glacialis

Appendix 2 : GLM results for Rimouski and Shediac Valley stations. Significance of the year and month effects as well as the adjusted R squared of the regression for nutrients and chlorophyll *a* are presented.

Station	Index	Year (*p*)	Month (*p*)	R^2
Rimouski	Chlorophyll *a* (0–100m)	<0.0001	<0.0001	0.42
	Nitrate (0–50m)	<0.0001	<0.0001	0.39
	Nitrate (50–150m)	<0.0001	<0.0001	0.28
	Nitrate (150–320m)	<0.0001	<0.0001	0.39
Shediac Valley	Chlorophyll *a* (0–100m)	<0.001	<0.0001	0.32
	Nitrate (0–50m)	<0.0001	<0.0001	0.37
	Nitrate (50–84m)	<0.0001	<0.0001	0.4

Appendix 3 : GLM results for Rimouski and Shediac Valley stations. Significance of the year and month effects as well as the adjusted R squared of the regression for phytoplankton groups are presented.

Station	Index	Year (*p*)	Month (*p*)	R^2
Rimouski	Diatoms	<0.0001	<0.0001	0.34
	Dinoflagellates	<0.0001	<0.0001	0.5
	Flagellates	<0.0001	<0.0001	0.37
	Ciliates	<0.0001	<0.0001	0.36
	Total	<0.0001	<0.0001	0.26
	Diatoms/Dinoflagellates	<0.0001	0.001	0.1
	Diatoms/Flagellates	<0.0001	0.01	0.13
Shediac Valley	Diatoms	<0.0001	<0.001	0.32
	Dinoflagellates	<0.0001	0.04	0.27
	Flagellates	<0.0001	<0.0001	0.42
	Ciliates	0.2	0.5	0.04
	Total	<0.0001	<0.001	0.31
	Diatoms/Dinoflagellates	0.007	0.02	0.16
	Diatoms/Flagellates	0.01	<0.0001	0.39

Appendix 4 : GLM results for Gulf regions. Significance of the year, season, and station effects as well as the adjusted R squared of the regression for nutrients or chlorophyll a are presented.

Region	Index	Year (*p*)	Season (*p*)	Station(*p*)	R^2
Estuary/NW Gulf	Chlorophyll *a* (0–100m)	<0.0001	<0.0001	<0.0001	0.31
	Nitrate (0–50m)	<0.0001	<0.0001	<0.0001	0.63
	N:P (0–50m)	<0.0001	<0.0001	<0.0001	0.59
	Si:N (0–50m)	<0.0001	<0.0001	<0.0001	0.3
	Nitrate (50–150m)	<0.0001	<0.0001	<0.0001	0.34
	N:P (50–150m)	<0.0001	<0.0001	<0.0001	0.28
	Si:N (50–150m)	<0.0001	<0.0001	<0.0001	0.35
	Nitrate (150-btm)	<0.0001	<0.0001	<0.0001	0.94
	N:P (150-btm)	<0.0001	<0.001	<0.0001	0.32
	Si:N (150-btm)	<0.0001	<0.001	<0.0001	0.65
Northeast Gulf	Chlorophyll *a* (0–100m)	<0.0001	<0.0001	0.2	0.24
	Nitrate (0–50m)	<0.0001	<0.0001	0.04	0.59
	N:P (0–50m)	<0.0001	<0.0001	0.05	0.53
	Si:N (0–50m)	<0.0001	<0.0001	<0.0001	0.24
	Nitrate (50–150m)	<0.0001	<0.0001	<0.0001	0.55
	N:P (50–150m)	<0.0001	<0.0001	<0.0001	0.58
	Si:N (50–150m)	<0.0001	0.6	<0.0001	0.29
	Nitrate (150-btm)	<0.0001	<0.0001	<0.0001	0.92
	N:P (150-btm)	<0.0001	<0.0001	<0.0001	0.59
	Si:N (150-btm)	<0.0001	<0.0001	<0.0001	0.57
Central Gulf/Cabot Strait	Chlorophyll *a* (0–100m)	<0.0001	<0.0001	0.1	0.15
	Nitrate (0–50m)	<0.0001	<0.0001	<0.0001	0.71
	N:P (0–50m)	<0.0001	<0.0001	<0.0001	0.65
	Si:N (0–50m)	<0.0001	0.01	<0.001	0.21
	Nitrate (50–150m)	<0.0001	<0.0001	<0.0001	0.46
	N:P (50–150m)	<0.0001	<0.0001	<0.0001	0.46
	Si:N (50–150m)	<0.0001	<0.001	<0.0001	0.48
	Nitrate (150-btm)	<0.0001	<0.0001	<0.0001	0.92
	N:P (150-btm)	<0.0001	<0.0001	<0.0001	0.48
	Si:N (150-btm)	<0.0001	0.001	<0.0001	0.56
Magdalen Shallows	Chlorophyll *a* (0–100m)	<0.0001	<0.0001	<0.0001	0.23
	Nitrate (0–50m)	<0.0001	<0.0001	<0.0001	0.44
	N:P (0–50m)	<0.0001	<0.0001	<0.0001	0.36
	Si:N (0–50m)	<0.0001	<0.0001	<0.0001	0.27
	Nitrate (50–150m)	0.03	<0.0001	<0.0001	0.51
	N:P (50–150m)	<0.0001	<0.0001	<0.0001	0.46
	Si:N (50–150m)	<0.0001	0.006	<0.0001	0.42

Appendix 5 : GLM results for Rimouski and Shediac Valley stations. Significance of the year and month effects as well as the adjusted R squared of the regression for each zooplankton index are presented.

Station	Index	Year (*p*)	Month (*p*)	R^2
Rimouski	*Calanus finmarchicus*	<0.0001	<0.0001	0.51
	Pseudocalanus spp.	<0.0001	<0.0001	0.57
	Total copepods	<0.0001	<0.0001	0.59
	Non-copepods	<0.0001	<0.0001	0.46
	Calanus hyperboreus	<0.0001	<0.0001	0.43
	Small calanoids	<0.0001	<0.0001	0.7
	Large calanoids	<0.0001	<0.0001	0.34
	Cyclopoids	<0.0001	<0.0001	0.59
	Copepods: Warm	<0.0001	0.8	0.5
	Copepods: Cold	<0.0001	<0.0001	0.44
	Dry weight	<0.0001	<0.0001	0.68
Shediac Valley	*Calanus finmarchicus*	<0.0001	<0.0001	0.32
	Pseudocalanus spp.	0.07	0.1	0.07
	Total copepods	0.2	<0.0001	0.18
	Non-copepods	<0.001	<0.0001	0.22
	Calanus hyperboreus	<0.0001	<0.0001	0.67
	Small calanoids	0.005	<0.0001	0.2
	Large calanoids	<0.0001	<0.0001	0.34
	Cyclopoids	0.4	<0.0001	0.24
	Copepods: Warm	0.09	0.1	0.07
	Copepods: Cold	0.02	<0.0001	0.3
	Dry weight	<0.0001	<0.0001	0.36

Appendix 6 : GLM results for Gulf regions. Significance of the year, season, and station effects as well as the adjusted R squared of the regression for each zooplankton index are presented.

Region	Index	Year (*p*)	Season (*p*)	Station(*p*)	R^2
Estuary and Northwest Gulf	*Calanus finmarchicus*	<0.0001	0.001	<0.0001	0.66
	Pseudocalanus spp.	<0.0001	<0.0001	<0.0001	0.55
	Total copepods	<0.0001	<0.0001	<0.0001	0.76
	Non-copepods	<0.0001	<0.0001	<0.0001	0.57
	Calanus hyperboreus	0.01	<0.0001	<0.0001	0.6
	Small calanoids	<0.0001	<0.0001	<0.0001	0.68
	Large calanoids	<0.0001	0.002	<0.0001	0.77
	Cyclopoids	<0.0001	<0.0001	<0.0001	0.73
	Copepods: Warm	<0.0001	0.001	<0.0001	0.53
	Copepods: Cold	<0.0001	<0.001	<0.0001	0.66
	Dry weight	<0.0001	0.05	<0.0001	0.76
Northeast Gulf	*Calanus finmarchicus*	0.0001	<0.0001	0.007	0.22
	Pseudocalanus spp.	<0.0001	0.002	<0.0001	0.31
	Total copepods	<0.0001	<0.0001	<0.001	0.39
	Non copepods	<0.0001	0.008	<0.0001	0.45
	Calanus hyperboreus	<0.001	<0.0001	<0.0001	0.59
	Small calanoids	<0.0001	0.6	<0.0001	0.41
	Large calanoids	0.009	<0.0001	<0.0001	0.45
	Cyclopoids	<0.0001	<0.0001	0.1	0.5
	Copepods: Warm	<0.0001	<0.0001	0.002	0.51
	Copepods: Cold	<0.0001	<0.0001	<0.0001	0.43
	Dry weight	<0.0001	<0.0001	<0.0001	0.68
Central Gulf and Cabot Strait	*Calanus finmarchicus*	<0.0001	<0.001	0.007	0.26
	Pseudocalanus spp.	<0.0001	<0.0001	<0.0001	0.28
	Total copepods	<0.001	<0.0001	<0.001	0.18
	Non-copepods	<0.0001	<0.0001	<0.0001	0.46
	Calanus hyperboreus	<0.0001	<0.001	<0.0001	0.51
	Small calanoids	<0.0001	0.9	<0.0001	0.31
	Large calanoids	<0.0001	0.9	<0.0001	0.32
	Cyclopoids	<0.0001	<0.0001	0.005	0.24
	Copepods: Warm	<0.0001	<0.0001	<0.0001	0.49
	Copepods: Cold	<0.001	0.3	0.3	0.09
	Dry weight	<0.0001	0.5	<0.0001	0.6
Magdalen Shallows	*Calanus finmarchicus*	<0.0001	<0.0001	<0.0001	0.32
	Pseudocalanus spp.	<0.0001	<0.0001	0.6	0.12
	Total copepods	<0.0001	<0.0001	<0.0001	0.21
	Non-copepods	<0.0001	<0.0001	<0.0001	0.49
	Calanus hyperboreus	<0.0001	<0.0001	<0.0001	0.48
	Small calanoids	<0.0001	0.001	0.004	0.19
	Large calanoids	<0.0001	<0.0001	<0.0001	0.5
	Cyclopoids	<0.0001	<0.0001	<0.0001	0.31
	Copepods: Warm	<0.0001	<0.0001	0.005	0.51
	Copepods: Cold	<0.0001	<0.0001	<0.0001	0.4
	Dry weight	<0.0001	<0.0001	<0.0001	0.47

Appendix 7 : Spring bloom fit for 2022 in all Gulf ocean colour polygons using the Phytofit application v1.0.0 (Clay et al. 2021) with the standard AZMP parameters listed below.

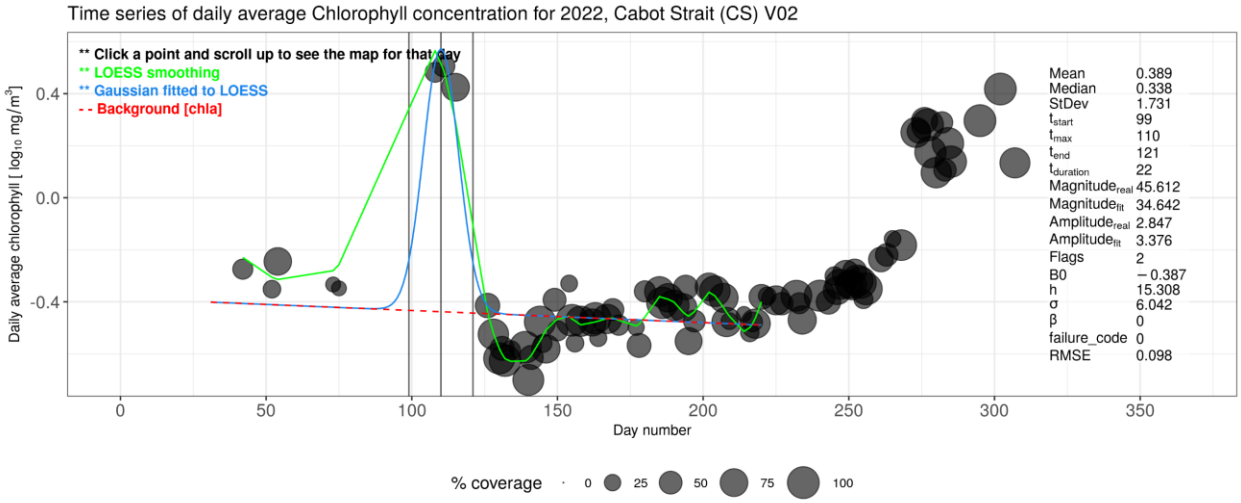

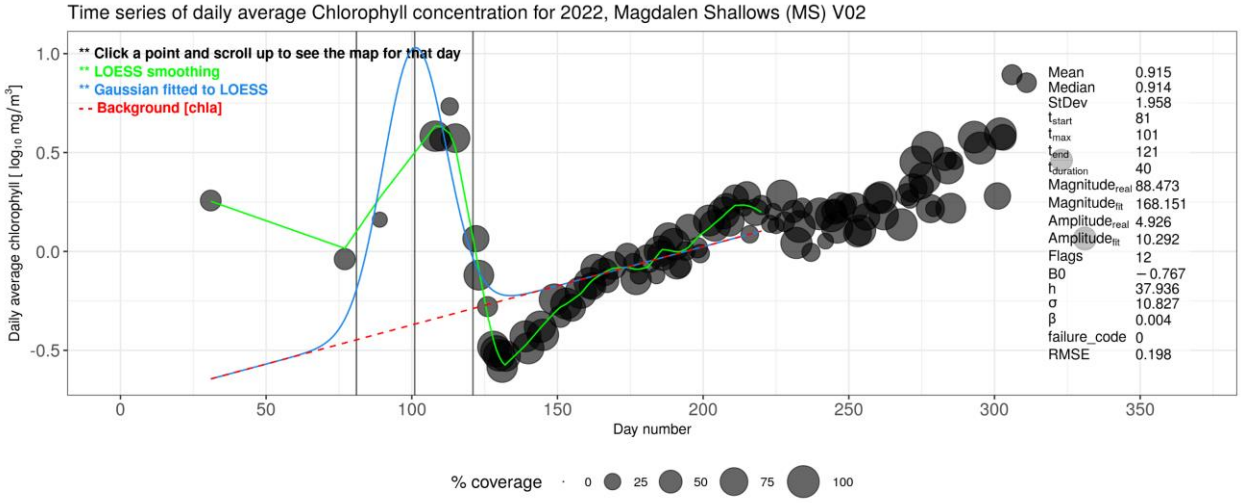

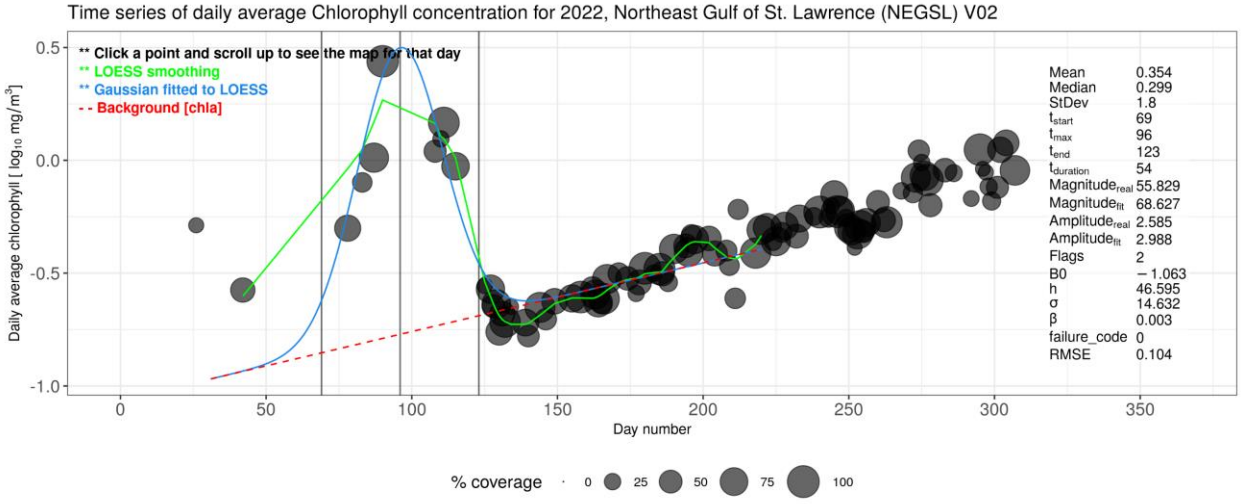

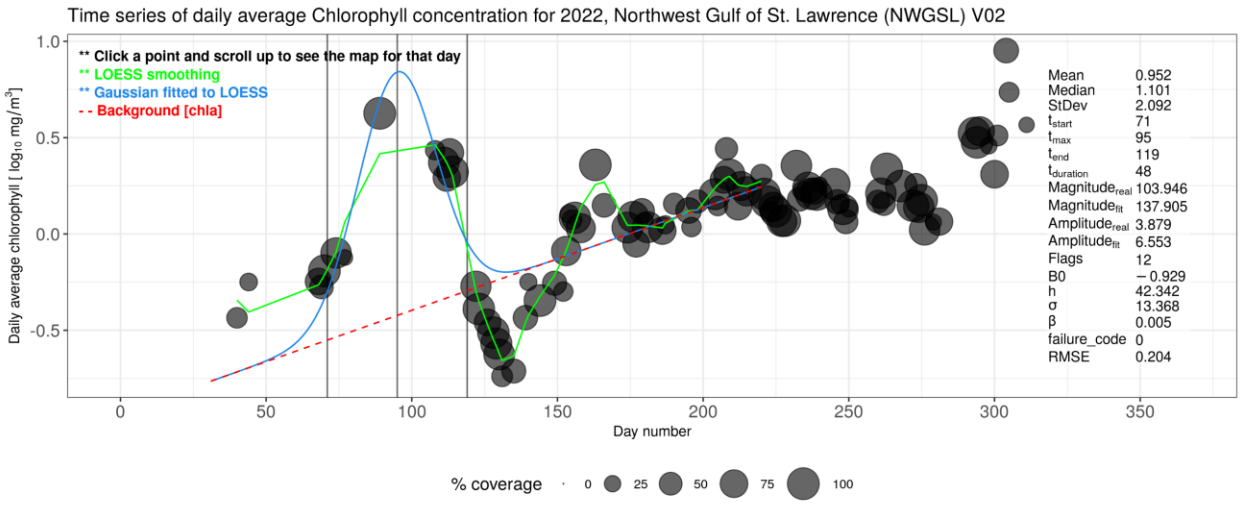

Parameters	Value
Settings_region	Gulf of Saint Lawrence 4 km
Settings_sat_alg	modisaquar2022.0_chleof
Settings_concentration_type	full
Settings_interval	daily
Settings_log_chla	TRUE
Settings_yearday_slide	1
Settings_percent	20
Settings_outlier	sd3
Settings_dailystat	average
Settings_pixrange1	-
Settings_pixrange2	-
Settings_fitmethod	gauss
Settings_bloomShape	symmetric
Settings_smoothMethod	loess
Settings_loessSpan	0,2
Settings_t_range	31,22
Settings_ti_limits	58, 150
Settings_tm_limits	91,181
Settings_ti_threshold_type	percent_thresh
Settings_ti_threshold_constant	0,1
Settings_tm	TRUE
Settings_beta	TRUE
Settings_use_weights	TRUE
Settings_rm_bkrnd	TRUE
Settings_flag1_lim1	0.75
Settings_flag1_lim2	1.25
Settings_flag2_lim1	0.85
Settings_flag2_lim2	1.15
Settings_threshcoef	1.05